Near-infrared Emissive Hypervalent Compounds with Germanium(IV)-Fused Azobenzene π-Conjugated Systems

Masayuki Gon,[a] Misao Yaegashi,[a] Kazuo Tanaka,*[a] and Yoshiki Chujo[a]

[a]   Dr. M. Gon, Misao Yaegashi, Prof. Dr. K. Tanaka, Prof. Dr. Y. Chujo
       Department of Polymer Chemistry, Graduate School of Engineering, Kyoto University, Katsura, Nishikyo-ku, Kyoto 615-8510, Japan
       E-mail: tanaka@poly.synchem.kyoto-u.ac.jp

       Supporting information for this article is given via a link at the end of the document.

Abstract: A novel molecular design for showing near-infrared (NIR) emission is still required for satisfying growing demands for NIR-light technology. In this research, we discover hypervalent compounds with germanium(Ge)-fused azobenzene (GAz) scaffolds can exhibit NIR emission (λ_{PL} = 690~721 nm, Φ_{PL} = 0.03~0.04) despite compact π-conjugated systems. The unique optical properties are derived from trigonal bipyramidal geometry of the hypervalent compounds constructed by combination of Ge and azobenzene-based tridentate ligands. Experimental and theoretical calculation results disclose that germanium–nitrogen (Ge−N) coordination at the equatorial position strongly reduces the energy level of LUMO (lowest unoccupied molecular orbital), and the three-center four-electron (3c-4e) bond in the apical position effectively rises the energy level of HOMO (highest occupied molecular orbital). It is emphasized that large narrowing of the HOMO–LUMO energy gap is achieved just by forming the hypervalent bond. In addition, the narrow-energy-gap property can be enhanced by extension of π-conjugation. The obtained π-conjugated polymer shows efficient NIR emission both in solution (λ_{PL} = 770 nm and Φ_{PL} = 0.10) and film (λ_{PL} = 807 nm and Φ_{PL} = 0.04). These results suggest that collaboration of a hypervalent bond and a π-conjugated system is a novel and effective strategy for tuning electronic properties even in the NIR region.

Introduction

Near-infrared (NIR) light has attracted attention because of unique features, such as invisibility to human eyes, good biotissue permeability, and lower light scattering compared to visible light.[1] Development of NIR emissive molecules has been actively conducted, and various chemical scaffolds have been proposed so far, for example, cyanine, squaraine, rhodamine, boron-dipyrromethene, and donor–acceptor (D–A) dyes.[2] However, wide π-conjugated systems are commonly required to realize the narrow energy gap for NIR emission. Therefore, there are often difficulties in tuning of optical properties by chemical modification based on expanded π-conjugated systems due to low solubility. Furthermore, solid-state luminescent properties are spoiled by concentration quenching caused by non-specific intermolecular interactions in the condensed state. Therefore, it is still necessary to develop compact molecular structures which can provide NIR emission.

Introduction of heteroatoms into the chemical backbones is effective for tuning optical properties without changes of the molecular skeletons.[3] We have recently proposed that the replacement of the skeletal carbon to nitrogen at "the isolated FMO (frontier molecular orbital)" position where only one of

FMOs is distributed in the π-conjugated system is a facile protocol for selectively lowering energy levels.[4] On the basis of this concept, azobenzene (Ph–N=N–Ph) is a representative candidate.[5] Based on stilbene (Ph–CH=CH–Ph), which is one of conventional repeating units for emissive organic materials, such as poly(p-phenylene vinylene)s (PPVs), NIR emission can be potentially generated from the narrow energy gap between FMOs consisting of the largely-lowered LUMO (lowest unoccupied molecular orbital) by the nitrogen replacement and the moderately-lowered HOMO (highest occupied molecular orbital).[6,7]

Pristine azobenzene is the non-emissive unit because of fast internal conversion of excited energy via non-radiative deactivation process often accompanied with *cis–trans* photoisomerization.[8] Recently, it was reported that boron–azobenzene coordination dramatically changed azobenzene properties and succeeded in inducing bright emission from the azobenzene scaffold.[9] There were other studies regarding emission from the azobenzene derivatives mainly by restricting the molecular motion.[10] Our research group also found that boron-fused azobenzene (BAz) showed aggregation-induced emission (AIE)[11] in which the emission is quenched in solution, while emission enhancement is observable only in aggregation.[12] BAz can be also used as an electron-accepting comonomer for NIR emissive D–A type π-conjugated oligomers and polymers[12a,13], and an PPV-type π-conjugated polymer[14] because boron–nitrogen (B−N) coordination additionally lowered the LUMO energy level of the azobenzene unit. As other examples, we revealed that the boron-fused azomethine (BAm) derivatives showed AIE and crystallization-induced emission enhancement (CIEE)[12b,15] properties and worked as moderate electron-accepting units for bright emissive π-conjugated polymer from yellow to NIR region in solution and film.[16] More recently, we revealed that tin(Sn)-fused azobenzene (TAz) derivatives showed emission bands in the longer wavelength region than BAz ones.[17] That was attributed to a hypervalent bond of a five-coordinated Sn with distorted trigonal bipyramidal geometry. In addition, the optical properties were able to be controlled by reversible coordination numbers between five and six. Moreover, NIR absorption and emission of the TAz scaffold were accomplished by extension of π-conjugation with constructing PPV-type π-conjugated system.[18] Therefore, combination of a hypervalent bond and azobenzene is expected to be a versatile candidate for a fundamental scaffold of a NIR emissive material.

In this research, we focused on germanium (Ge) belonging to 4th period of group 14 elements in periodic table and constructed hypervalent Ge-fused azobenzene (GAz) compounds with distorted trigonal bipyramidal geometry. Ge-

containing π-conjugated systems and their properties including σ*–π* conjugation[19] have been actively studied sometimes by focusing on the properties depending on group 14 elements.[20] Although optical properties based on hypervalent Ge compounds were also reported, there are much room to discuss the role of the element in optical properties.[21] In the case of distorted trigonal bipyramidal geometry focused by us here, it is expected that the GAz compounds have much more ideal geometry with smaller distortion than Sn ones because of shorter atomic radii of Ge (1.25 Å) than that of Sn (1.45 Å).[22] As a result, we confirmed the less distorted geometry both from a single crystal X-ray diffraction (SC-XRD) analysis and the optimized modeling structure from theoretical calculations. As we presumed, the GAz derivatives showed NIR emission which was longer wavelength than TAz derivatives despite the small π-conjugated system composed of azobenzene. Furthermore, the emission and chemical stability were highly reinforced by forming π-conjugated polymeric system. The concept of functional monomers with heteroatoms have been proposed as element-block materials[23] by our research group, and the GAz derivatives should be versatile units for constructing NIR-emissive materials.

Results and Discussion

Synthesis. Scheme 1 shows the synthesis of halogenated Ge-fused azobenzene compounds **GAz-X** (X = F, Cl, Br, I). By stirring a reaction mixture of each halogenated tridentate ligand **AzOH-X** (X = F, Cl, Br, I), triethylamine (Et$_3$N) and distilled diisopropyldichlorogermane (iPr$_2$GeCl$_2$) at ambient temperature under nitrogen atmosphere, the respective compounds **GAz-X** were obtained. The reaction quantitatively proceeded, and the compounds were finally obtained with moderate yields after recrystallization (39~84%). The isopropyl groups at the Ge atom were introduced to improve chemical stability of the hypervalent compounds by preventing the Ge center from attacks of nucleophiles such as water. Additionally, halogens play roles in the enhancement of crystallinity and stability in solution and solid. Indeed, the pure hydrogen-substituted compound (**GAz-H**) was hardly obtained due to high reactivity and low crystallinity. Crystallization was the main tool to obtain pure compounds because we avoided purifying them by silica gel chromatography in which **GAz-X** would be adsorbed and decomposed by nucleophilic Si-OH groups. The chemical structure of the Sn-fused azobenzene compound (**TAz-F**) which was previously reported is also shown in Scheme 1 as a model compound to evaluate the difference depending on the elements.[17]

Next, we synthesized a π-conjugated alternating copolymer including the GAz unit in the main chain (Scheme 2). The Migita–Kosugi–Stille cross-coupling[24] polymerization with **GAz-Br** and 5,5′-bis(trimethylstannyl)-3,3′-didodecyl-2,2′-bithiophene (**BT**) were carried out under a catalytic condition using Pd$_2$(dba)$_3$ (dba = dibenzylideneacetone) and 2-dicyclohexylphosphino-2′,4′,6′-triisopropylbiphenyl (XPhos) to provide a copolymer, and **P-GAz** was obtained in 90% isolated yield. The coupling reaction was performed under a neutral condition for suppressing decomposition of the hypervalent compound units. The relative molecular weights of **P-GAz** ($M_n = 1.4 \times 10^4$, $M_w = 3.6 \times 10^4$, $M_w/M_n = 2.5$) were determined by gel permeation chromatography (GPC) with polystyrene standards by using
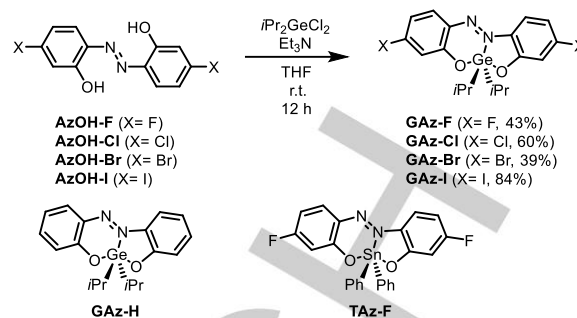
Scheme 1. Synthesis of halogenated the Ge-fused azobenzene compounds, **GAz-X** (X = F, Cl, Br, I). Chemical structures of **GAz-H** and Sn-fused azobenzene compound **TAz-F**.
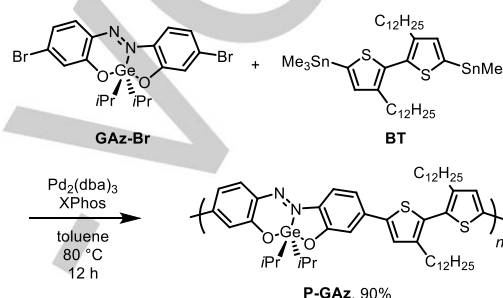
Scheme 2. Synthesis of the π-conjugated polymer **P-GAz** containing a hypervalent Ge moiety in the main chain.

chloroform (CHCl$_3$) as an eluent. All synthesized compounds showed good solubility in common organic solvents such as toluene, CHCl$_3$, dichloromethane and tetrahydrofuran (THF). They were characterized by ^{1}H and ^{13}C NMR spectroscopy, high-resolution mass spectrometry (HRMS) and elemental analyses (see Supporting Information) and had enough stability to use in solution and solid under ambient conditions. In addition, polymerization enhanced thermal stability and water resistance compared to the monomer because degradation was suppressed in the polymers (Figures S1, S2 and Table S1). From the characterization data, we concluded that the samples had the designed structures and enough purity for further analyses.

Crystal Structures. Figures 1A and 1B show the structures obtained from the analysis with SC-XRD of **GAz-F** and **GAz-Br**, respectively. The data clearly indicate that the GAz compounds had five-coordinated Ge centers with distorted trigonal bipyramidal geometry. To the best of our knowledge, they are the first examples to offer hypervalent Ge-fused azobenzene compounds. As a series of the similar hypervalent compounds constructed by group 14 elements and azobenzene tridentate ligands, another research group and our group found the Sn-fused azobenzene compounds with distorted trigonal bipyramidal geometry.[17,25] Interestingly, compared with silicon (Si)-fused azobenzene compounds which form square pyramidal geometry, the Ge and Sn compounds exhibit significant different structures.[27] In addition, similar distorted trigonal bipyramidal geometry of the five-coordinated Ge compound with the azomethine (Schiff base) ligand was also reported.[27] The bond lengths of **GAz-F** and **GAz-Br** between N(1) and N(2) were
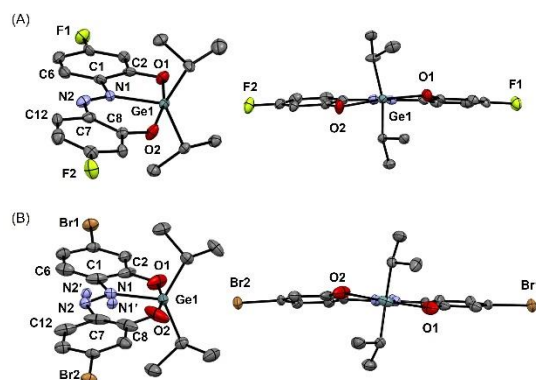
Figure 1. ORTEP drawings of (A) **GAz-F**, (B) **GAz-Br** (50% probability for thermal ellipsoids). Hydrogen atoms are omitted to clarify. All crystallographic data including **GAz-Cl** and **GAz-I** are shown in Supporting Information.

Table 1. Spectroscopic data of TAz and GAz derivatives

	λ_{abs}[b] /nm	λ_{PL}[b,c] /nm	Φ_{PL}[b,c,d]	τ[b,e] /ns [α]	k_r[f] /10^8 s^{-1}	k_{nr}[f] /10^8 s^{-1}
TAz-F [a]	523	640	0.21	3.1	0.69	2.6
GAz-F	560	690	0.04	0.72	0.57	13
GAz-Cl	583	706	0.04	0.61	0.67	16
GAz-Br	587	712	0.04	0.59	0.71	16
GAz-I	597	720	0.03	0.53	0.64	18
P-GAz	693	770	0.10	0.42 [96%]	2.3	20
	(710) [g]	(807) [g]	(0.04) [g]	1.0 [4%]		

[a] From ref. 17. [b] In CHCl$_3$ (1.0×10^{-5} M). [c] Excited at λ_{abs}. [d] Determined as an absolute value. [e] PL lifetime monitored at λ_{PL}, excited at 532 nm. [f] k_r = Φ_{PL}/τ_{av}, k_{nr} = $(1 - \Phi_{PL})/\tau_{av}$, τ_{av} = $\Sigma\alpha_i\tau_i$. α: relative amplitude. [g] In film.
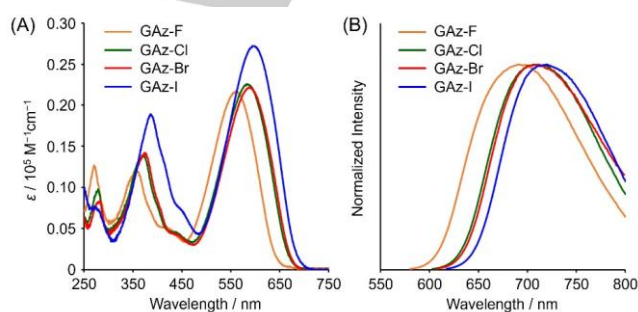

Figure 2. (A) UV–vis absorption and (B) PL spectra of **GAz-X** (X = F, Cl, Br, I) in CHCl$_3$ (1.0×10^{-5} M), excited at wavelengths of absorption maxima.

1.27~1.28 Å, meaning that these bonds can be assigned as an N=N bond.[17,26,28] The absolute values of dihedral angles of C(1)–N(1)–N(2)–C(7) were 178.3° and 179.6° for **GAz-F** and **GAz-Br**, respectively, indicating that the azobenzene π-conjugated system should have highly planar structures. On the other hand, the absolute values of dihedral angles of C(2)−O(1)−O(2)−C(8) were 20.84° and 21.46° for **GAz-F** and **GAz-Br**, respectively, indicating that Ge coordination should be slightly distorted in crystal. Compared to **TAz-F**,[17] the Ge–N bond (2.02 Å) was shorter than the Sn–N bond (2.20 Å). Additionally, the angle of O(1)−Ge(1)−O(2) (164.7°) was closer to straight than that of O(1)−Sn(1)−O(2) (157.5°). These results suggest that distortion of trigonal bipyramidal geometry is smaller in GAz than in TAz as we expected. There were disordered nitrogen atoms in **GAz-Br** which were often detected in similar heteroatom-fused azobenzene compounds.[12,17,26] Details in crystallographic data including **GAz-Cl** and **GAz-I** are described in Tables S2–S5 and Figures S3–S6. The information of representative bond lengths, angles and dihedral angles is listed in Table S6. From those data, we confirmed that the five-coordinated hypervalent GAz compounds with partially-distorted trigonal bipyramidal geometry can be obtained regardless of the type of halogens.

Optical Properties. To investigate optical properties of the GAz derivatives, we performed UV–vis and photoluminescence (PL) measurements in CHCl$_3$ (1.0×10^{-5} M). The results are summarized in Figure 2 and Table 1. Accordingly, **GAz-X** (X = F, Cl, Br, I) exhibited emission around 690~720 nm, and the PL quantum yields (Φ_{PL}s) were 0.03~0.04. These data mean that the GAz derivatives can be a versatile platform for obtaining NIR emission. Interestingly, owing to the small π-conjugated system consisting of azobenzene, all complexes show high solubility, which is precious for various applications.[29] To comprehend emission mechanisms, a radiative rate constants (k_r) and a non-radiative rate constant (k_{nr}) were estimated from a PL lifetime measurement (Figure S7). From all **GAz-X**, the k_r values were found in the moderate range (~10^7 s^{-1}) while the k_{nr} values were relatively large (~10^9 s^{-1}), comparing to the previous tin compounds such as **TAz-F** in Table 1.[17] The effect of intersystem crossing is limited because **TAz-F** containing heavier atom showed smaller k_{nr} value than **GAz-F**. To obtain deep insight on the large values of k_{nr}, PL and lifetime measurements at 77 K in vitrified 2-methyl tetrahydrofuran (2Me-

THF) were conducted with **GAz-Br** (Figure S8 and Table S7). It was observed that PL spectrum showed hypsochromic shift with vibrational structure, and significantly the Φ_{PL} increased from 0.04 to 0.16 corresponded to decreases in k_{nr}. These data suggest that structural relaxation after photo excitation should be the main process for non-radiative decay. When **GAz-Br** was dispersed in the polystyrene film in which molecular motions should be loosely restricted even at room temperature, the enhancement of Φ_{PL} from 0.04 to 0.06 was also detected (Figure S9 and Table S8). This fact also supports the speculation that intramolecular motions in the excited state should occur in **GAz-X**, followed by lowering Φ_{PL}s. Moreover, we conducted variable-temperature ^{1}H NMR measurements with **GAz-Br**. Accordingly, the signal peaks observed in the aromatic area (6.7~7.6 ppm) gradually became sharp by cooling from 20 to −60 °C (Figure S10). This result clearly indicates that the structure of **GAz-X** is also non-rigid at room temperature in the ground state and these motions should be suppressed by cooling. In the case of the Si-fused azobenzene derivative, it was also reported that there were two conformations in equilibrium composed of replacing five- and six-membered rings originating from the pedal motion of azobenzene.[26b,30] In the case of the GAz derivatives, similar molecular motions might occur in solution at room temperature.

Introduction of conjugated molecules into polymer main-chains is one of effective strategies not only for inducing longer-wavelength light emission but also for enhancing PL quantum yields.[12a,13] The synthesized π-conjugated polymer **P-GAz**
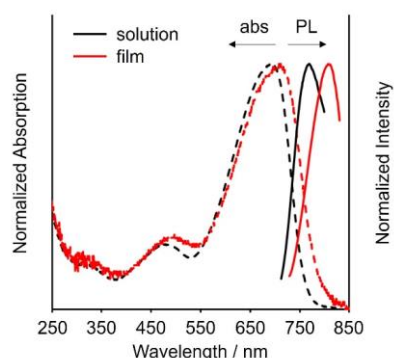
Figure 3. UV–vis absorption (dotted line) and PL spectra (solid line) of **P-GAz** in CHCl₃ (1.0×10⁻⁵ M) and in film prepared by a spin-coating method (1000 rpm, 30 s) on a quartz substrate (0.9 cm×5 cm) from CHCl₃ solutions (100 μL of 1 mg/300 μL), excited at wavelengths of absorption maxima.

showed dramatical bathochromic shift of the absorption band (λ_{abs} = 693 nm) compared to the monomer **GAz-Br** (λ_{abs} = 587 nm) (Figure 3 and Table 1). It should be emphasized that **P-GAz** showed NIR emission with the highest emission quantum yields (λ_{PL} = 770 nm and Φ_{PL} = 0.10) in the synthesized GAz derivatives. According to the kinetic parameter calculation, elevation of the k_r value without momentous change in k_{nr} was observed. The molecular motions of the GAz moiety, which are the main path for non-radiation decay, should be restricted by the incorporation into the π-conjugated polymeric system. It should be mentioned that as is often the case with the NIR-luminescent materials, bathochromic shifts of a PL spectrum generally lead to increase in k_{nr} values due to the effect represented by the energy-gap law.[1a,31] In this study, the loss of emission efficiency caused by such acceleration of k_{nr} could be limited. The emission from **P-GAz** was also detectable in film (λ_{PL} = 807 nm and Φ_{PL} = 0.04). In addition, the spectra shapes were maintained before and after 100 °C annealing for 1 h under vacuum condition (Figure S11). Hence, π-conjugated polymerization is beneficial for enhancement of parameters for applications as stable NIR-emissive materials.

Cyclic Voltammetry. The origin of narrow-energy-gap properties of the GAz derivatives was evaluated by cyclic voltammetry (CV). We calculated experimental values of HOMO and LUMO energy levels from onset potentials of oxidation and reduction curves in voltammogram, respectively (Figure S12 and Table S9). Accordingly, it was found that **GAz-X** had high HOMO (−5.59 ~ −5.65 eV) and low LUMO energy levels (−3.53 ~ −3.72 eV). These data are the considerable evidence of long wavelength of optical properties. We previously reported that the narrow-energy-gap behavior should be attributed to the effect of asymmetric chemical bonds of trigonal bipyramidal geometry composed of 3c-4e bond at apical positions and sp^2 hybrid orbital at equatorial positions.[17] In **P-GAz**, elevation of HOMO energy level (−5.36 eV) was derived from the electron-donating comonomer, bithiophene, and that was one of main factors for bathochromic shift of the absorption and emission spectra.

Theoretical Calculation. To obtain further insight of optical properties of the GAz derivatives, density functional theory (DFT) and time-dependent (TD)-DFT calculations were executed (Figures 4 and S13–S15). Similarly to our previous results on the TAz compounds, the optimized structures of GAz had
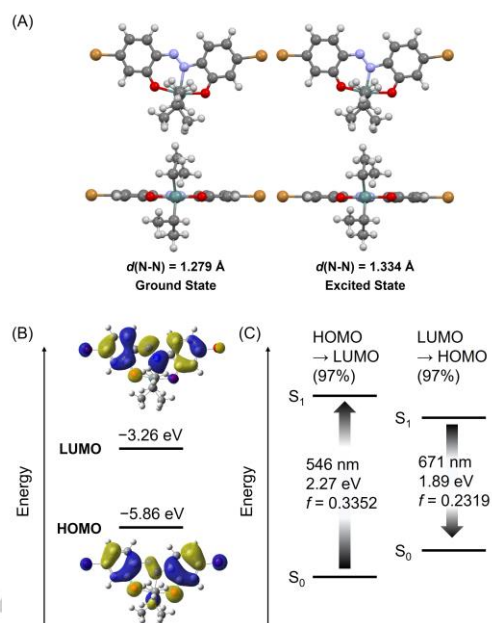

Figure 4. Calculation results of **GAz-Br**. (A) Top and front views of optimized structures in the ground and excited states, respectively. (B) Kohn–Sham orbitals (isovalue = 0.02) and energy diagrams of HOMO and LUMO. (C) Oscillator strength (*f*), transition energy of S₀→S₁ transition from the optimized ground state and S₁→S₀ transition from the optimized excited state. Calculation details and all results for **GAz-X** (X = F, Cl, Br, I) are shown in Supporting Information.
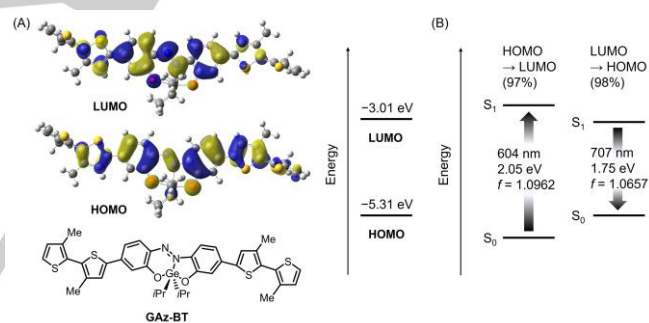

Figure 5. Calculation results of **GAz-BT** as a model compound of **P-GAz**. (A) Chemical structure, Kohn–Sham orbitals (isovalue = 0.02) and energy diagrams of HOMO and LUMO. (B) Oscillator strength (*f*), transition energy of S₀→S₁ transition from the optimized ground state and S₁→S₀ transition from the optimized excited state. Calculation details are shown in Supporting Information.

partially-distorted trigonal bipyramidal geometries (Figures 4A and S13).[17] In addition, it was shown that the S₀→S₁ transition assigned to the π–π* one was allowed by making Ge−N coordination and was consisted of almost pure HOMO–LUMO transitions (Figures 4B, 4C, S14 and S15). The energy gap was large in the following order: **GAz-F** >> **GAz-Cl** > **GAz-Br** > **GAz-I**, and the tendency was good agreement with experimental data from absorption and emission measurements. The optimized structures were highly planar in the ground state, while structural relaxation driven by elongation of the N=N bond was proposed in the excited state (Figures 4A and S13). In **P-GAz**, the model compound **GAz-BT** supported the expansion of π-conjugated system to the comonomer units linked at both ends (Figure 5A and S16). In addition, the estimated both absorption and

4

emission wavelengths were larger than **GAz-Br**. Therefore, it can be said that extension of π-conjugation involving the hypervalent Ge atoms can be realized.

By compering experimental data with our previous report based on TAz,[17] it was noted that the energy gaps of GAz were narrower than those of TAz. We evaluated the origin of the difference derived from the period in group 14 elements by using the simplified hypervalent compounds **GAzMe-H** and **TAzMe-H** without substituents on azobenzene moieties and with two methyl groups at Ge and Sn atoms. The result of calculation was well reproduced with the same tendency of the energy gaps. In summary, the narrower energy gaps of GAz should be mainly caused by elevation of HOMO and reduction of LUMO energy revels in **GAzMe-H** (Figure S17). It was found that the degree of distortion in trigonal bipyramidal geometry was smaller in **GAzMe-H** than in **TAzMe-H** because of the difference in the atomic size, which was also observed in crystallographic data. Shorter bond length of Ge−N reduced LUMO energy revel, and more linear angle of the 3c-4e bond (O−Ge−O) increased HOMO energy level compering to TAz (Figure S17A). A natural bond orbital (NBO) calculation also suggested stronger interaction of Ge−N (ΔE = 163.24 kcal mol^{-1}) than that of Sn−N (ΔE = 79.40 kcal mol^{-1}) (Figures S18 and S19), leading to strong decrease in LUMO energy level of **GAzMe-H**. From the data on energy levels of oxygen atoms in NBO calculation, the values of average energy were −7.80 eV for **GAzMe-H** and −7.88 eV for **TAzMe-H** (Figure S20). This implied that the electron-donating ability of oxygen atoms was slightly enhanced by Ge coordination. The NBO calculation was also supported existence of the 3c-4e bond in both GAz and TAz (Figures S18 and S19). From these data, the close-to-ideal structure for trigonal bipyramidal geometry should be responsible for reduction of energy gaps of the π-conjugated system in the ligand.

Conclusion

We synthesized hypervalent compounds composed of five-coordinated Ge and azobenzene-based π-conjugated systems. It was found that the halogenated GAz derivatives exhibited absorption and emission in long wavelength region despite the compact π-conjugated systems consisting of azobenzene. To the best of our knowledge, this is the first report on NIR emission beyond 700 nm from the azobenzene-based small molecular conjugated system. The data from theoretical calculations support that these outstanding optical properties should be attributed to the asymmetric hypervalent bonds originating from trigonal bipyramidal geometry containing a 3c-4e bond. In addition, the smaller atomic size of Ge than that of Sn contributes to the improvement of planarity in trigonal bipyramidal geometry, leading to narrowing HOMO−LUMO energy gaps of the connected π-conjugated system. We obtained highly-efficient NIR emissive polymer both in solution (λ_{PL} = 770 nm and Φ_{PL} = 0.10) and film (λ_{PL} = 807 nm and Φ_{PL} = 0.04) owing to a synergistic effect between a hypervalent bond and extension of π-conjugation. Those results should open a novel research field of hypervalent compounds for controlling energy gaps of π-conjugated system, which has a potential to apply for development of NIR emissive materials.

[1] a) A. Zampetti, A. Minotto, F. Cacialli, *Adv. Funct. Mater.* **2019**, *29*, 1807623; b) M. Gon, S. Ito, K. Tanaka, Y. Chujo, *Bull. Chem. Soc. Jpn* **2021**, *94*, 2290–2301.

[2] J. Wu, Z. Shi, L. Zhu, J. Li, X. Han, M. Xu, S. Hao, Y. Fan, T. Shao, H. Bai, B. Peng, W. Hu, X. Liu, C. Yao, L. Li, W. Huang, *Adv. Optical Mater.* **2022**, *10*, 2102514.

[3] a) V. H. K. Fell, A. Mikosch, A.-K. Steppert, W. Ogieglo, E. Senol, D. Canneson, M. Bayer, F. Schoenebeck, A. Greilich, A. J. C. Kuehne, *Macromolecules* **2017**, *50*, 2338–2343; b) R. Inaba, K. Oka, T. Iwami, Y. Miyake, H. Tajima, H. Imoto, K. Naka, *Inorg. Chem.* **2022**, *61*, 7318–7326. c) T. Matsumoto, H. Takamine, K. Tanaka, Y. Chujo, *Chem. Lett.* **2015**, *44*, 1658–1660; d) T. Matsumoto, K. Tanaka, K. Tanaka, Y. Chujo, *Dalton Trans.* **2015**, *44*, 8697–8707; e) S. Ito, A. Hirose, M. Yamaguchi, K. Tanaka, Y. Chujo, **2017**, *9*, 68; f) M. Planells, B. C. Schroeder, I. McCulloch, *Macromolecules* **2014**, *47*, 5889–5894; g) Y. Matsumura, K. Fukuda, S. Inagi, I. Tomita, *Macromol. Rapid Commun.* **2015**, *36*, 660–664; h) M. Detty, P. Prasad, D. Donnelly, T. Ohulchanskyy, S. Gibson, R. Hilf, *Bioorg. Med. Chem.* **2004**, *12*, 2537–2544; i) B. Calitree, D. J. Donnelly, J. J. Holt, M. K. Gannon, C. L. Nygren, D. K. Sukumaran, J. Autschbach, M. R. Detty, *Organometallics* **2007**, *26*, 6248–6257; j) G. Qian, B. Dai, M. Luo, D. Yu, J. Zhan, Z. Zhang, D. Ma, Z. Y. Wang, *Chem. Mater.* **2008**, *20*, 6208–6216; h) R. Yoshii, H. Yamane, A. Nagai, K. Tanaka, H. Taka, H. Kita, Y. Chujo, *Macromolecules* **2014**, *47*, 2316–2323; i) M.-S. Su, C.-Y. Kuo, M.-C. Yuan, U.-S. Jeng, C.-J. Su, K.-H. Wei, *Adv. Mater.* **2011**, *23*, 3315–3319; j) S. Otep, Y.-C. Lin, H. Matsumoto, T. Mori, K.-H. Wei, T. Michinobu, *Org. Electron.* **2020**, *87*, 105986; k) J.-M. Jiang, P. Raghunath, H.-K. Lin, Y.-C. Lin, M. C. Lin, K.-H. Wei, *Macromolecules* **2014**, *47*, 7070–7080.

[4] a) K. Tanaka, Y. Chujo, *Chem. Lett.* **2021**, *50*, 269–279; b) H. Watanabe, K. Tanaka, Y. Chujo, *Asian J. Org. Chem.* **2022**, *11*, e202200221.

[5] E. Merino, *Chem. Soc. Rev.* **2011**, *40*, 3835–3853.

[6] a) C.-L. Liu, F.-C. Tsai, C.-C. Chang, K.-H. Hsieh, J.-L. Lin, W.-C. Chen, *Polymer* **2005**, *46*, 4950–4957; b) Y. Wang, J. Ma, Y. Jiang, *J. Phys. Chem. A* **2005**, *109*, 7197–7206.

[7] a) A. J. Blayney, I. F. Perepichka, F. Wudl, D. F. Perepichka, *Isr. J. Chem.* **2014**, *54*, 674–688; b) N. C. Greenham, S. C. Moratti, D. D. C. Bradley, R. H. Friend, A. B. Holmes, *Nature* **1993**, *365*, 628–630.

[8] a) A. Cembran, F. Bernardi, M. Garavelli, L. Gagliardi, G. Orlandi, *J. Am. Chem. Soc.* **2004**, *126*, 3234–3243; b) T. Fujino, S. Y. Arzhantsev, T. Tahara, *J. Phys. Chem. A* **2001**, *105*, 8123–8129; c) H. M. D. Bandara, S. C. Burdette, *Chem. Soc. Rev.* **2012**, *41*, 1809–1825; d) H. Rau, *Angew. Chem. Int. Ed. Engl.* **1973**, *12*, 224–235; *Angew. Chem.* **1973**, *85*, 248–258.

[9] a) J. Yoshino, N. Kano, T. Kawashima, *Chem. Commun.* **2007**, 559–561; b) J. Yoshino, A. Furuta, T. Kambe, H. Itoi, N. Kano, T. Kawashima, Y. Ito, M. Asashima, *Chem. Eur. J.* **2010**, *16*, 5026–5035; c) N. Kano, A. Furuta, T. Kambe, J. Yoshino, Y. Shibata, T. Kawashima, N. Mizorogi, S.

Nagase, *Eur. J. Inorg. Chem.* **2012**, 1584–1587; c) J. Yoshino, N. Kano, T. Kawashima, *Dalton Trans.* **2013**, *42*, 15826–15834.

[10] a) H. Bisle, H. Rau, *Chem. Phys. Lett.* **1975**, *31*, 264–266; b) M. Ghedini, D. Pucci, G. Calogero, F. Barigelletti, *Chem. Phys. Lett.* **1997**, *267*, 341–344; c) A.-Y. Jee, Y. Lee, M. Lee, M. H. Kim, *J. Chem. Phys.* **2012**, *136*, 121104; f) M. Han, S. J. Cho, Y. Norikane, M. Shimizu, A. Kimura, T. Tamagawa, T. Seki, *Chem. Commun.* **2014**, *50*, 15815–15818; e) M. Yamauchi, K. Yokoyama, N. Aratani, H. Yamada, S. Masuo, *Angew. Chem. Int. Ed.* **2019**, *58*, 14173–14178; *Angew. Chem.* **2019**, *131*, 14311–14316; f) Q. Zhu, S. Wang, P. Chen, *Org. Lett.* **2019**, *21*, 4025–4029.

[11] a) J. Mei, N. L. C. Leung, R. T. K. Kwok, J. W. Y. Lam, B. Z. Tang, *Chem. Rev.* **2015**, *115*, 11718–11940; b) J. Luo, Z. Xie, J. W. Y. Lam, L. Cheng, H. Chen, C. Qiu, H. S. Kwok, X. Zhan, Y. Liu, D. Zhu, B. Z. Tang, *Chem. Commun.* **2001**, 1740–1741.

[12] a) M. Gon, K. Tanaka, Y. Chujo, *Angew. Chem. Int. Ed.* **2018**, *57*, 6546–6551; *Angew. Chem.* **2018**, *130*, 6656–6661; b) Gon, M.; Tanaka, K.; Chujo, Y. *Chem. Rec.* **2021**, *21*, 1358–1373.

[13] a) M. Gon, J. Wakabayashi, K. Tanaka, Y. Chujo, *Chem. Asian J.* **2019**, *14*, 1837–1843; b) M. Gon, J. Wakabayashi, M. Nakamura, K. Tanaka, Y. Chujo, *Chem. Asian J.* **2021**, *16*, 696–703; c) M. Gon, J. Wakabayashi, M. Nakamura, K. Tanaka, Y. Chujo, *Macromol. Rapid Commun.* **2021**, *42*, 2000566; d) M. Nakamura, M. Gon, S. Natsuda, Y. Tamai, H. Ohkita, K. Tanaka, Y. Chujo, *Dalton Trans.* **2022**, *51*, 74–84.

[14] J. Wakabayashi, M. Gon, K. Tanaka, Y. Chujo, *Macromolecules* **2020**, *53*, 4524–4532.

[15] a) Y. Dong, J. W. Y. Lam, A. Qin, Z. Li, J. Sun, H. H.-Y. Sung, I. D. Williams, B. Z. Tang, *Chem. Commun.* **2007**, 40–42; b) S. Ohtani, M. Gon, K. Tanaka, Y. Chujo, *Chem. Eur. J.* **2017**, *23*, 11827–11833; c) S. Ohtani, Y. Takeda, M. Gon, K. Tanaka, Y. Chujo, *Chem. Commun.* **2020**, *56*, 15305–15308; d) S. Ohtani, M. Gon, K. Tanaka, Y. Chujo, *Crystals* **2020**, *10*, 615.

[16] a) S. Ohtani, M. Gon, K. Tanaka, Y. Chujo, *Macromolecules* **2019**, *52*, 3387–3393; b) S. Ohtani, N. Yamada, M. Gon, K. Tanaka, Y. Chujo, *Polym. Chem.* **2021**, *12*, 2752–2759; d) S. Ohtani, M. Nakamura, M. Gon, K. Tanaka, Y. Chujo, *Chem. Commun.* **2020**, *56*, 6575–6578.

[17] M. Gon, K. Tanaka, Y. Chujo, *Chem. Eur. J.* **2021**, *27*, 7561–7571.

[18] M. Gon, K. Tanimura, M. Yaegashi, K. Tanaka, Y. Chujo, *Polym. J.* **2021**, *53*, 1241–1249.

[19] S. Yamaguchi, Y. Itami, K. Tamao, *Organometallics* **1998**, *17*, 4910–4916.

[20] a) S. M. Parke, M. P. Boone, E. Rivard, *Chem. Commun.* **2016**, *52*, 9485–9505; b) M. Shimizu, D. Ryuse, T. Kinoshita, *Chem. Eur. J.* **2017**, *23*, 14623–14630; c) B. L. Lucht, M. A. Buretea, T. D. Tilley, *Organometallics* **2000**, *19*, 3469–3475; d) Y. H. Park, Yongmin Kim, Honglae Sohn, *J. Korean Phys. Soc.* **2011**, *59*, 2318–2323; e) G. L. Gibson, D. Gao, A. A. Jahnke, J. Sun, A. J. Tilley, D. S. Seferos, *J. Mater. Chem. A* **2014**, *2*, 14468–14480; f) R. Stalder, S. R. Puniredd, M. R. Hansen, U. Koldemir, C. Grand, W. Zajaczkowski, K. Müllen, W. Pisula, J. R. Reynolds, *Chem. Mater.* **2016**, *28*, 1286-1297; g) K. Murakami, Y. Ooyama, H. Higashimura, J. Ohshita, *Organometallics* **2016**, *35*, 20–26; h) F.-B. Zhang, Y. Adachi, Y. Ooyama, J. Ohshita, *Organometallics* **2016**, *35*, 2327–2332; i) F.-B. Zhang, Y. Ooyama, J. Ohshita, *ChemistrySelect* **2017**, *2*, 3106–3109; j) Y. Adachi, Y. Ooyama, N. Shibayama, J. Ohshita, *Chem. Lett.* **2016**, *46*, 310–312; k) Y. Adachi, T. Nomura, J. Ohshita, *Chem. Eur. J.* **2019**, *25*, 4974–4983; l) W. Sun, Y. Adachi, J. Ohshita, *Dyes Pigm.* **2022**, *203*, 110333; m) H. Tanimoto, T. Nagao, Y. Nishiyama, T. Morimoto, F. Iseda, Y. Nagato, T. Suzuka, K. Tsutsumi, K. Kakiuchi, *Dalton Trans.* **2014**, *43*, 8338–8343; n) H. Arii, Y. Iwanami, D. Nakane, H. Masuda, J. Matsumoto, T. Shiragami, K. Mochida, T. Kawashima, *Organometallics* **2021**, *40*, 1363–1370; o) F.

Zheng, A. Tanudjaja, Z. Gao, S. Inagi, I. Tomita, *Polymer* **2020**, *204*, 122809; p) R. Suzuki, R. Tada, Y. Miura, N. Yoshioka, *J. Mol. Struct.* **2016**, *1106*, 399–406.

[21] a) M. Yamamura, M. Albrecht, M. Albrecht, Y. Nishimura, T. Arai, T. Nabeshima, *Inorg. Chem.* **2014**, *53*, 1355–1360; b) R. R. Maar, S. D. Catingan, V. N. Staroverov, J. B. Gilroy, *Angew. Chem. Int. Ed.* **2018**, *57*, 9870–9874; *Angew. Chem.* **2018**, *130*, 10018–10022; c) A. S. Gowda, T. S. Lee, M. C. Rosko, J. L. Petersen, F. N. Castellano, C. Milsmann, *Inorg. Chem.* **2022**, *61*, 7338–7348.

[22] E. Clementi, D. L. Raimondi, W. P. Reinhardt, *J. Chem. Phys.* **1967**, *47*, 1300–1307.

[23] a) Y. Chujo, K. Tanaka, *Bull. Chem. Soc. Jpn.* **2015**, *88*, 633–643; b) M. Gon, K. Tanaka, Y. Chujo, *Polym. J.* **2018**, *50*, 109–126; c) K. Tanaka, Y. Chujo, *Polym. J.* **2020**, *52*, 555–566.

[24] a) M. Kosugi, K. Sasazawa, Y. Shimizu, T. Migita, *Chem. Lett.* **1977**, *6*, 301–302; b) D. Milstein, J. K. Stille, *J. Am. Chem. Soc.* **1978**, *100*, 3636–3638.

[25] K. E. Bessler, J. A. dos Santos, V. M. Deflon, S. de Souza Lemos, E. Niquet, *Z. anorg. allg. Chem.* **2004**, *630*, 742–745.

[26] a) U. Böhme, S. Jähnigen, *Acta Cryst.* **2008**, *C64*, o364–o366; b) A. S. Soldatenko, I. V. Sterkhova, N. F. Lazareva, *J. Organomet. Chem.* **2019**, *903*, 120997.

[27] A. A. Diamantis, J. M. Gulbis, M. Manikas, E. R. T. Tiekink, *Phosphorus Sulfur Silicon Relat. Elem.* **1999**, *150*, 251–259.

[28] J. Harada, K. Ogawa, S. Tomoda, *Acta Cryst.* **1997**, *B53*, 662–672.

[29] N. Nagashima, S. Ozawa, M. Furuta, M. Oi, Y. Hori, T. Tomita, Y. Sohma, M. Kanai, *Sci. Adv.* **2021**, *7*, eabc9750.

[30] J. Harada, K. Ogawa, *Chem. Soc. Rev.* **2009**, *38*, 2244–2252.

[31] a) R. Englman, J. Jortner, *Mol. Phys.* **1970**, *18*, 145–164; b) V. Chynwat, H. A. Frank, *Chem. Phys.* **1995**, *194*, 237–244; c) L. Biczók, T. Bérces, H. Inoue, *J. Phys. Chem. A* **1999**, *103*, 3837–3842.

Entry for the Table of Contents
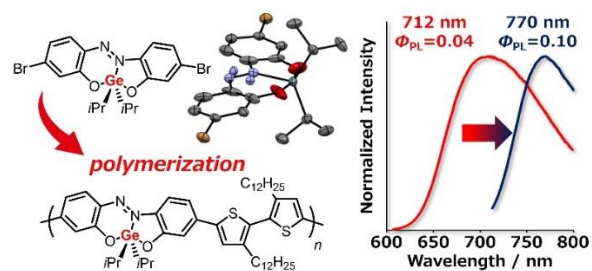
Ge-fused azobenzene compounds: Hypervalent compounds with a germanium(Ge)-fused azobenzene (GAz) scaffold exhibiting NIR emission despite the compact π-conjugated systems. Synergistic effect between a hypervalent bond and extension of π-conjugation is a novel and effective strategy for obtaining NIR emissive materials.

Supporting Information

Near-infrared Emissive Hypervalent Compounds with Germanium(IV)-Fused Azobenzene π-Conjugated Systems

Masayuki Gon, Misao Yaegashi, Kazuo Tanaka* and Yoshiki Chujo

Department of Polymer Chemistry, Graduate School of Engineering, Kyoto University Katsura, Nishikyo-ku, Kyoto 615-8510, Japan

E-mail: tanaka@poly.synchem.kyoto-u.ac.jp

Key words: germanium; azobenzene; hypervalent bond; trigonal bipyramidal geometry; near-infrared emission

Contents   page

General

^{1}H and ^{13}C NMR spectra were recorded on JEOL EX400, ECS400, ECZ400 and AL400 instruments at 400 and 100 MHz, respectively. High-resolution ^{13}C NMR spectra were recorded on ECZ500R and ECZ600R instruments at 125 and 150 MHz, respectively. Samples were analyzed in CDCl$_3$. The chemical shift values were expressed relative to Me$_4$Si for ^{1}H and ^{13}C NMR as an internal standard in CDCl$_3$. Analytical thin layer chromatography (TLC) was performed with silica gel 60 Merck F254 plates. Column chromatography was performed with Wakogel$^®$ C-300 silica gel. High-resolution mass (HRMS) spectrometry was performed at the Technical Support Office (Department of Synthetic Chemistry and Biological Chemistry, Graduate School of Engineering, Kyoto University), and the HRMS spectra were obtained on a Thermo Fisher Scientific EXACTIVE spectrometer for electrospray ionization (ESI), a Thermo Fisher Scientific EXACTIVE spectrometer for atmospheric pressure chemical ionization (APCI) and a Bruker Daltonics ultrafleXtreme for matrix assisted laser desorption ionization (MALDI). UV–vis spectra were recorded on a SHIMADZU UV-3600 spectrophotometer, and samples were analyzed at room temperature. HORIBA JOBIN YVON Fluorolog-3 and Oxford Optistat DN2 were used for PL spectra. Absolute photoluminescence quantum efficiency (Φ_{PL}) was recorded on a Hamamatsu Photonics Quantaurus-QY Plus C13534-01. Cyclic voltammetry (CV) was conducted on a BASALS-Electrochemical-Analyzer Model 600D with a grassy carbon working electrode, a Pt counter electrode, an Ag/AgCl reference electrode, and the ferrocene/ferrocenium (Fc/Fc$^+$) external reference at a scan rate of 0.1 V s^{-1}. The PL lifetime measurement was performed on a Horiba FluoreCube spectrofluorometer system; excitation was conducted using visible diode lasers (NanoLED 532 nm). Elemental analyses were performed at the Microanalytical Center of Kyoto University. X-ray crystallographic analysis was conducted by Rigaku R-AXIS RAPID-F graphite-monochromated MoKα radiation diffractometer with imaging plate or Rigaku Saturn 724+ with MicroMax-007HF CCD diffractometer with Varimax Mo optics using graphite-monochromated MoKα radiation. A symmetry-related absorption correction was conducted by using the program ABSCOR.[1] The analysis was carried out with Yadokari-XG.[2] The program ORTEP3[3] and Mercury-4.2.0 were used to generate the X-ray structural diagram. TGA was performed on an EXSTAR STA7200RV, a Hitachi High-Tech Science Corporation., with the heating rate of 10 °C/min up to 550 °C under nitrogen flowing (200 mL/min). Residual water was removed by keeping on the aluminum pan at 110 °C for 20 min. before the curve profiling. The decomposition temperatures (T_d) were

determined from the onset of the weight loss.

Materials

Commercially available compounds used without purification:

4-Chloro-2-methoxyaniline (**NH2-Cl**) (Combi-Blocks, Inc.)

Manganese(IV) Oxide, Powder (MnO_2) (FUJIFILM Wako Pure Chemical Corporation)

Boron tribromide (17% in CH_2Cl_2, ca. 1 M) (BBr_3 in CH_2Cl_2) (Tokyo Chemical Industry Co, Ltd.)

o-Anisidine (**NH2-H**) (Tokyo Chemical Industry Co, Ltd.)

Calcium carbonate ($CaCO_3$) (Nacalai Tesque, Inc.)

$Pd_2(dba)_3$ (dba = dibenzylideneacetone) (Tokyo Chemical Industry Co, Ltd.)

2-Dicyclohexylphosphino-2′,4′,6′-triisopropylbiphenyl (XPhos) (Strem Chemicals, Inc.)

Commercially available solvents:

MeOH, toluene, $CHCl_3$, CH_2Cl_2, acetone, hexane, ethyl acetate and acetonitrile were purchased from FUJIFILM Wako Pure Chemical Corporation and used without purification.

THF (FUJIFILM Wako Pure Chemical Corporation) and Et_3N (Kanto Chemical Co., Inc.) were purified by passage through solvent purification columns under N_2 pressure.[4]

Compounds prepared as described in the literatures:

Diisopropyldichlorogermane (*i*Pr_2GeCl_2)[5]

4,4′-Difluoro-2,2′-dihydroxyazobenzene (**AzOH-F**)[6]

4,4′-Dibromo-2,2′-dihydroxyazobenzene (**AzOH-Br**)[7]

Benzyltriethylammonium dichloroiodate[8]

5,5′-Bis(trimethylstannyl)-3,3′-didodecyl-2,2′-bithiophene (**BT**)[9]

Synthetic procedures and characterization

Synthesis of GAz-F
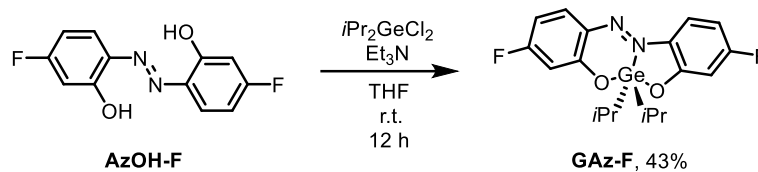
AzOH-F (50.0 mg, 0.200 mmol) in Et$_2$O (20 mL) was added to the solution of diisopropyldichlorogermane (84.3 μL, 0.360 mmol) and Et$_3$N (0.726 g cm^{-3}, 0.111 mL, 0.799 mmol) in Et$_2$O (5 mL) under Ar. The reaction mixture was stirred at room temperature for 12 h, and then filtered to remove precipitated salts. The product was purified by recrystallization from hexane to afford **GAz-F** (34.9 mg, 0.0857 mmol, 43%) as a black solid.

^{1}H NMR (CDCl$_3$, 400 MHz) δ 7.65–7.55 (br, 1H), 7.50–7.40 (br, 1H), 6.60–6.35 (br, 4H), 1.91–1.80 (m, 2H), 1.19 (d, J = 7.4 Hz, 12H) ppm. ^{13}C{^{1}H} NMR (CDCl$_3$, 125 MHz) δ 168.9 (J_{C-F} = 260.2 Hz), 167.3 (J_{C-F} = 250.2 Hz), 163.9 (J_{C-F} = 12.6 Hz), 163.7 (J_{C-F} = 15.8 Hz), 136.4 (J_{C-F} = 12.6 Hz), 134.0, 132.7, 118.3 (J_{C-F} = 12.7 Hz), 108.2 (J_{C-F} = 24.2 Hz), 107.5 (J_{C-F} = 21.2 Hz), 106.0 (J_{C-F} = 25.3 Hz), 103.7 (J_{C-F} = 23.2 Hz), 28.5, 18.5 (J_{C-Ge} = 35.8 Hz) ppm. HRMS (ESI) calcd. for C$_{18}$H$_{21}$F$_2$GeN$_2$O$_2$ [M+H]$^+$: 409.0777, found: 409.0780. Elemental analysis calcd. for C$_{18}$H$_{20}$F$_2$GeN$_2$O$_2$: C 53.12 H 4.95 N 6.88, found: C 53.13 H 5.04 N 6.63.
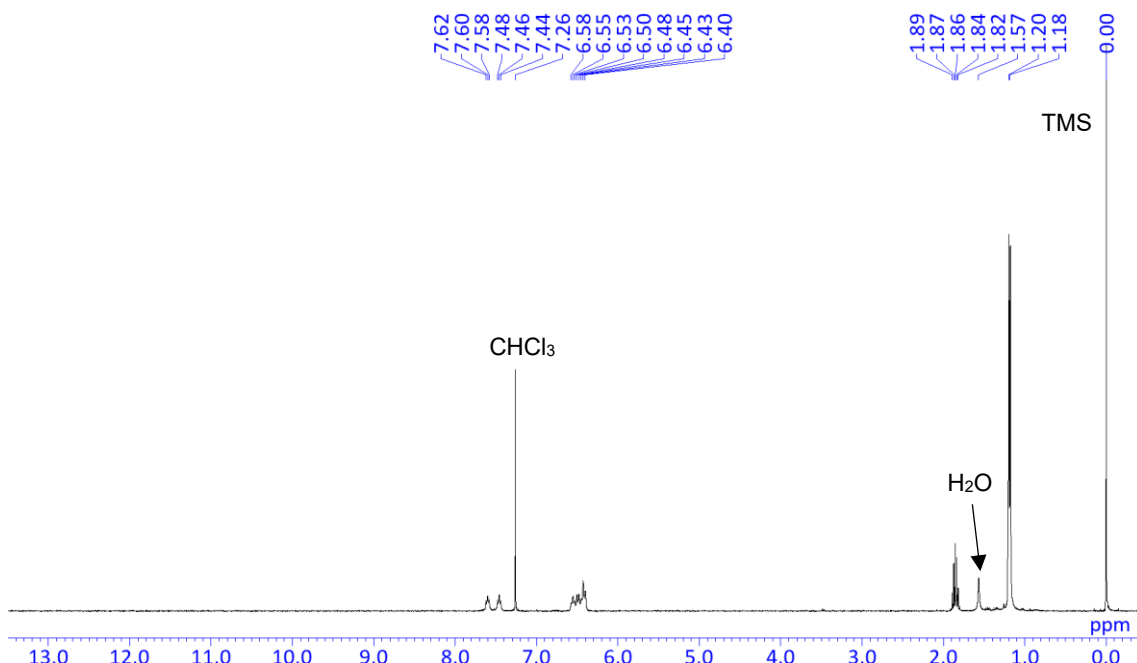
Chart S1. ^{1}H NMR spectrum of **GAz-F** in CDCl$_3$ at 400 MHz.
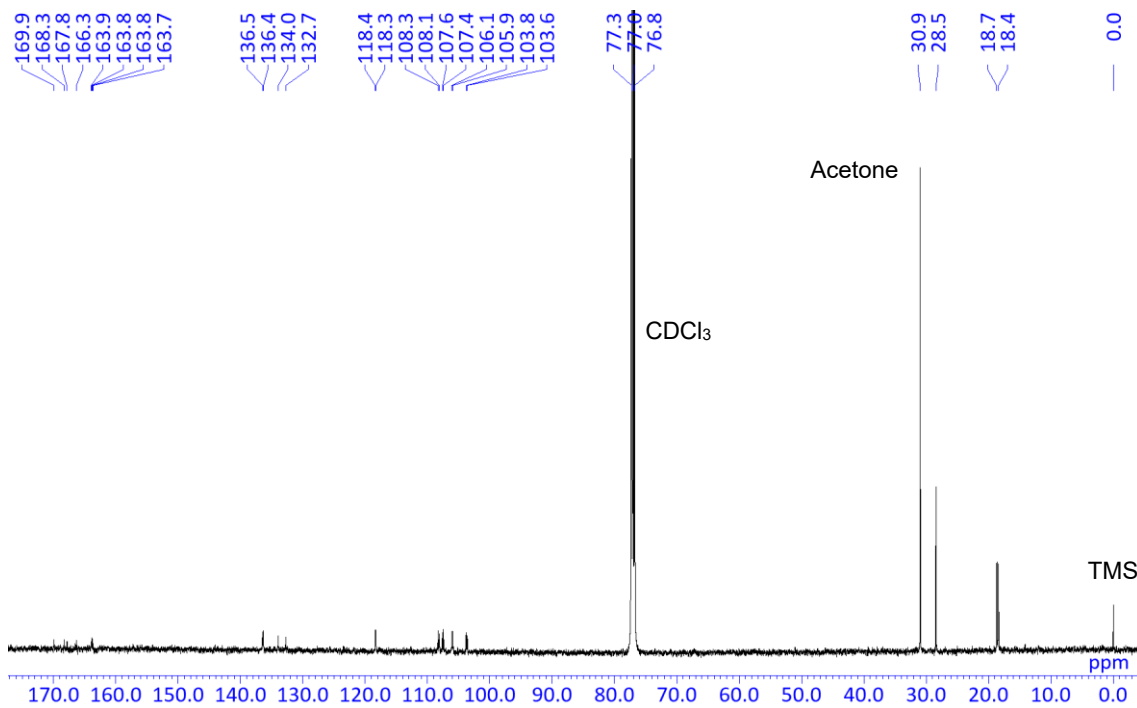
Chart S2. ^{13}C{^{1}H} NMR spectrum of **GAz-F** in CDCl$_3$ at 125 MHz.

Synthesis of 4,4′-dichloro-2,2′-dimethoxyazobenzene (AzOMe-Cl)
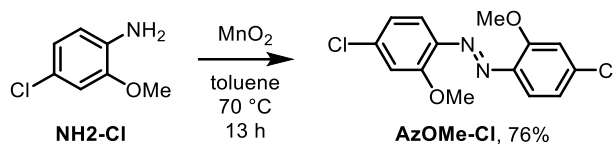
A mixture of 4-chloro-2-methoxyaniline (**NH2-Cl**) (4.00 g, 25.4 mmol), MnO$_2$ (8.83 g, 102 mmol) and toluene (100 mL) was placed in a round-bottom flask equipped with a magnetic stirring bar. The mixture was reacted at 70 °C for 13 h. After the reaction, MnO$_2$ was removed by filtration through celite and silica and washed with CHCl$_3$. The residue was purified by recrystallization with MeOH (poor solvent) and CHCl$_3$ (good solvent) to afford **AzOMe-Cl** (3.00 g, 9.64 mmol, 76%) as a brown solid.

^{1}H NMR (CDCl$_3$, 400 MHz) δ 7.59 (d, J = 8.6 Hz, 2H), 7.06 (d, J = 2.0 Hz, 2H), 6.98 (dd, J = 8.6, 2.1 Hz, 2H), 4.01 (s, 6H) ppm. ^{13}C{^{1}H} NMR (CDCl$_3$, 100 MHz) δ 157.3, 141.3, 138.1, 121.1, 118.4, 113.3, 56.6 ppm. HRMS (APCI) calcd. for C$_{14}$H$_{13}$Cl$_2$N$_2$O$_2$ [M+H]$^+$: 311.0349, found: 311.0347. Elemental analysis calcd. for C$_{14}$H$_{12}$Cl$_2$N$_2$O$_2$: C 54.04 H 3.89 N 9.00, found: C 54.20 H 3.80 N 9.14.
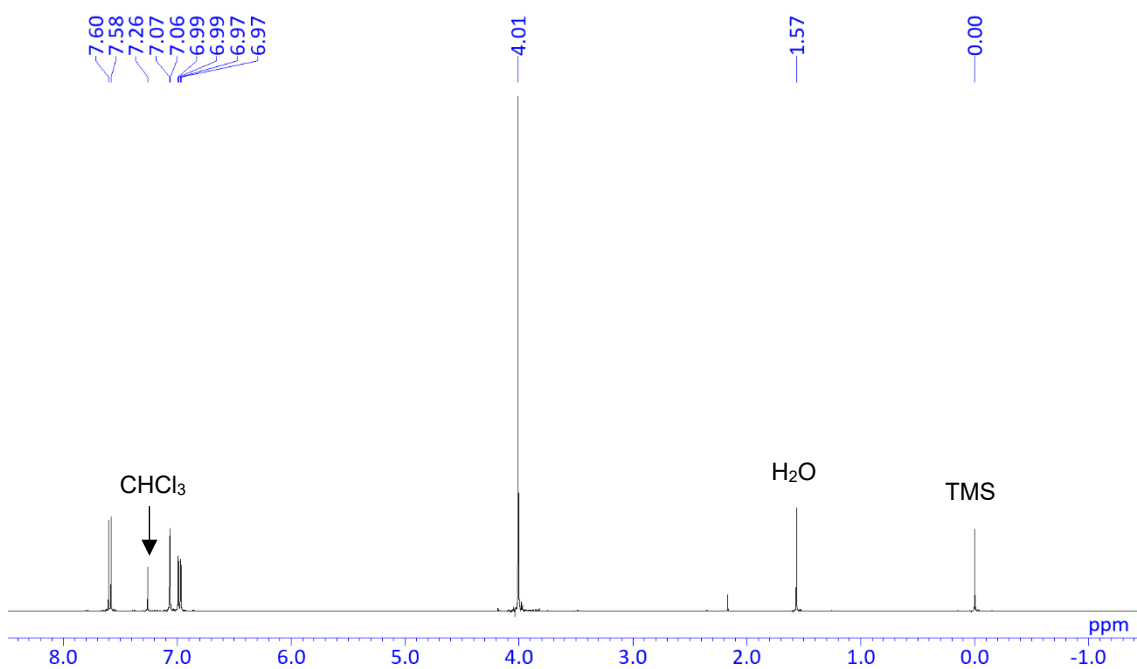
Chart S3. ^{1}H NMR spectrum of **AzOMe-Cl** in CDCl$_3$ at 400 MHz.
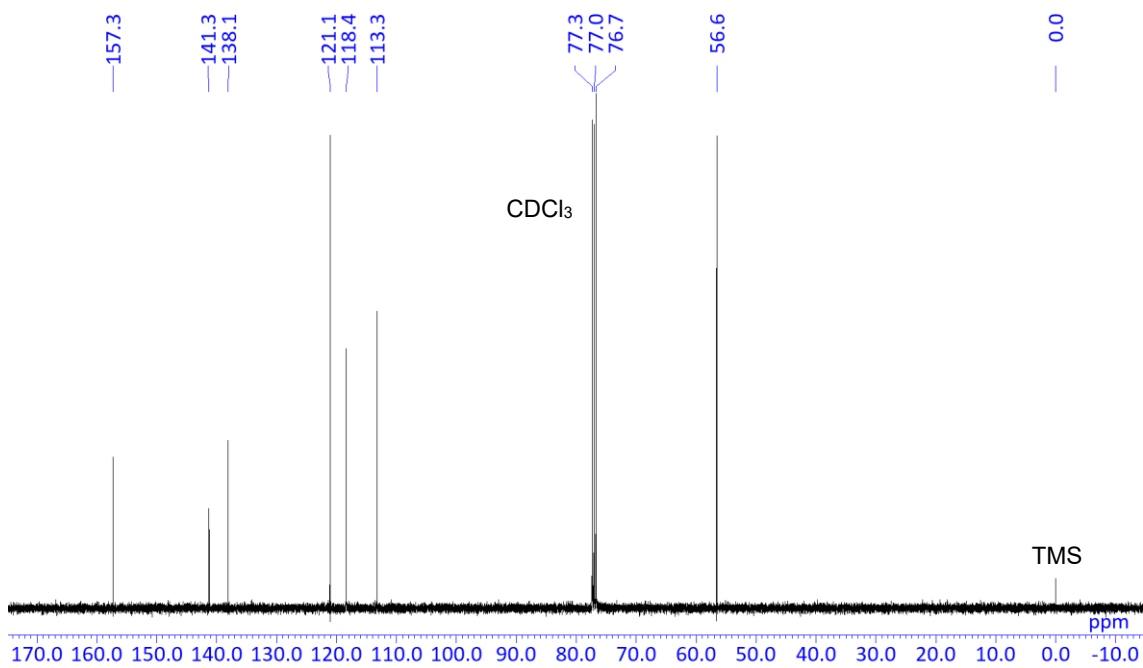
Chart S4. ^{13}C{^{1}H} NMR spectrum of **AzOMe-Cl** in CDCl$_3$ at 100 MHz.

Synthesis of 4,4′-dichloro-2,2′-dihydroxyazobenzene (AzOH-Cl)
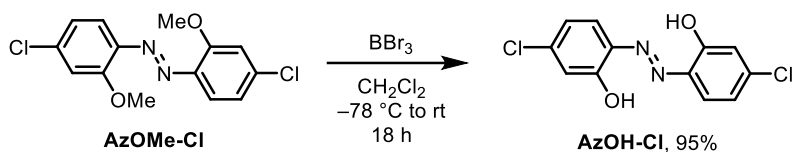
AzOMe-Cl (3.00 g, 9.64 mmol) was placed in a round-bottom flask equipped with a magnetic stirring bar. After degassing and filling Ar three times, CH_2Cl_2 (200 mL) was added to the flask. After cooling the mixture to −78 °C, BBr_3 (1 M in CH_2Cl_2, 24.1 mL, 24.1 mmol) was dropwisely added. The reaction was carried out at room temperature for 18 h. After the reaction, MeOH was carefully added at 0 °C for quenching the reaction. Then, the target compound was immediately precipitated as an orange solid. The solid was collected and washed with MeOH to afford **AzOH-Cl** (2.61 g, 9.18 mmol, 95%) as an orange solid.

^{1}H NMR (CDCl$_3$, 400 MHz) δ 12.25 (s, 2H), 7.63 (dd, J = 8.3, 0.5 Hz, 2H), 7.06 (dd, J = 2.2, 0.5 Hz, 2H), 7.05 (dd, J = 8.3, 2.1 Hz, 2H) ppm. ^{13}C{^{1}H} NMR (CDCl$_3$, 100 MHz) δ 153.6, 139.3, 133.7, 132.0, 121.1, 118.9 ppm. HRMS (ESI) calcd. for $C_{12}H_7Cl_2N_2O_2$ [M−H]$^-$: 280.9890, found: 280.9889. Elemental analysis calcd. for $C_{12}H_8Cl_2N_2O_2$: C 50.91 H 2.85 N 9.90, found: C 50.67 H 2.71 N 9.74.
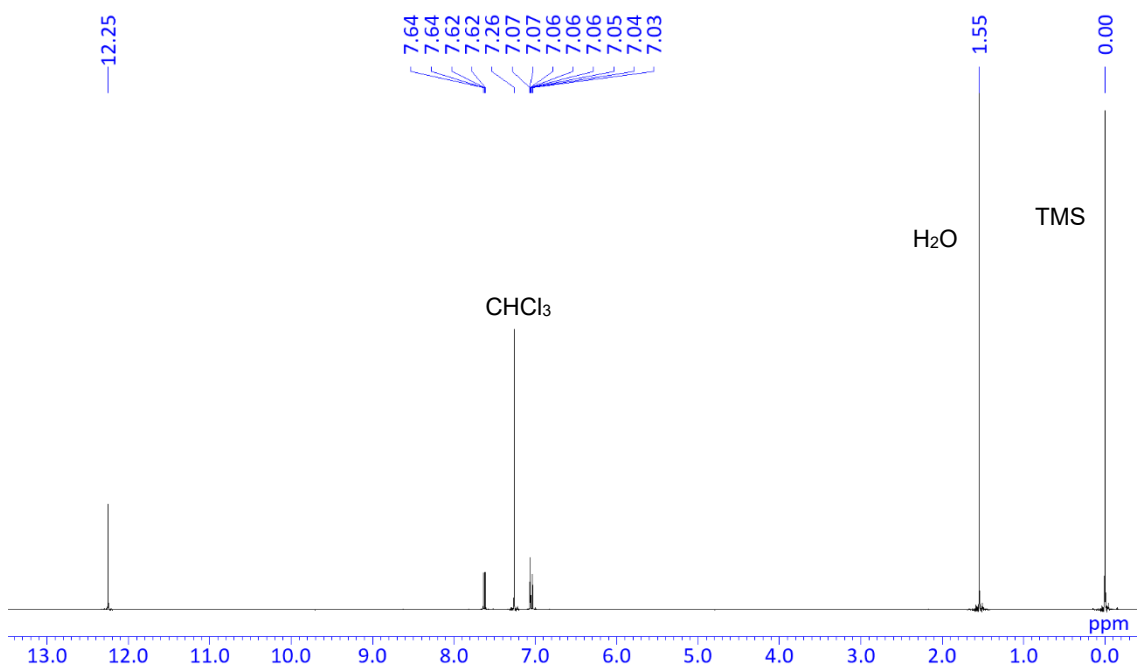
Chart S5. ^{1}H NMR spectrum of **AzOH-Cl** in CDCl$_3$ at 400 MHz.
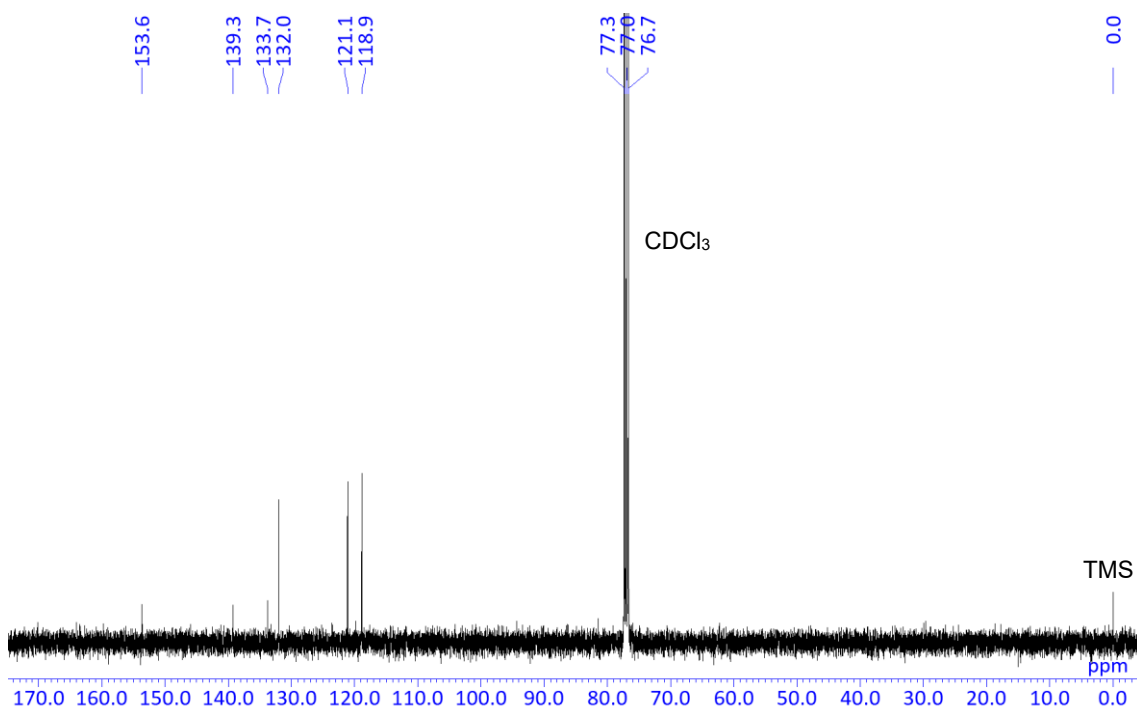
Chart S6. ^{13}C{^{1}H} NMR spectrum of **AzOH-Cl** in CDCl$_3$ at 100 MHz.

Synthesis of GAz-Cl
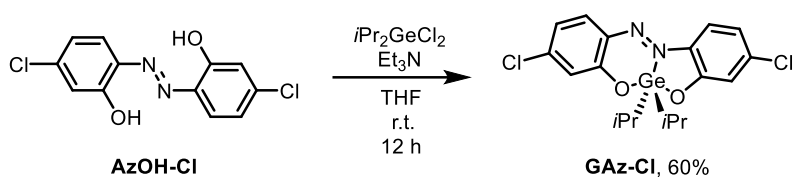
AzOH-Cl (50.0 mg, 0.177 mmol,) in Et$_2$O (10 mL) was added to the solution of diisopropyldichlorogermane (1.27 g cm^{-3}, 45.5 μL, 0.194 mmol) and Et$_3$N (0.726 g cm^{-3}, 49.2 μL, 0.353 mmol) in Et$_2$O (3 mL) under Ar. The reaction mixture was stirred at room temperature for 12 h, and then filtered to remove precipitated salts. The product was purified by recrystallization from hexane to afford **GAz-Cl** (46.6 mg, 0.106 mmol, 60%) as a black solid.

^{1}H NMR (CDCl$_3$, 400 MHz) δ 7.60–7.50 (br, 1H), 7.46–7.34 (br, 1H), 6.90–6.60 (br, 4H), 1.91–1.80 (m, 2H), 1.19 (d, J = 7.3 Hz, 12H) ppm. ^{13}C{^{1}H} NMR (CDCl$_3$, 125 MHz) δ 162.9, 161.8, 144.1, 140.3, 135.1, 134.9, 134.7, 122.1, 119.7, 118.5, 117.8, 117.6, 28.6, 18.5 ($J_{C–Ge}$ = 30.5 Hz) ppm. HRMS (ESI) calcd. for C$_{18}$H$_{21}$Cl$_2$GeN$_2$O$_2$ [M+H]$^+$: 441.0186, found: 441.0189. Elemental analysis calcd. for C$_{18}$H$_{20}$Cl$_2$GeN$_2$O$_2$: C 49.15 H 4.58 N 6.37, found: C 49.19 H 4.47 N 6.37.
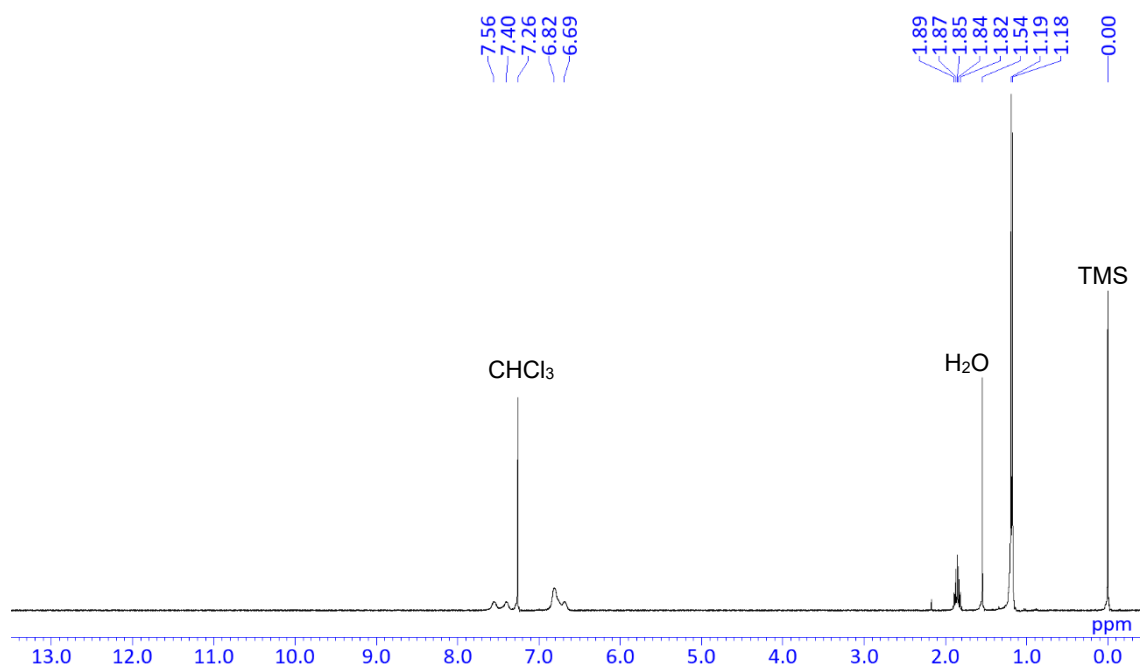
Chart S7. ^{1}H NMR spectrum of **GAz-Cl** in CDCl$_3$ at 400 MHz.
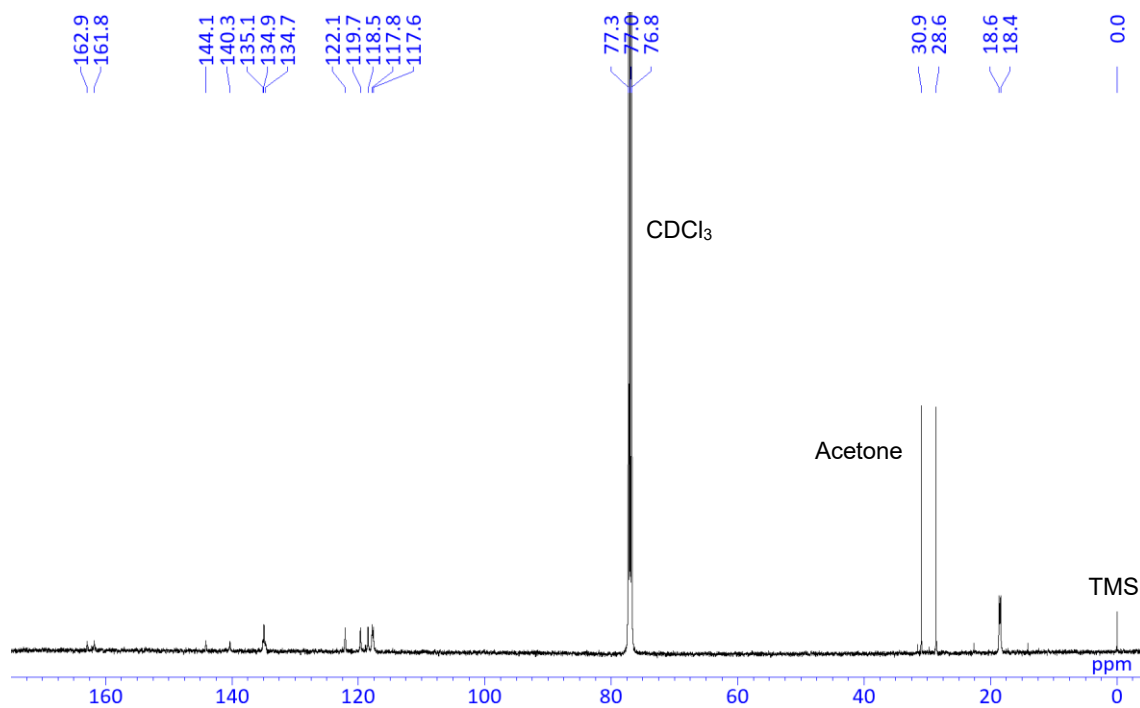
Chart S8. ^{13}C{^{1}H} NMR spectrum of **GAz-Cl** in CDCl$_3$ at 125 MHz.

Synthesis of GAz-Br
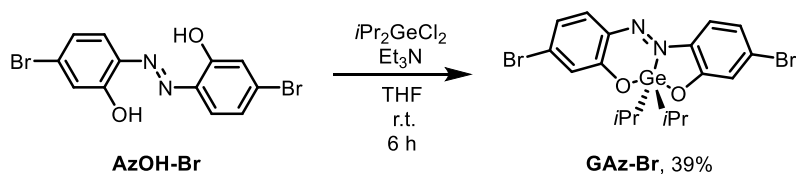
AzOH-Br (200 mg, 0.538 mmol) in THF (40 mL) was added to the solution of diisopropyldichlorogermane (1.27 g cm^{-3}, 0.226 mL, 0.968 mmol) and Et$_3$N (0.726 g cm^{-3}, 0.300 mL, 2.15 mmol) in THF (4 mL). The reaction mixture was stirred at ambient temperature for 6 h under argon atmosphere, and then filtered to remove salt. the product was purified by recrystallization from acetone to afford pure **GAz-Br** (110 mg, 0.208 mmol, 39%) as a black solid.

^{1}H NMR (CDCl$_3$, 400 MHz) δ 7.55–7.40 (br, 1H), 7.40–7.20 (br, 1H), 7.10–6.75 (br, 4H), 1.91–1.80 (m, 2H), 1.19 (d, J = 7.4 Hz, 12H) ppm. ^{13}C{^{1}H} NMR (CDCl$_3$, 150 MHz) δ 163.0, 161.6, 135.3, 135.1, 134.8, 133.4, 129.0, 125.4, 122.4, 121.3, 120.8, 118.0, 28.7, 18.5 (br) ppm. HRMS (ESI): calcd. for C$_{18}$H$_{21}$Br$_2$GeN$_2$O$_2$ [M+H]$^+$: 528.9165, found: 528.9178. Elemental analysis calcd. for C$_{18}$H$_{20}$Br$_2$GeN$_2$O$_2$: C 40.88 H 3.81 N 5.30, found: C 40.68 H 3.85 N 5.09.
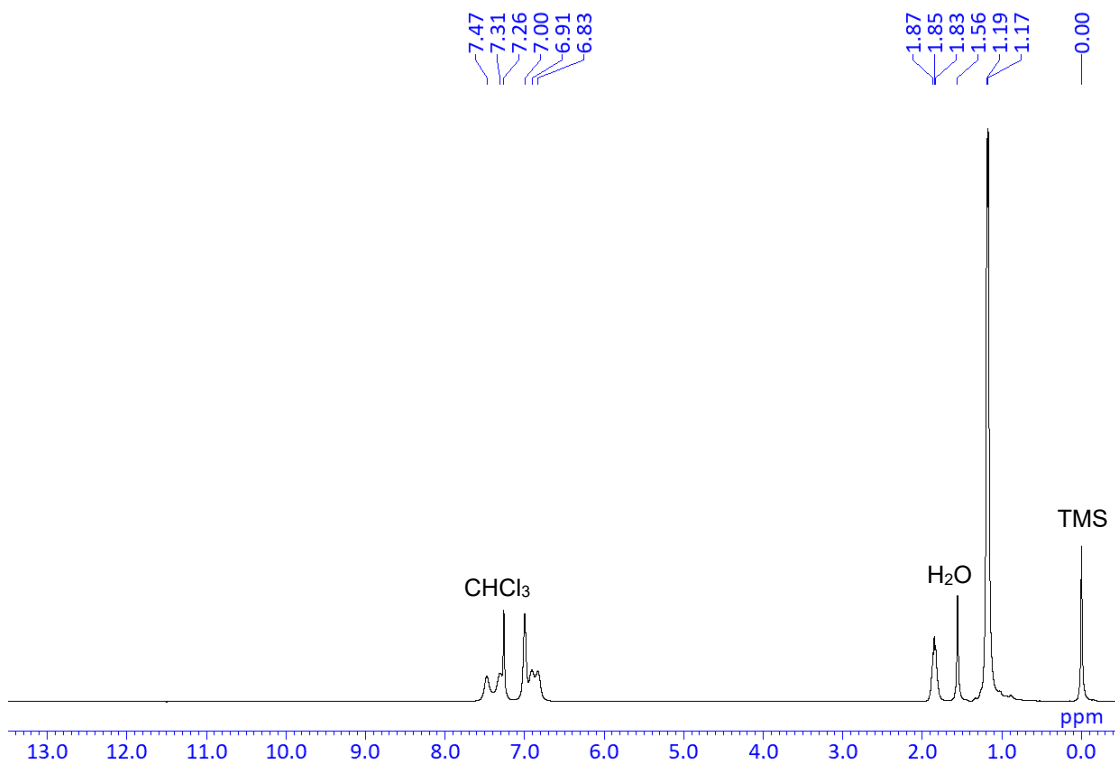
Chart S9. ^{1}H NMR spectrum of **GAz-Br** in CDCl$_3$ at 400 MHz.
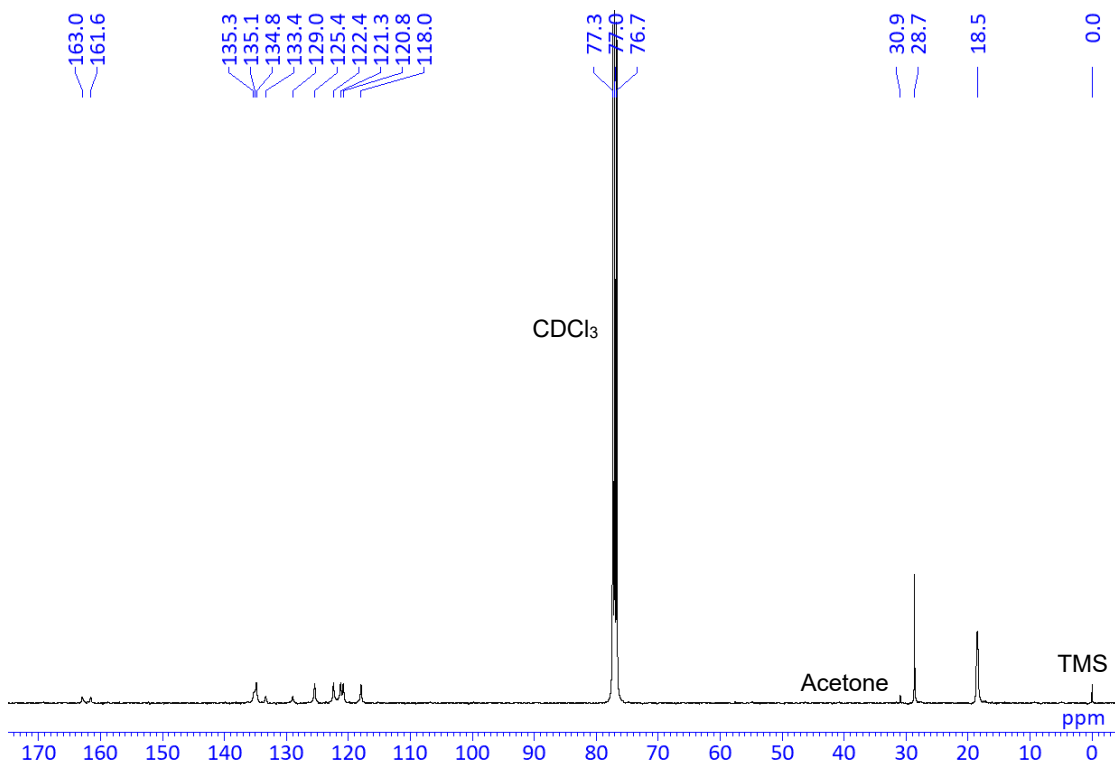
Chart S10. ^{13}C{^{1}H} NMR spectrum of **GAz-Br** in CDCl$_3$ at 150 MHz.

Synthesis of 4-iodo-2-methoxyaniline (NH2-I)
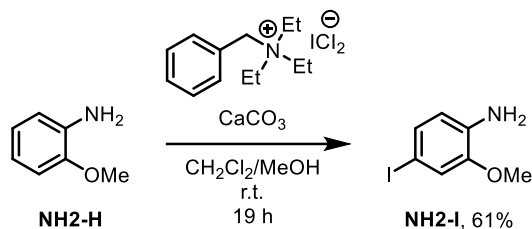
In a 1000 mL round bottom flask, o-anisidine (**NH2-H**) (6.50 g, 52.8 mmol) was dissolved in 500 mL CH$_2$Cl$_2$ and 200 mL methanol. CaCO$_3$ (10.6 g, 106 mmol) and then benzyltriethylammonium dichloroiodate (21.6 g, 55.4 mmol) was added. The reaction mixture was stirred at ambient temperature for 19 h. After filtering to remove CaCO$_3$, volatile materials were removed by evaporation under reduced pressure. The product was purified by silica gel column chromatography (eluted with hexane/ethyl acetate = 3/1 v/v, R_f = 0.51) to afford pure **NH2-I** (8.07 g, 32.4 mmol, 61%) as a brown solid.

^{1}H NMR (CDCl$_3$, 400 MHz) δ 7.07 (dd, J = 8.1, 1.7 Hz, 1H), 7.01 (d, J = 1.7 Hz, 1H), 6.46 (d, J = 8.1 Hz, 1H), 3.81 (s, 3H), 3.80 (s, 2H) ppm. ^{13}C{^{1}H} NMR (CDCl$_3$, 100 MHz) δ 148.0, 136.1, 129.9, 119.2, 116.3, 78.3, 55.6 ppm. HRMS (ESI): calcd. for C$_7$H$_9$INO [M+H]$^+$: 249.9723, found: 249.9724. Elemental analysis calcd. for C$_7$H$_8$INO: C 33.76 H 3.24 N 5.62, found: C 33.93 H 3.32 N 5.59.
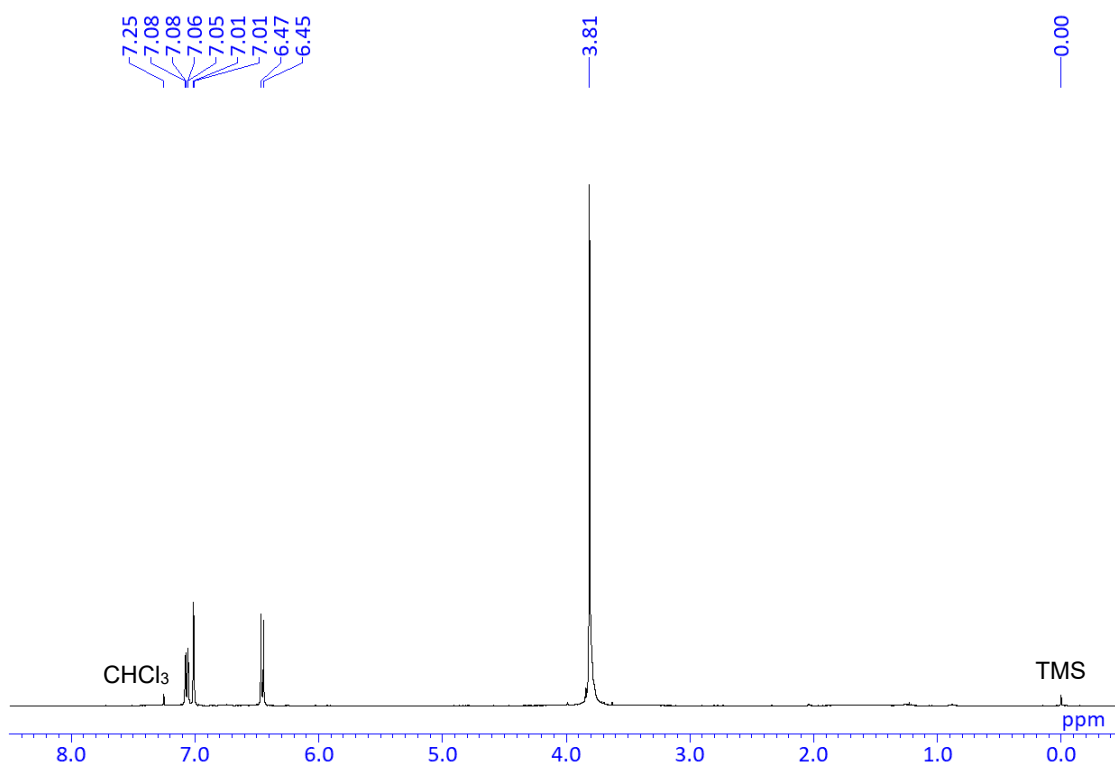
Chart S11. ^{1}H NMR spectrum of **NH2-I** in CDCl$_3$ at 400 MHz.
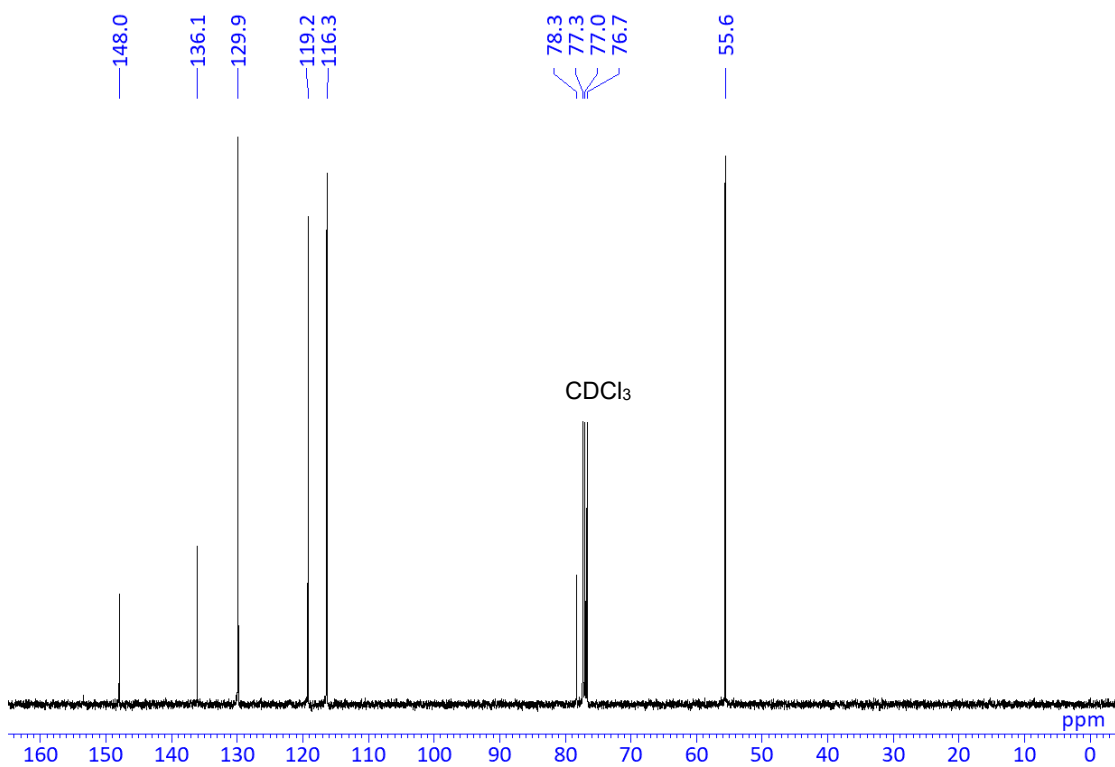
Chart S12. ^{13}C{^{1}H} NMR spectrum of **NH2-I** in CDCl$_3$ at 100 MHz.

Synthesis of 4,4′-iodo-2,2′-dimethoxyazobenzene (AzOMe-I)
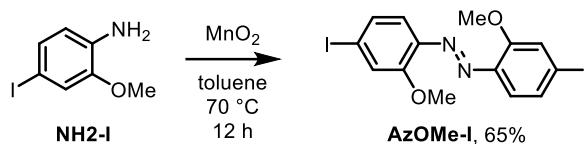
NH2-I (6.34 g, 25.5 mmol) and 100 mL toluene were added to 300 mL round bottom flask. After warming to 70 °C, MnO_2 (8.85 g, 102 mmol) was added and stirred for 12 h. Upon cooling to ambient temperature, the reaction mixture was filtered through celite and silica. Volatile materials were removed by evaporation under reduced pressure, the product was purified by recrystallization from mixed solvent of methanol/chloroform and washed with methanol to afford pure **AzOMe-I** (4.10 g, 8.30 mmol, 65%) as a brown solid.

^{1}H NMR (CDCl$_3$, 400 MHz) δ 7.40 (d, J = 1.4 Hz, 2H), 7.37–7.32 (m, 4H), 4.00 (s, 6H) ppm. ^{13}C{^{1}H} NMR (CDCl$_3$, 100 MHz) δ 157.1, 142.4, 130.3, 122.4, 118.7, 98.4, 56.7 ppm. HRMS (ESI): [M+Na]$^+$ calcd. for C$_{14}$H$_{12}$I$_2$N$_2$O$_2$Na [M+Na]$^+$: 516.8880, found: 516.8882. Elemental analysis calcd. for C$_{14}$H$_{12}$I$_2$N$_2$O$_2$: C 34.03 H 2.45 N 5.67, found: C 34.28 H 2.53 N 5.61.
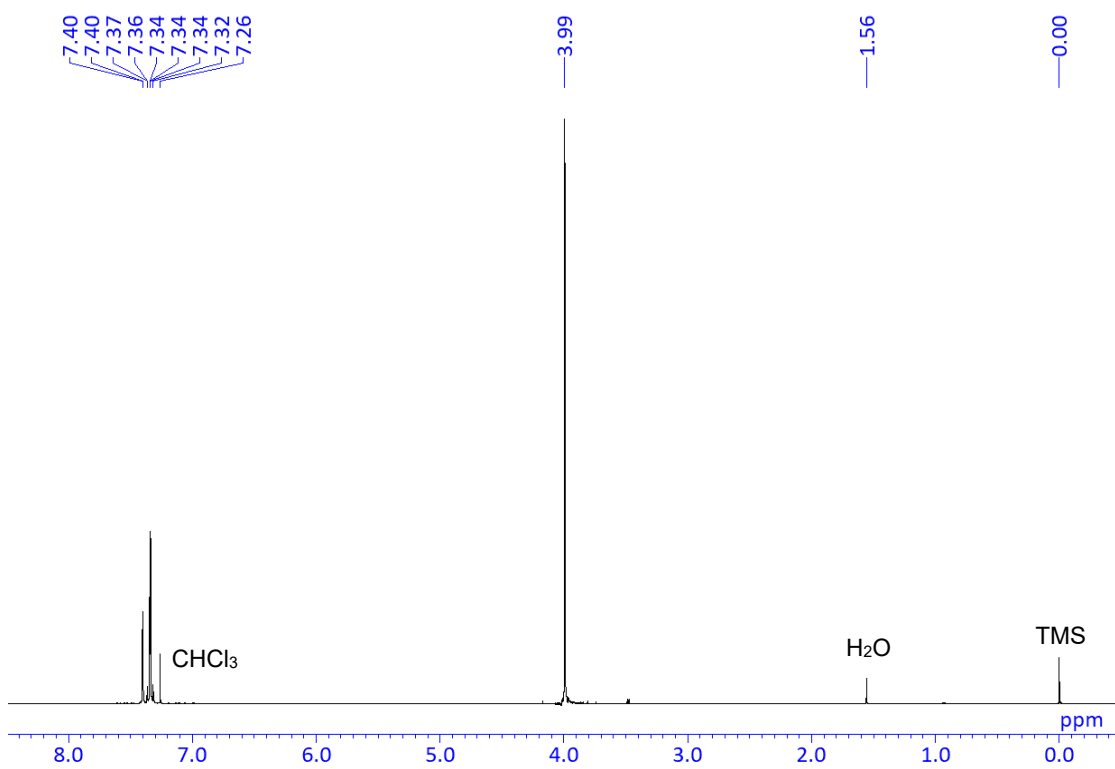
Chart S13. ^1H NMR spectrum of **AzOMe-I** in CDCl$_3$ at 400 MHz.
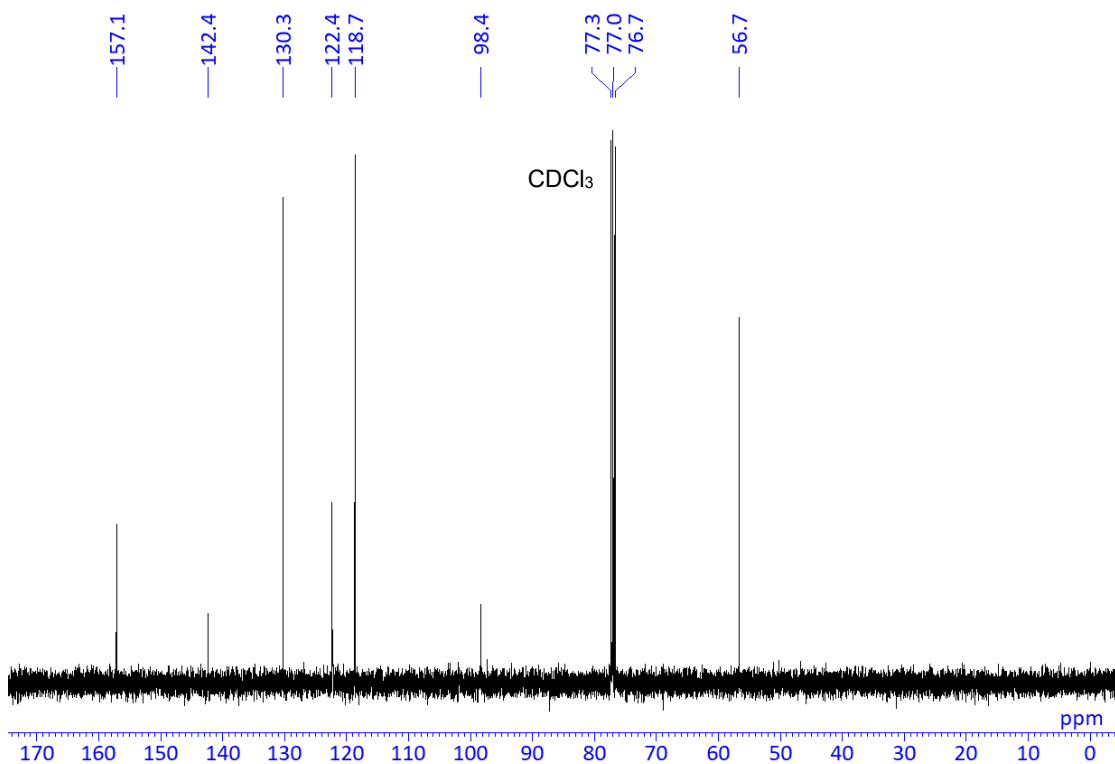
Chart S14. $^{13}C\{^1H\}$ NMR spectrum of **AzOMe-I** in CDCl$_3$ at 100 MHz.

S-18

Synthesis of 4,4′-iodo-2,2′-dihydroxyazobenzene (AzOH-I)
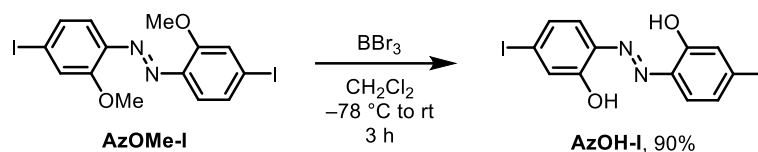
AzOMe-I (2.00 g, 4.05 mmol) and 90 mL CH_2Cl_2 were added to 200 mL round bottom two neck flask equipped with a rubber septum. After cooling to –78 °C, BBr_3 (1 M in CH_2Cl_2, 10.1 mL, 10.1 mmol) was added. The reaction mixture was stirred at ambient temperature for 3 h under argon atmosphere. The reaction was quenched by methanol, and volatile materials were removed by evaporation under reduced pressure, the product was purified by recrystallization from mixed solvent of methanol/chloroform and washed with methanol to afford pure **AzOH-I** (1.69 g, 3.63 mmol, 90%) as a yellow solid.

^{1}H NMR (CDCl$_3$, 400 MHz) δ 12.14 (s, 2H), 7.43–7.37 (m, 4H) ppm. ^{13}C{^{1}H} NMR (CDCl$_3$, 100 MHz) δ 153.0, 134.6, 132.0, 130.0, 128.2, 100.3 ppm. HRMS (ESI): calcd. for $C_{12}H_7I_2N_2O_2$ [M−H]$^-$: 464.8602, found: 464.8598. Elemental analysis calcd. for $C_{12}H_8I_2N_2O_2$: C 30.93 H 1.73 N 6.01, found: C 30.80 H 1.81 N 6.01.
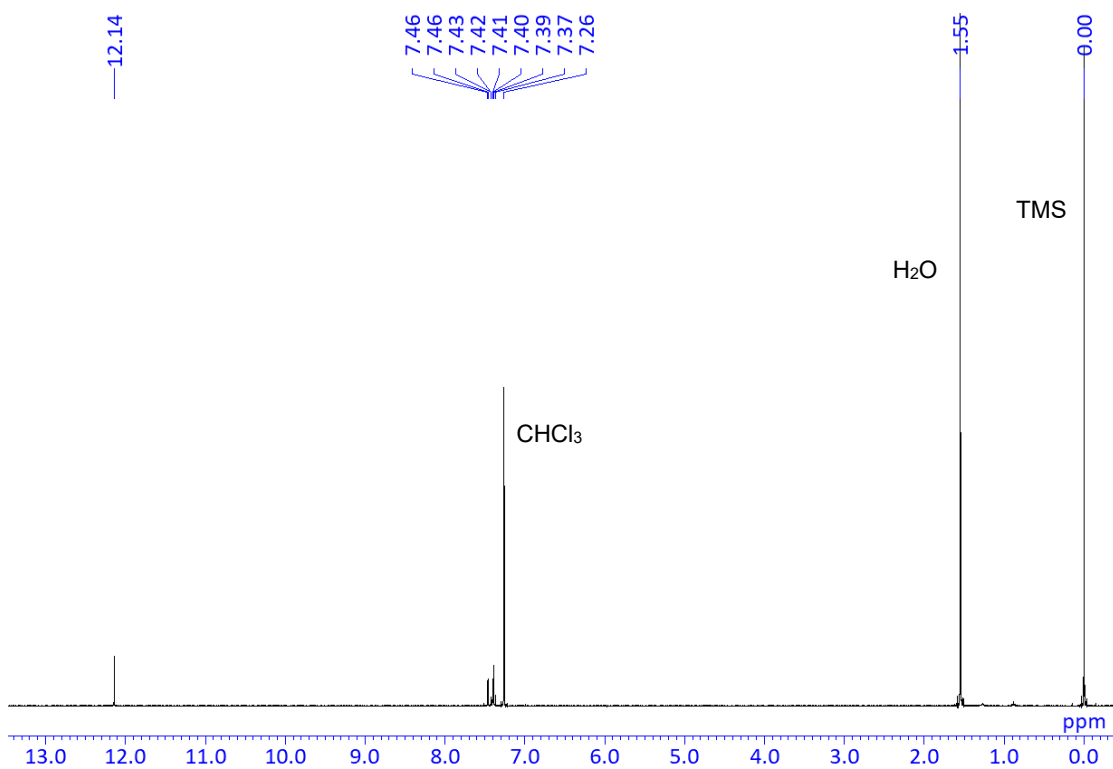
Chart S15. ^{1}H NMR spectrum of **AzOH-I** in CDCl$_3$ at 400 MHz.
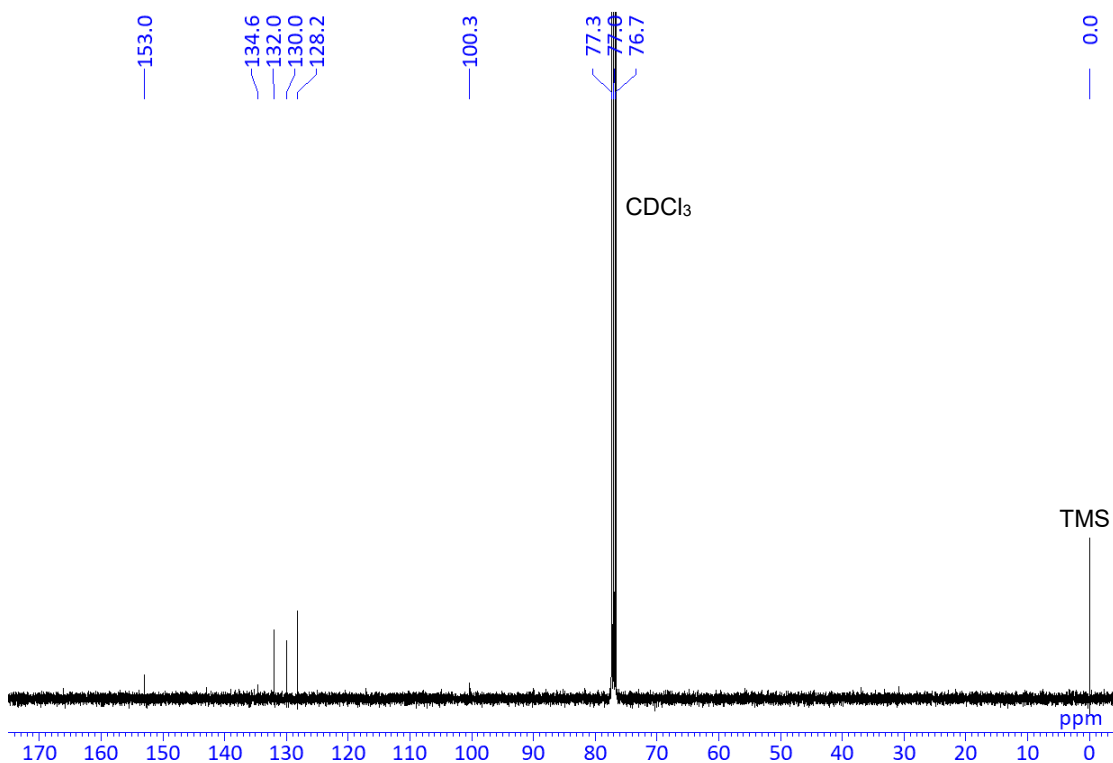
Chart S16. ^{13}C{^{1}H} NMR spectrum of **AzOH-I** in CDCl$_3$ at 100 MHz.

Synthesis of GAz-I
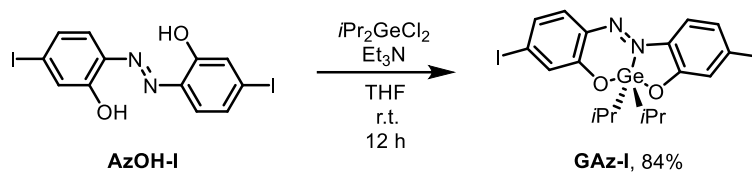
AzOH-I (250 mg, 0.536 mmol) in THF (40 mL) was added to the solution of diisopropyldichlorogermane (1.27 g cm^{-3}, 0.226 mL, 0.966 mmol) and Et$_3$N (0.726 g cm^{-3}, 0.299 mL, 2.15 mmol) in THF (4 mL). The reaction mixture was stirred at ambient temperature for 12 h under argon atmosphere, and then filtered to remove salt. the product was purified by recrystallization from acetone to give pure **GAz-I** (280 mg, 0.450 mmol, 84%) as a black solid.

^{1}H NMR (CDCl$_3$, 400 MHz) δ 7.36–7.206 (br, 4H), 7.20–7.00 (br, 2H), 1.89–1.78 (m, 2H), 1.17 (d, J = 7.4 Hz, 12H) ppm. ^{13}C{^{1}H} NMR (CDCl$_3$, 125 MHz) δ 162.7, 161.1, 135.8, 135.8, 134.6, 132.2, 128.1, 127.2, 127.1, 118.0, 107.3, 101.7, 28.7, 18.5 (br) ppm. HRMS (ESI): calcd. for C$_{18}$H$_{21}$I$_2$GeN$_2$O$_2$ [M+H]$^+$:624.8899, found: 624.8903. Elemental analysis calcd. for C$_{18}$H$_{20}$I$_2$GeN$_2$O$_2$: C 34.71 H 3.24 N 4.50, found: C 34.77 H 3.28 N 4.31.
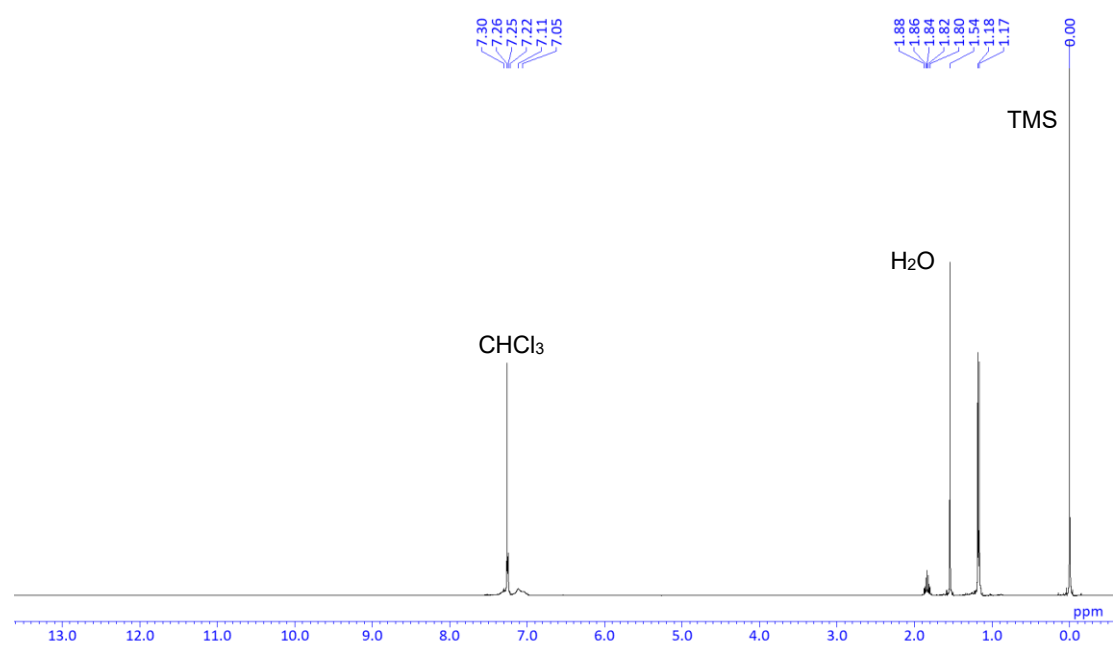
Chart S17. ^{1}H NMR spectrum of **GAz-I** in CDCl$_3$ at 400 MHz.
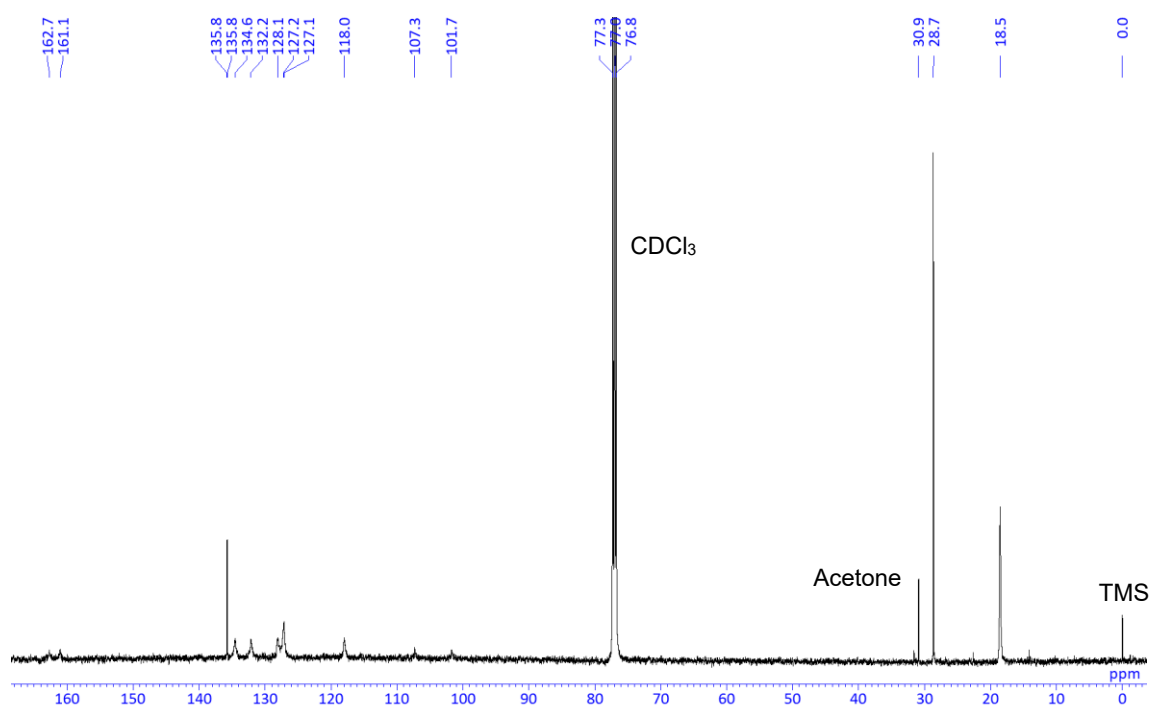
Chart S18. ^{13}C{^{1}H} NMR spectrum of **GAz-I** in CDCl$_3$ at 125 MHz.

Synthesis of P-GAz
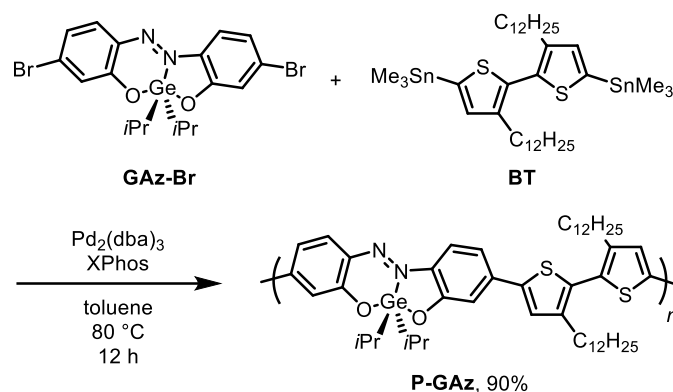
In a round-bottom flask, **GAz-Br** (54.3 mg, 0.103 mmol), 5,5′-bis(trimethylstannyl)-3,3′-didodecyl-2,2′-bithiophene (**BT**) (85.0 mg, 0.103 mmol), $Pd_2(dba)_3$ (2.82 mg, 0.0031 mmol), XPhos (2.93 mg, 0.0062 mmol) were dissolved in toluene (2.0 mL). The solution was stirred at 80 °C for 12 h under nitrogen atmosphere. Upon cooling to ambient temperature, chloroform (2.0 ml) was added. The solution was filtered through cotton and reprecipitated from acetonitrile. The polymer collected by filtration was dried in vacuo to afford **P-GAz** (82.8 mg, 90%) as a black solid.

M_n = 14,000, M_w = 36,000, M_w/M_n = 2.50. ^{1}H NMR (CDCl$_3$, 400 MHz) δ 7.74–7.62 (br, 1H), 7.50–7.38 (m, 2H), 7.34–7.20 (br, 1H), 7.11–7.01 (m, 4H), 2.70–2.45 (br, 4H), 1.92–1.86 (m, 2H), 1.68–1.50 (br, 4H), 1.38–1.10 (br, 36H), 0.87 (t, J = 6.8 Hz, 6H) ppm. ^{13}C NMR (CDCl$_3$, 100 MHz) δ 31.9, 30.7, 29.7, 29.5, 29.4, 29.1, 28.5, 22.7, 18.9, 18.6, 14.1 ppm. The peaks in an aromatic area are unclear due to broadened peaks.
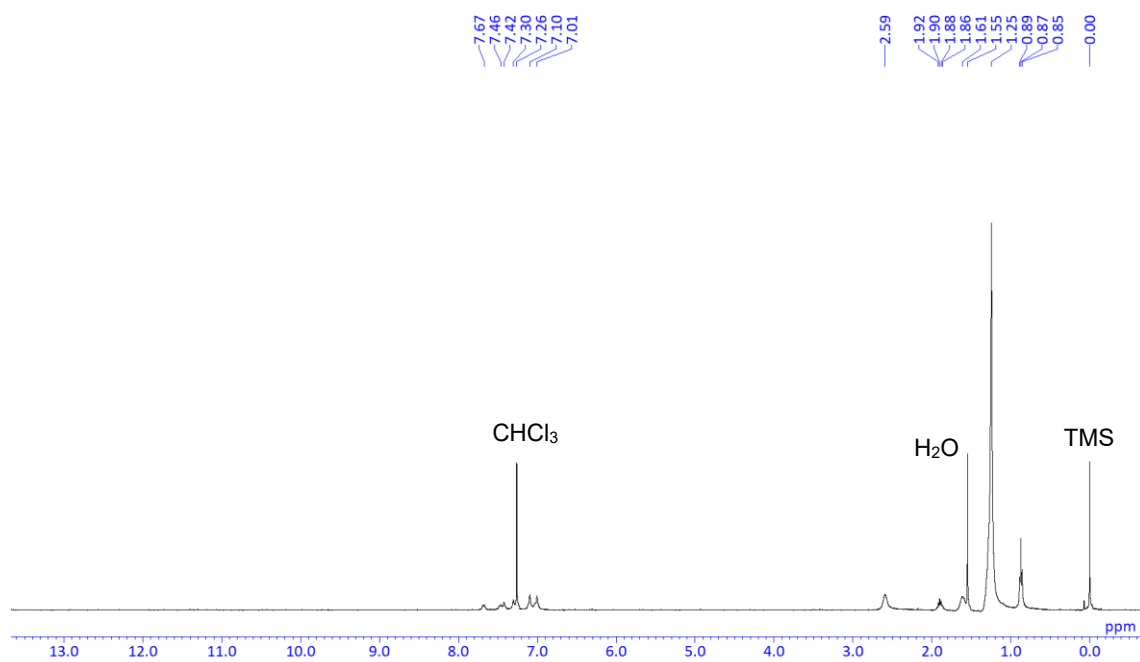
Chart S19. ^{1}H NMR spectrum of **P-GAz** in CDCl$_3$ at 400 MHz.
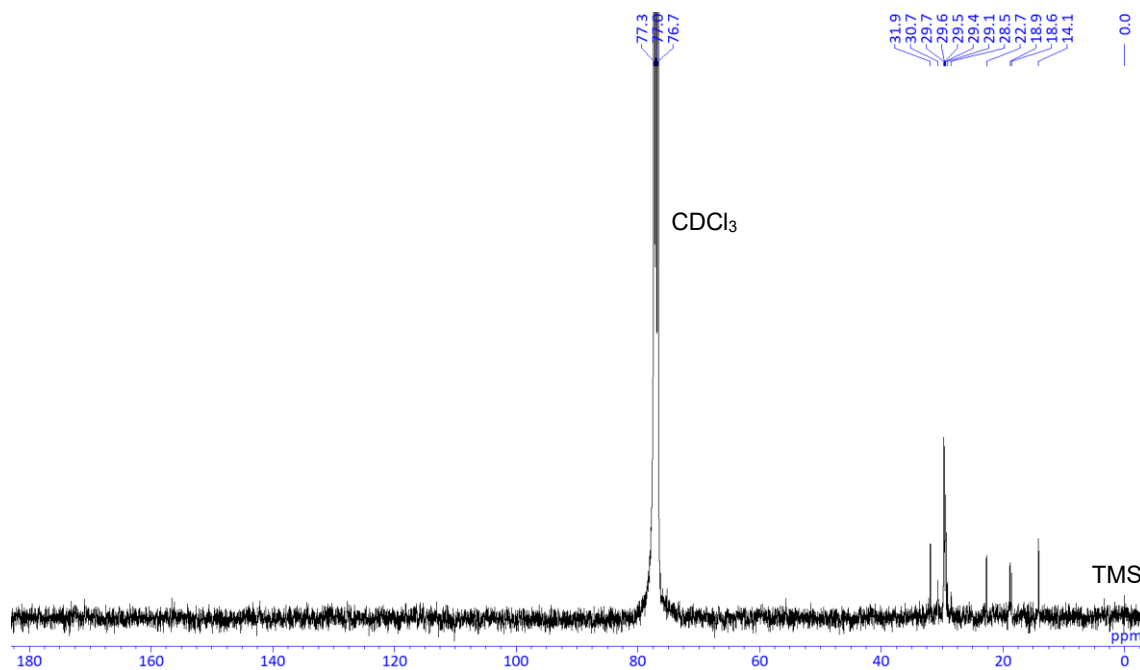
Chart S20. ^{13}C{^{1}H} NMR spectrum of **P-GAz** in CDCl$_3$ at 100 MHz.
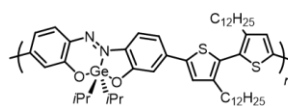
repeating unit
$C_{50}H_{72}GeN_2O_2S_2$
m/z: 870

Matrix: DCTB (*trans*-2-[3-(4-*tert*-butylphenyl)-2-methyl-2-propenylidene]malononitrile)
Cationization agent: TFA-Na
Linear mode
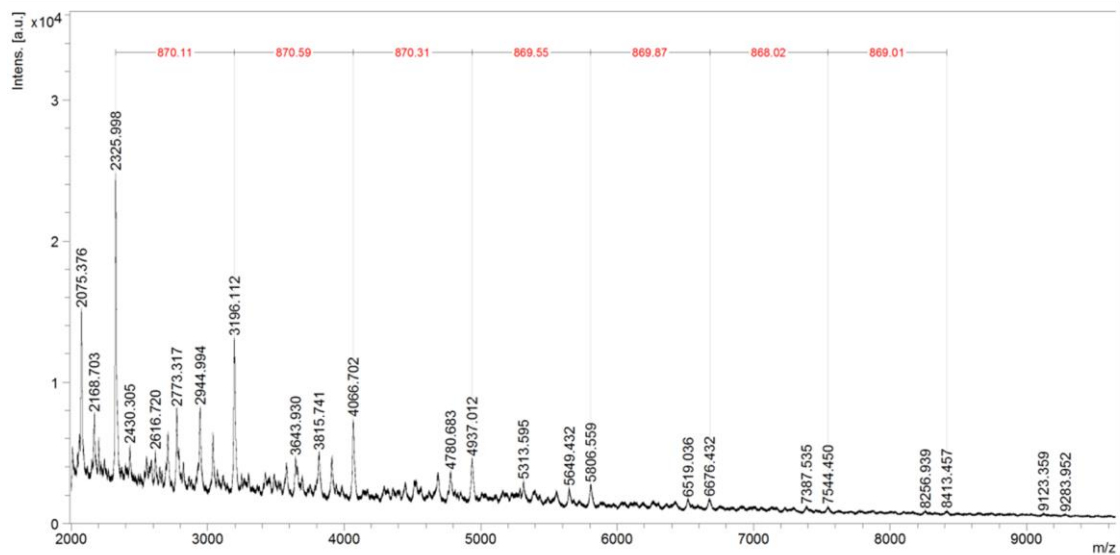
Chart S21. MALDI-TOF mass spectrum of **P-GAz**.

Thermal stability with thermogravimetric analysis (TGA)

The thermogravimetric (TGA) analysis indicated that polymerization provided higher thermal stability to **P-GAz** (T_d = 288 °C, T_d: decomposition temperature) than to **GAz-Br** (T_d = 250 °C) (Figure S1 and Table S1). It is likely that molecular motions and subsequent pyrolysis would be suppressed by polymerization.
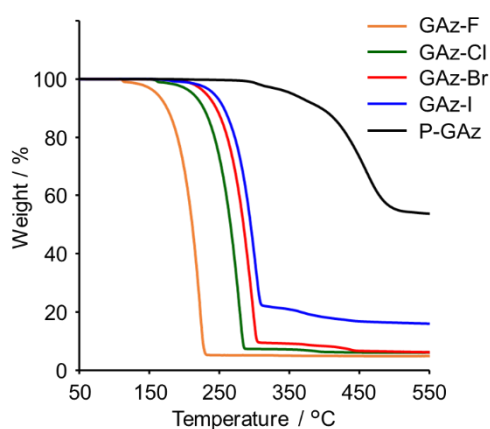
Figure S1. TGA curves of GAz derivatives, under N_2 (scan rate, 10 °C min^{-1}).

Table S1. Decomposition temperatures of GAz derivatives

	$T_d{}^a$ /°C
GAz-F	170
GAz-Cl	232
GAz-Br	250
GAz-I	249
P-GAz	288

[a] Onset temperature of the degradation curve calculated from an extrapolation method

Water sensitivity

Water sensitivity of GAz was evaluated with monomer **GAz-Br** and polymer **P-GAz**. The sensitivity test was conducted in the mixed solutions (THF/H$_2$O = 99/1 v/v, 1.0×10^{-5} M) monitoring alteration of absorption properties. Initially, the stock solution of each sample was prepared (1.0×10^{-3} M in THF), and then 50 μL of it was diluted in 4.90 mL of THF. The test was started just when 50 μL of H$_2$O was added into the solution. Absorption spectra were recorded at 0 h, 0.5 h, 1 h, 2 h, 6 h, 1 d and 2 d after adding H$_2$O (Figure S2). In **GAz-Br**, the intensity of absorption band around 600 nm gradually decreased and completely disappeared after 1 h, meanwhile new absorption band around 400 nm originating from the ligand **AzOH-Br** gradually increased.[7] This indicates that Ge coordination should be irreversibly decomposed by nucleophilic attack by H$_2$O. In contrast, the original spectrum can be significantly preserved until after 2 h in **P-GAz**. That means that **P-GAz** possesses higher resistance to H$_2$O than **GAz-Br**. Strong chemical bonds and hydrophobicity of the π-conjugated polymeric system could play a critical role in higher water resistance. Owing to applicability of the GAz compound for polymerization, further stability can be enhanced.
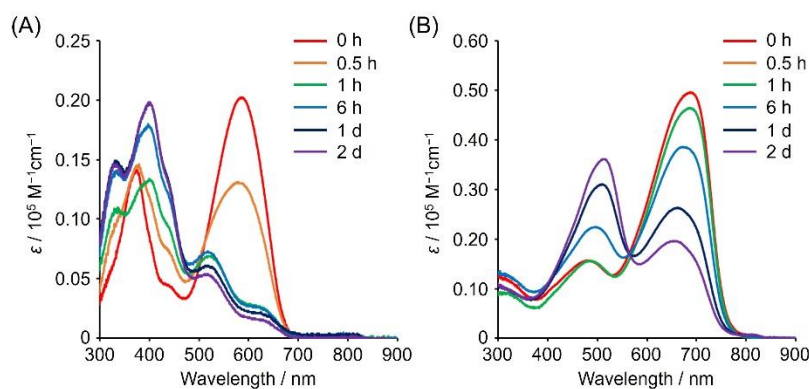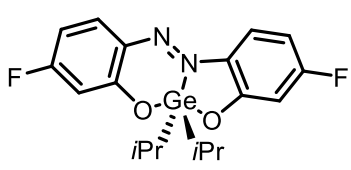
Figure S2. Water sensitivity test of (A) **GAz-Br** and (B) **P-GAz** in THF/H$_2$O = 99/1 v/v (1.0×10^{-5} M) with chronological change of UV–vis absorption spectra.

Single crystal X-ray structure analysis of GAz-F

Intensity data were collected on a Rigaku R-AXIS RAPID imaging plate area detector with graphite monochromated MoKα radiation (λ = 0.71069 Å). The structures were solved and refined by full-matrix least-squares procedures based on F^2 (SHELXL-2018/3).[10]

Table S2. Crystallographic data of **GAz-F**

Empirical formula	$C_{18}H_{20}F_2GeN_2O_2$
Formula weight	407.00
Temperature (K)	93(2)
Wavelength (Å)	0.71075
Crystal system, space group	Triclinic, $P-1$
Unit cell dimensions (Å)	a=7.1512(3)
	b=10.9485(5)
	c=11.7984(5)
Unit cell dimensions (º)	α=73.883(5)
	β=80.802(6)
	γ=81.188(6)
Volume (Å^3)	870.25(7)
Z, calculated density (g cm^{-3})	2, 1.553
Absorption coefficient	1.794
F(000)	416
Crystal size (mm)	0.50×0.30×0.20
θ range for data collection (°)	1.81-27.455
Limiting indices	$-9{\leq}h{\leq}9$, $-14{\leq}k{\leq}14$, $-13{\leq}l{\leq}15$
Reflections collected (unique)	8254/7655 [R(int)=0.0361]
Completeness to theta	0.981
Max. and min. transmission	1.000, 0.6238
Goodness-of-fit on F^2	1.157
Final R indices [$I > 2\sigma(I)$][a]	R_1 = 0.0446, wR_2 = 0.1078
R indices (all data)	R_1 = 0.0615, wR_2 = 0.1539

(structure of **GAz-F**, CCDC # 2191327)

[a] $R_1 = \Sigma(|F_0|-|F_c|)/\Sigma|F_0|$. w$R_2 = [\Sigma w(F^2_0-F^2_c)^2/\Sigma w(F^2_0)^2]^{1/2}$. w $= 1/[\sigma^2(F^2_0)+[(ap)^2+bp]]$, where $p = [\max(F^2_0,0)+2F^2_c]/3$.

(A)

Top View

Front View

(B)
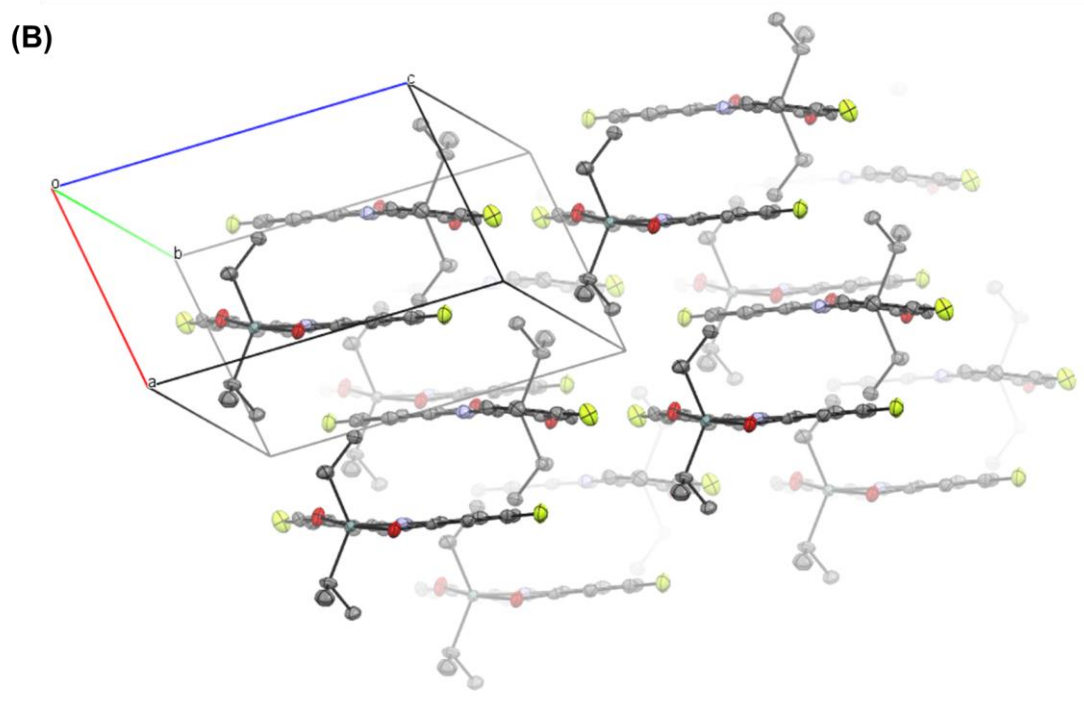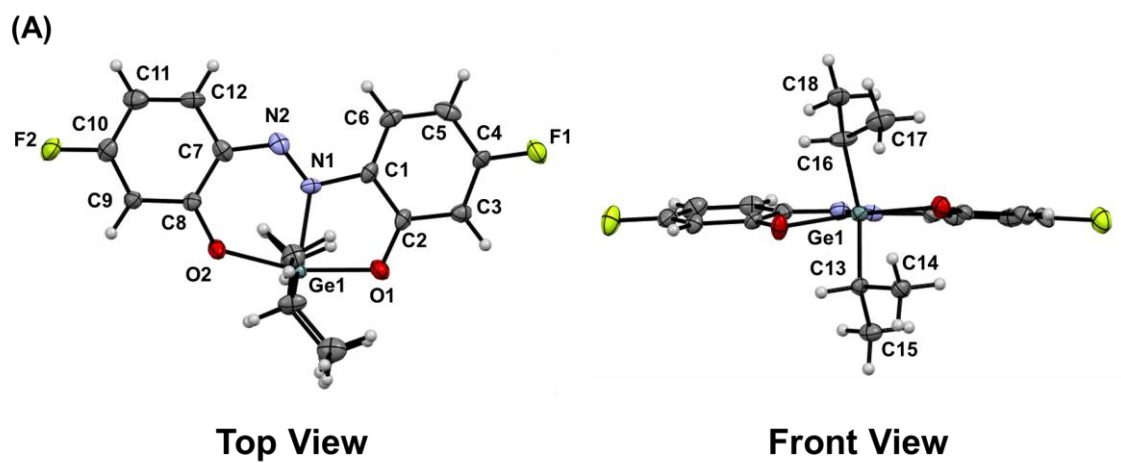
Figure S3. (A) ORTEP drawings and (B) packing diagrams of **GAz-F**. Thermal ellipsoids are scaled to the 50% probability level. Hydrogen atoms are omitted for clarity.

Single crystal X-ray structure analysis of GAz-Cl

Intensity data were collected on a Rigaku R-AXIS RAPID imaging plate area detector with graphite monochromated MoKα radiation (λ = 0.71069 Å). The structures were solved and refined by full-matrix least-squares procedures based on F^2 (SHELXL-2018/3).[10]

Table S3. Crystallographic data of **GAz-Cl**

Empirical formula	$C_{18}H_{20}Cl_2GeN_2O_2$
Formula weight	439.9000
Temperature (K)	93(2)
Wavelength (Å)	0.71075
Crystal system, space group	Monoclinic, $C\ 2/c$
Unit cell dimensions (Å)	a=14.7930(8)
	b=17.8136(8)
	c=6.9755(4)
Unit cell dimensions (º)	α=90
	β=90.569(6)
	γ=90
Volume (Å^3)	1838.07(17)
Z, calculated density (g cm^{-3})	4, 1.589
Absorption coefficient	1.972
F(000)	896
Crystal size (mm)	0.21×0.21×0.20
θ range for data collection (°)	1.79-27.455
Limiting indices	$-19 \leq h \leq 19$, $-22 \leq k \leq 23$, $-8 \leq l \leq 9$
Reflections collected (unique)	8447/7619 [R(int)=0.0355]
Completeness to theta	0.992
Max. and min. transmission	1.000, 0.7033
Goodness-of-fit on F^2	1.111
Final R indices [$I > 2\sigma(I)$][a]	R_1 = 0.0306, wR_2 = 0.0681
R indices (all data)	R_1 = 0.0368, wR_2 = 0.0709

[a] $R_1 = \Sigma(|F_0|-|F_c|)/\Sigma|F_0|$. w$R_2 = [\Sigma w(F^2_0-F^2_c)^2/\Sigma w(F^2_0)^2]^{1/2}$. w = $1/[\sigma^2(F^2_0)+[(ap)^2+bp]]$, where p = $[max(F^2_0,0)+2F^2_c]/3$.

(Image accompanying table:)
GAz-Cl

CCDC # 2191330

(A)

Top View

Front View
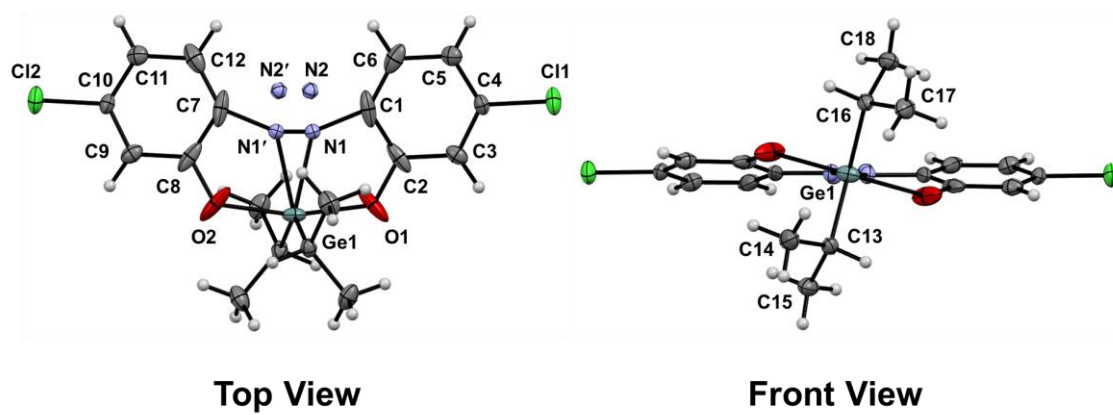
(B)
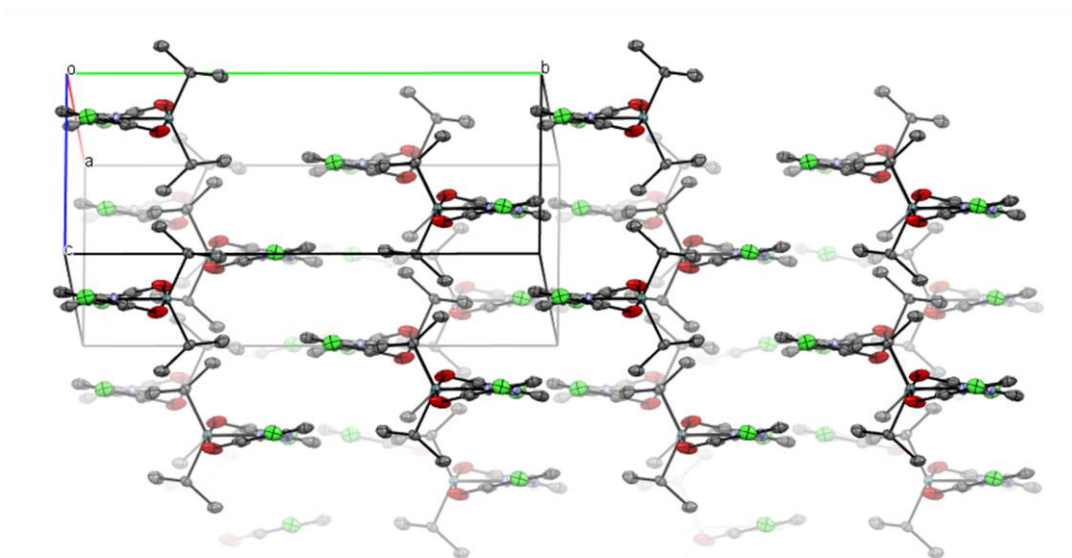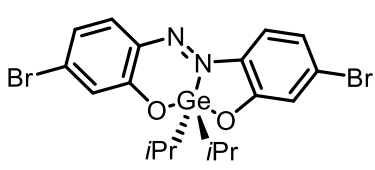
Figure S4. (A) ORTEP drawings and (B) packing diagrams of **GAz-Cl**. Thermal ellipsoids are scaled to the 50% probability level. Hydrogen atoms are omitted for clarity.

Single crystal X-ray structure analysis of GAz-Br

Intensity data were collected on a Rigaku Saturn 724+ with MicroMax-007HF CCD diffractometer with Varimax Mo optics using graphite-monochromated MoKα radiation. The structures were solved and refined by full-matrix least-squares procedures based on F^2 (SHELXL-2018/3).[10]

Table S4. Crystallographic data of **GAz-Br**

Empirical formula	$C_{18}H_{20}Br_2GeN_2O_2$
Formula weight	528.81
Temperature (K)	143
Wavelength (Å)	0.71075
Crystal system, space group	Orthorhombic, *Pbcn*
Unit cell dimensions (Å)	a=18.116(3)
	b=7.0572(10)
	c=29.558(5)
Unit cell dimensions (º)	α=90
	β=90
	γ=90
Volume (Å^3)	3778.9(10)
Z, calculated density (g cm^{-3})	8, 1.859
Absorption coefficient	5.865
F(000)	2080
Crystal size (mm)	0.25×0.14×0.14
θ range for data collection (°)	3.1-27.5
Limiting indices	$-22 \leq h \leq 21$, $-9 \leq k \leq 9$, $-38 \leq l \leq 38$
Reflections collected (unique)	28128/11813 [R(int)=0.0478]
Completeness to theta	0.982
Max. and min. transmission	1.000, 0.658
Goodness-of-fit on F^2	1.116
Final R indices [$I > 2\sigma(I)$][a]	$R_1 = 0.0325$, w$R_2 = 0.0726$
R indices (all data)	$R_1 = 0.0361$, w$R_2 = 0.0749$

[a] $R_1 = \Sigma(|F_0|-|F_c|)/\Sigma|F_0|$. w$R_2 = [\Sigma w(F^2_0-F^2_c)^2/\Sigma w(F^2_0)^2]^{1/2}$. w = 1/[$\sigma^2(F^2_0)+[(ap)^2+bp]$], where $p = [\max(F^2_0,0)+2F^2_c]/3$.

(A)

Top View   **Front View**
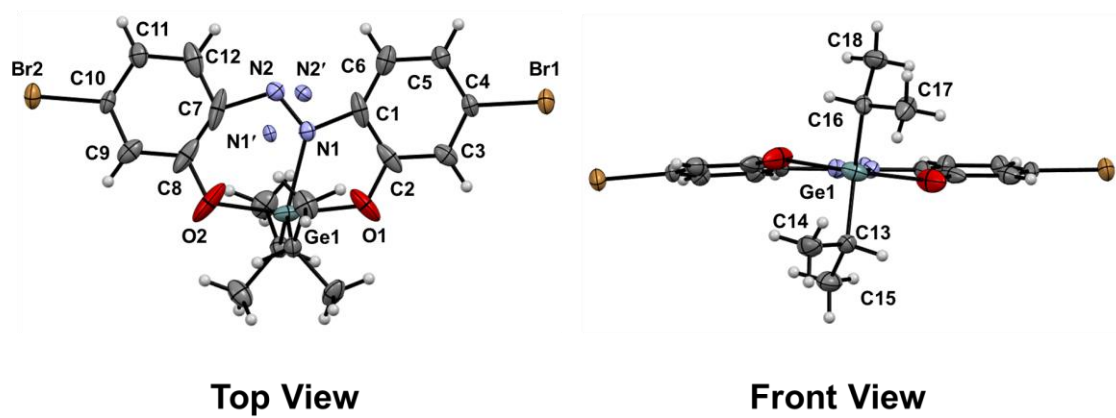
(B)
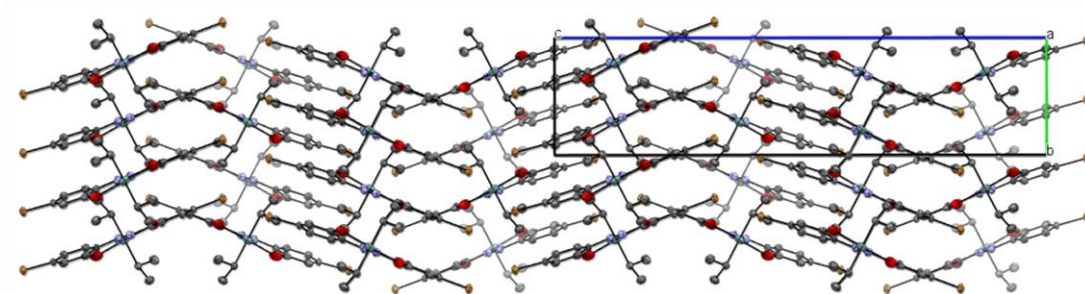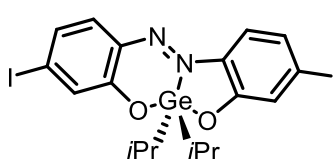
Figure S5. (A) ORTEP drawings and (B) packing diagrams of **GAz-Br**. Thermal ellipsoids are scaled to the 50% probability level. Hydrogen atoms are omitted for clarity.

Single crystal X-ray structure analysis of GAz-I

Intensity data were collected on a Rigaku Saturn 724+ with MicroMax-007HF CCD diffractometer with Varimax Mo optics using graphite-monochromated MoKα radiation. The structures were solved and refined by full-matrix least-squares procedures based on F^2 (SHELXL-2018/3).[10]

Table S5. Crystallographic data of **GAz-I**

Empirical formula	$C_{18}H_{20}I_2GeN_2O_2$
Formula weight	622.81
Temperature (K)	143
Wavelength (Å)	0.71075
Crystal system, space group	Orthorhombic, *Pbcn*
Unit cell dimensions (Å)	a=18.220(4)
	b=7.2691(16)
	c=30.396(7)
Unit cell dimensions (º)	α=90
	β=90
	γ=90
Volume (Å^3)	4025.7(16)
Z, calculated density (g cm^{-3})	8, 2.055
Absorption coefficient	4.603
F(000)	2368
Crystal size (mm)	0.13×0.10×0.10
θ range for data collection (°)	3.0-27.5
Limiting indices	$-23 \leq h \leq 23$, $-9 \leq k \leq 9$, $-29 \leq l \leq 39$
Reflections collected (unique)	28769/12475 [R(int)=0.0478]
Completeness to theta	0.997
Max. and min. transmission	1.000, 0.766
Goodness-of-fit on F^2	1.098
Final R indices [$I > 2\sigma(I)$][a]	$R_1 = 0.0325$, w$R_2 = 0.0729$
R indices (all data)	$R_1 = 0.0349$, w$R_2 = 0.0749$

GAz-I

CCDC # 2191341

[a] $R_1 = \Sigma(|F_0|-|F_c|)/\Sigma|F_0|$. w$R_2 = [\Sigma w(F^2_0-F^2_c)^2/\Sigma w(F^2_0)^2]^{1/2}$. w = $1/[\sigma^2(F^2_0)+[(ap)^2+bp]]$, where $p = [\max(F^2_0,0)+2F^2_c]/3$.

(A)
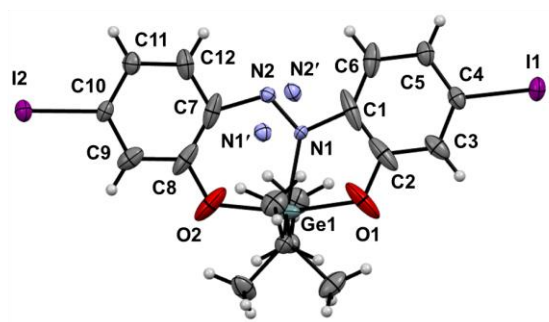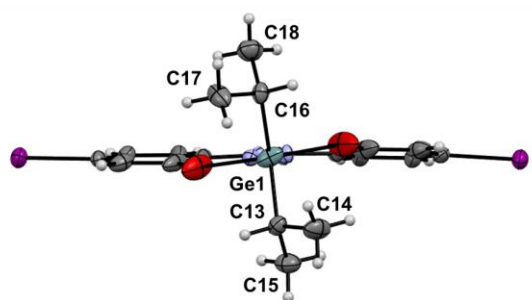
Top View   **Front View**

(B)
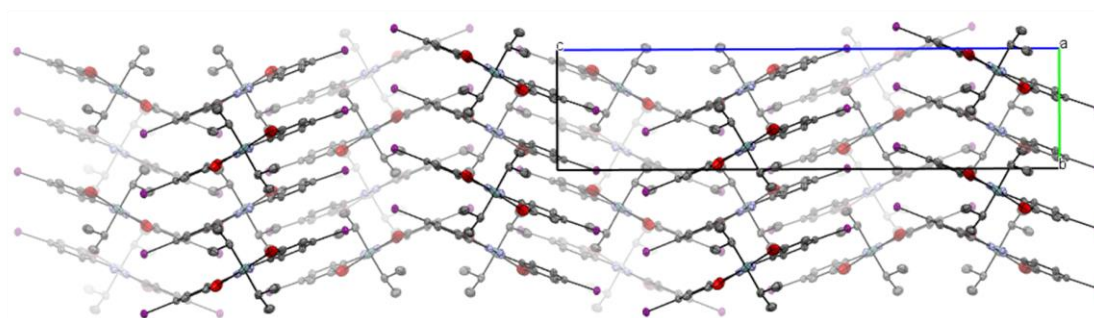
Figure S6. (A) ORTEP drawings and (B) packing diagrams of **GAz-I**. Thermal ellipsoids are scaled to the 50% probability level. Hydrogen atoms are omitted for clarity.

Selected bond lengths, angles and torsion angles

Table S6. Selected bond lengths, angles and torsion angles from single crystals of the TAz compounds

	GAz-F	GAz-Cl	GAz-Br	GAz-I
Bond / Å				
Ge(1)−C(13)	1.959(5)	1.950	1.949(3)	1.949(4)
Ge(1)−C(16)	1.955(5)	1.950	1.943(3)	1.944(4)
Ge(1)−O(1)	1.948(3)	1.967	1.967(3)	1.969(4)
Ge(1)−O(2)	1.992(3)	1.967	1.965(3)	1.964(3)
Ge(1)−N(1)	2.024(5)	2.056	2.107(5)	2.049(5)
N(1)−N(2)	1.276(6)	1.280	1.270(8)	1.286(8)
N(1)−C(1)	1.440(6)	1.447(4)	1.409(6)	1.410(7)
N(2)−C(7)	1.359(6)	1.447(4)	1.509(7)	1.477(7)
O(1)−C(2)	1.325(7)	1.320(3)	1.319(4)	1.325(6)
O(2)−C(8)	1.305(6)	1.320(3)	1.312(5)	1.317(6)
C(1)−C(2)	1.375(6)	1.408(4)	1.403(5)	1.398(8)
C(7)−C(8)	1.423(8)	1.408(4)	1.402(6)	1.407(7)
Angle / °				
C(13)−Ge(1)−C(16)	128.9(2)	130.30	129.5(1)	130.0(1)
N(1)−Ge(1)−C(13)	117.9(2)	116.50	112.9(2)	112.1(2)
N(1)−Ge(1)−C(16)	113.0(2)	112.02	116.2(2)	116.9(2)
O(1)−Ge(1)−O(2)	164.7(1)	165.30	165.8(1)	166.2(2)
N(1)−Ge(1)−O(1)	81.1(1)	70.65	69.8(1)	71.7(2)
N(1)−Ge(1)−O(2)	84.4(1)	94.66	96.2(2)	94.6(2)
Torsion Angle / °				
C(1)−N(1)−N(2)−C(7)	178.3(4)	176.70	−179.6(4)	177.6(5)
C(2)−O(1)−O(2)−C(7)	−20.84	−39.08	21.46	−21.15
C(6)−C(1)−C(7)−C(12)	−8.98	22.19	11.42	−9.89

PL lifetime decay curves
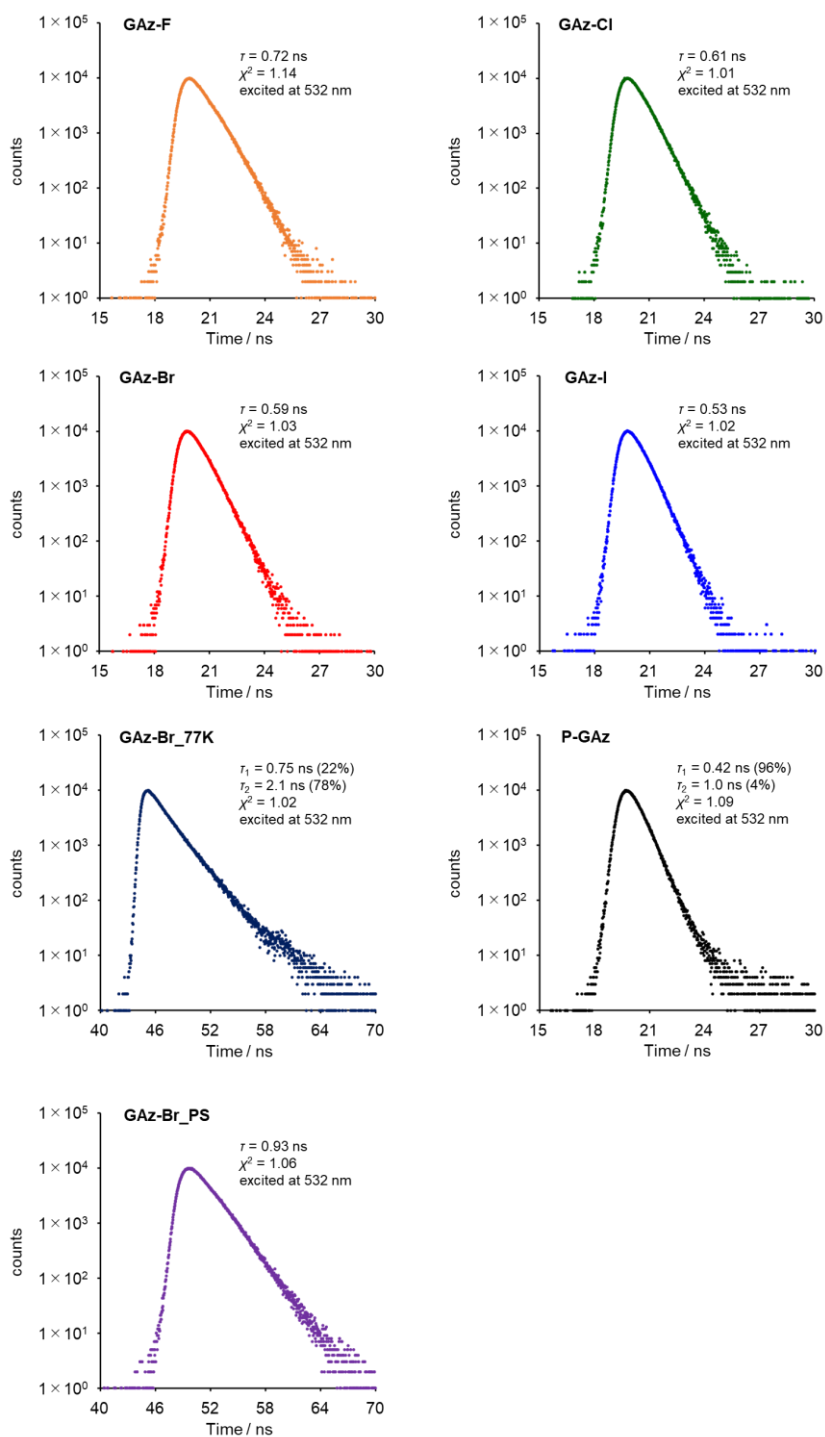
Figure S7. PL lifetime decay curves of **GAz** derivatives in CHCl₃ at room temperature, 77 K and in polystyrene film (1wt% **GAz-Br**) (**GAz-Br_PS**) (excited at 532 nm with a LED). Their emissions at the PL peak tops were monitored.

PL properties at 77 K
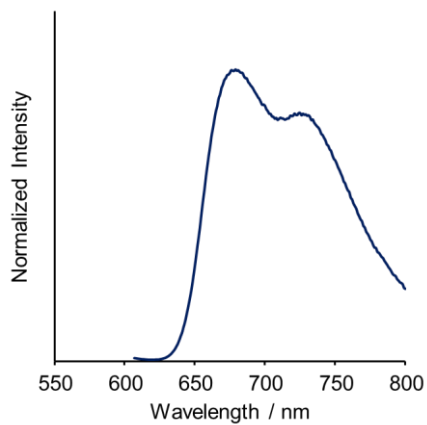
Figure S8. PL spectra of **GAz-Br** at 77 K in 2-MeTHF (1.0×10^{-5} M), excited at wavelengths of absorption maximum in CHCl$_3$ (1.0×10^{-5} M).

Table S7. Spectroscopic data of **GAz-Br** at 77 K in 2-MeTHF (1.0×10^{-5} M).

$\lambda_{PL}{}^a$ /nm	$\Phi_{PL}{}^{a,b}$	τ^c /ns [α]	$k_r{}^d$ /10^8 s^{-1}	$k_{nr}{}^d$ /10^8 s^{-1}
679	0.16	0.75 [22%], 2.1 [78%]	0.89	4.7

^{a} Excited at λ_{abs} in CHCl$_3$ (1.0×10^{-5} M).

^{b} Determined as an absolute value.

^{c} PL lifetime monitored at λ_{PL}, excited at 532 nm.

^{d} $k_r = \Phi_{PL}/\tau_{av}$, $k_{nr} = (1 - \Phi_{PL})/\tau_{av}$, $\tau_{av} = \Sigma\alpha_i\tau_i$. α: relative amplitude.

PL properties in polystyrene film
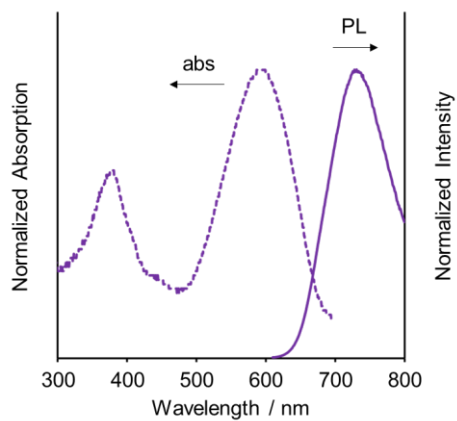
Figure S9. UV–vis absorption and PL spectra of **GAz-Br** in polystyrene film (1 wt% of **GAz-Br**), excited at wavelengths of absorption maximum.

Table S8. Spectroscopic data of **GAz-Br** in polystyrene film (1 wt% of **GAz-Br**).

λ_{abs} /nm	$\lambda_{PL}{}^a$ /nm	$\Phi_{PL}{}^{a,b}$	τ^c /ns	$k_r{}^d$ /10^8 s^{-1}	$k_{nr}{}^d$ /10^8 s^{-1}
591	731	0.06	0.93	0.65	10

[a] Excited at λ_{abs}.

[b] Determined as an absolute value.

[c] PL lifetime monitored at λ_{PL}, excited at 532 nm.

[d] $k_r = \Phi_{PL}/\tau$, $k_{nr} = (1 - \Phi_{PL})/\tau$.

Variable-temperature of ^{1}H NMR spectra
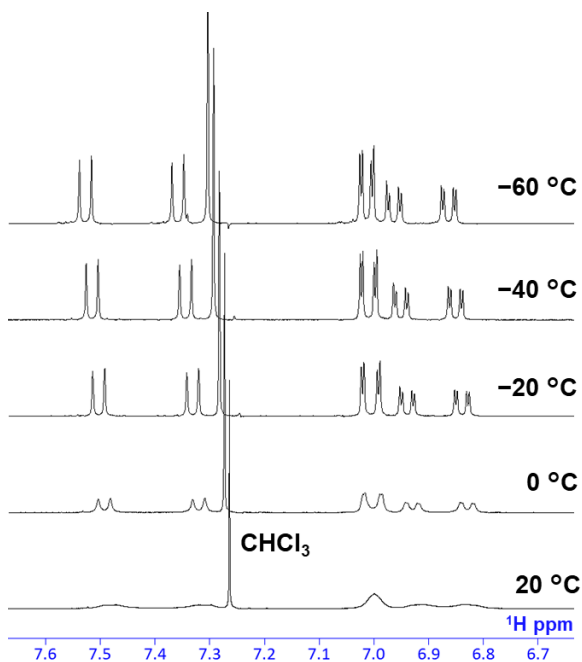
Figure S10. ^{1}H NMR spectra of **GAz-Br** in CDCl$_3$ at from 20 °C to −60 °C.

UV–vis absorption and PL spectra in film state
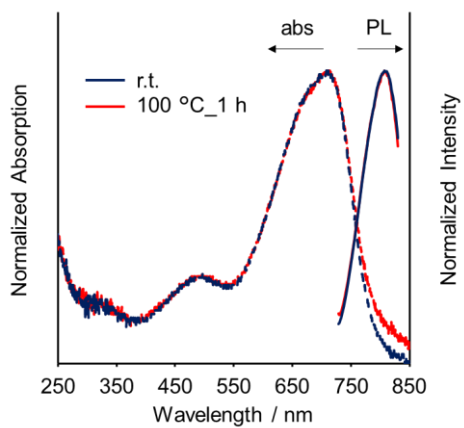
Figure S11. UV–vis absorption and PL spectra of **P-GAz** before and after annealing at 100 °C for 1 h, excited at wavelengths of absorption maximum.

Cyclic voltammograms

Experimental values of HOMO and LUMO energy levels (E_{HOMO} and E_{LUMO}, respectively) were estimated by onset potentials of oxidation (E_{onset}^{ox}) and reduction (E_{onset}^{red}) peaks by a cyclic voltammetry, respectively (Figure S12 and Table S9) according to the literature with the equation of E_{HOMO} /eV = −4.8 − E_{onset}^{ox} /V and E_{LUMO} /eV = −4.8 − E_{onset}^{red} /V.[11] Cyclic voltammograms of samples were recorded in CH_2Cl_2 (1.0×10^{-3} M) containing NnBu$_4$PF$_6$ (0.10 M) using a glassy carbon (GC) working electrode, a Pt wire counter electrode, an Ag/AgCl reference electrode, and a Fc/Fc$^+$ external standard at room temperature with a scan rate of 0.1 V s^{-1}.
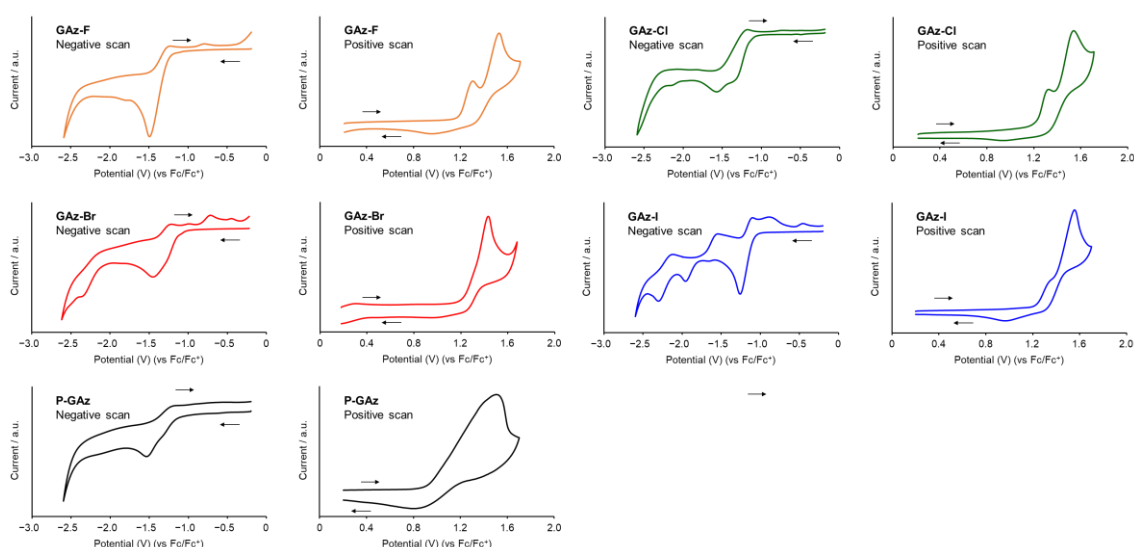
Figure S12. Cyclic voltammograms of GAz derivatives in CH_2Cl_2 (1.0×10^{-3} M for **GAz-X** (X = F, Cl, Br, I) and 1.0×10^{-3} M per repeating unit for **P-GAz**).

Table S9. Electrochemical data of GAz deravatives

	E_{onset}^{ox} /V	E_{onset}^{red} /V	E_{HOMO}^{a} /eV	E_{LUMO}^{a} /eV
GAz-F	+0.79	−1.27	−5.59	−3.53
GAz-Cl	+0.82	−1.15	−5.62	−3.65
GAz-Br	+0.85	−1.10	−5.65	−3.70
GAz-I	+0.83	−1.08	−5.63	−3.72
P-GAz	+0.56	−1.14	−5.36	−3.66

Computational details for theoretical calculation

The Gaussian 16 program package[12] was used for computation. We optimized the structures of the **GAz-F**, **GAz-Cl**, **GAz-Br**, **GAz-I**, **GAz-BT**, **GAzMe-H**, **TAzMe-H**, in the ground S_0 states and calculated their molecular orbitals. Chemical structures are described below. The density functional theory (DFT) was applied for the optimization of the structures in the S_0 states at B3LYP/LanL2DZ level for Sn, I and B3LYP/6-311G(d,p) level for the other atoms. The time-dependent (TD)-DFT was applied for the optimization of the structures in the S_1 states at B3LYP/LanL2DZ level for Sn, I and B3LYP/6-311+G(d,p) level for the other atoms. We calculated the energy of the $S_0 \rightarrow S_1$ and $S_1 \rightarrow S_0$ transitions with optimized geometries in the S_0 and S_1 states, respectively, by TD-DFT at B3LYP/LanL2DZ level for Sn, I and B3LYP/6-311G(d,p) level for the other atoms. Natural bond orbital (NBO) calculation was carried out by DFT at B3LYP/LanL2DZ level for Sn, I and B3LYP/6-311G(d,p) level for the other atoms.

Chemical Structures

GAz-F GAz-Cl GAz-Br GAz-I

GAz-BT

GAzMe-H TAzMe-H

GAz-F

d(N-N) = 1.278 Å
Ground State

d(N-N) = 1.334 Å
Excited State

GAz-Cl

d(N-N) = 1.278 Å
Ground State

d(N-N) = 1.334 Å
Excited State

GAz-Br

d(N-N) = 1.279 Å
Ground State

d(N-N) = 1.334 Å
Excited State

GAz-I

d(N-N) = 1.279 Å
Ground State

d(N-N) = 1.334 Å
Excited State
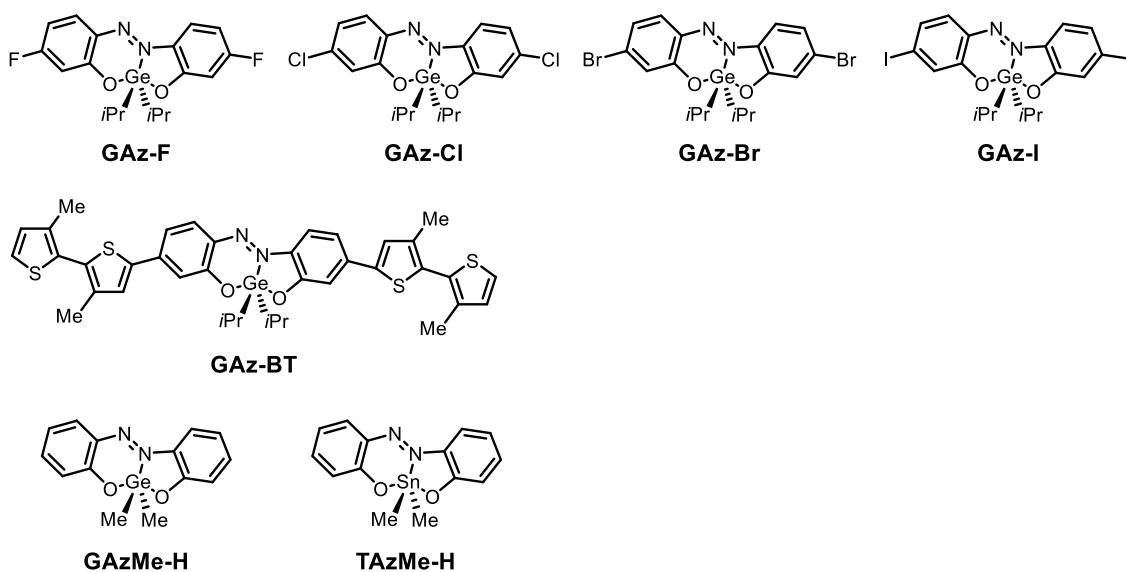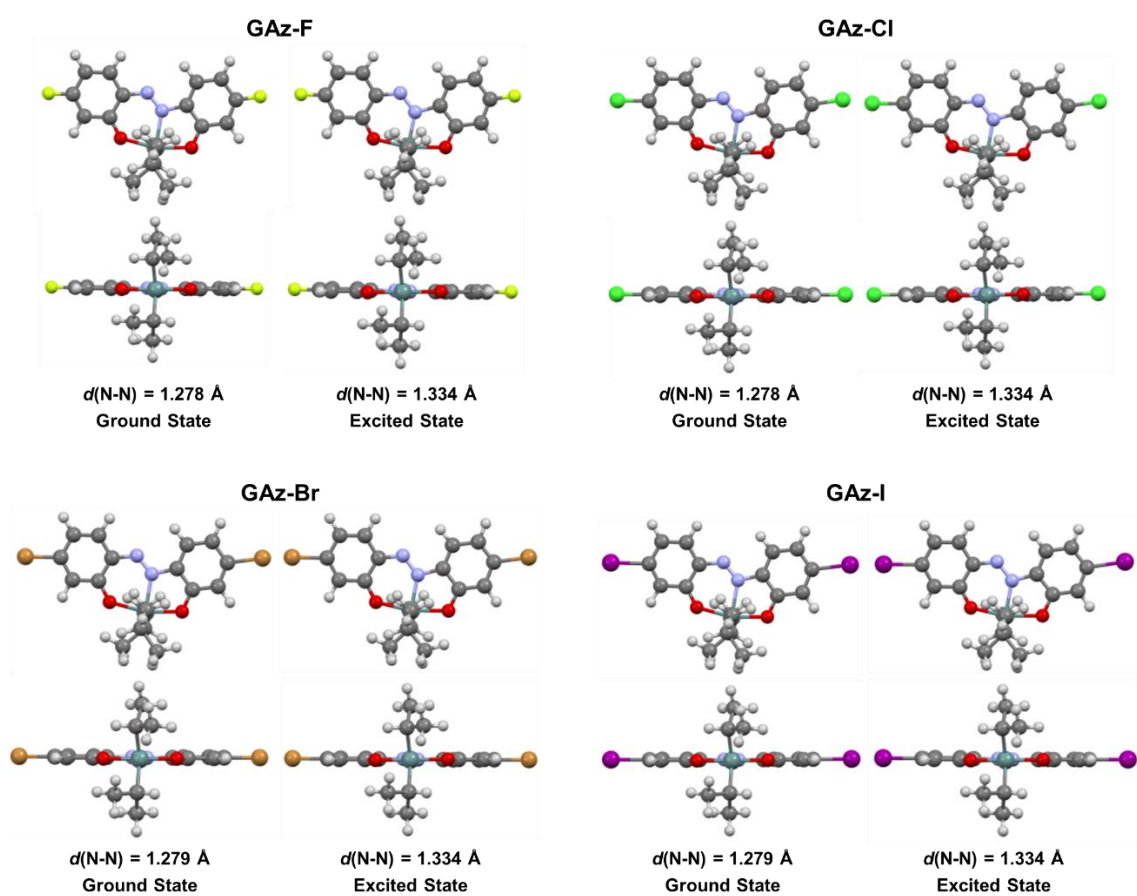
Figure S13. Top and front views of optimized structures of **GAz-X** (X = F, Cl, Br, I) in the ground and excited states.
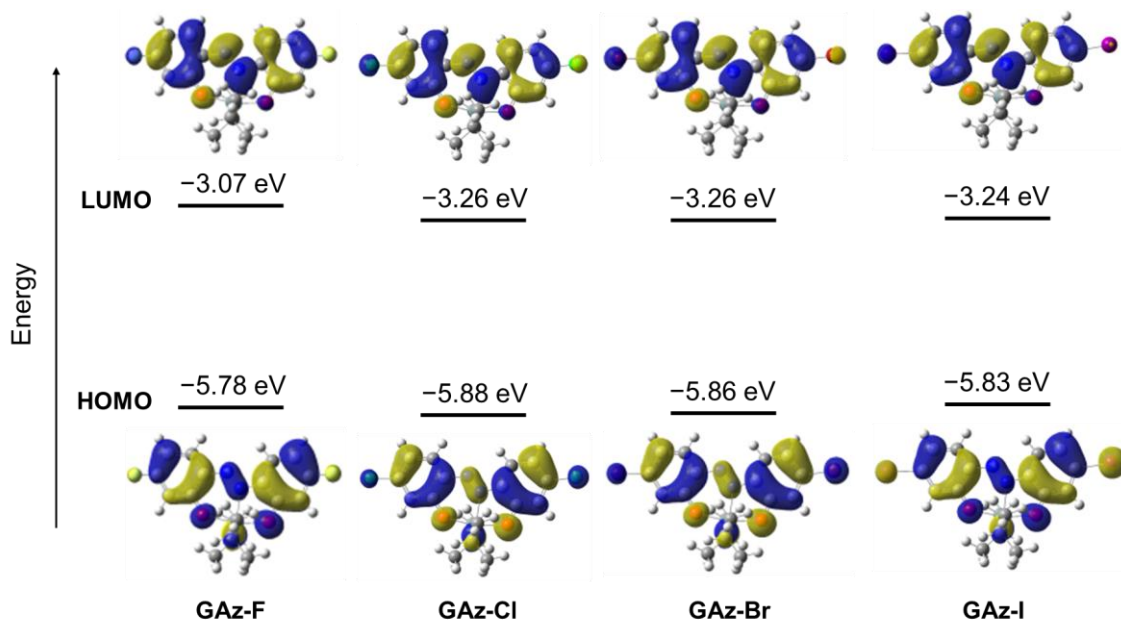
Figure S14. Kohn–Sham orbitals (isovalue = 0.02) and energy diagrams of HOMO and LUMO of **GAz-X** (X = F, Cl, Br, I) in the ground states.
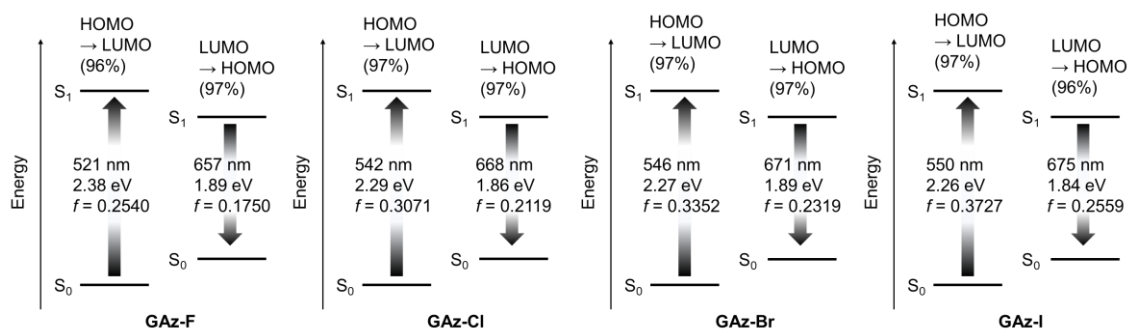
Figure S15. Oscillator strength (*f*), transition energy of $S_0 \rightarrow S_1$ transition from the optimized ground state and $S_1 \rightarrow S_0$ transition from the optimized excited state of **GAz-X** (X = F, Cl, Br, I).

d(N-N) = 1.282 Å
Ground State

d(N-N) = 1.336 Å
Excited State
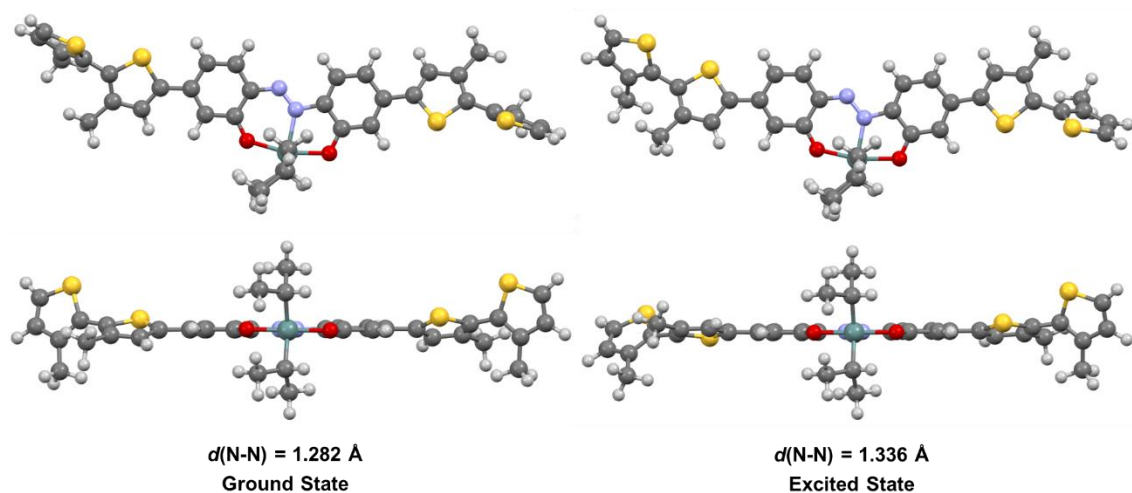
Figure S16. Top and front views of optimized structures of **GAz-BT** as a model compound of **P-GAz** in the ground and excited states.
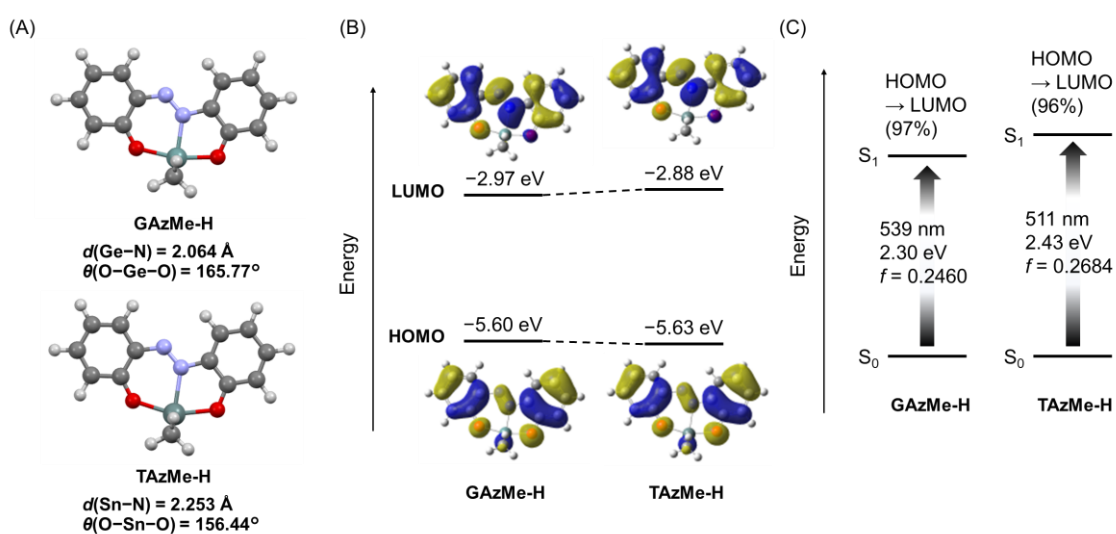
Figure S17. Calculation results of **GAzMe-H** and **TAzMe-H**. (A) Optimized structures in the ground state and selected chemical bond lengths and angles. (B) Kohn–Sham orbitals (isovalue = 0.02) and energy diagrams of HOMO and LUMO in the ground states. (C) Oscillator strength (f), transition energy of $S_0{\rightarrow}S_1$ transition from the optimized ground state.
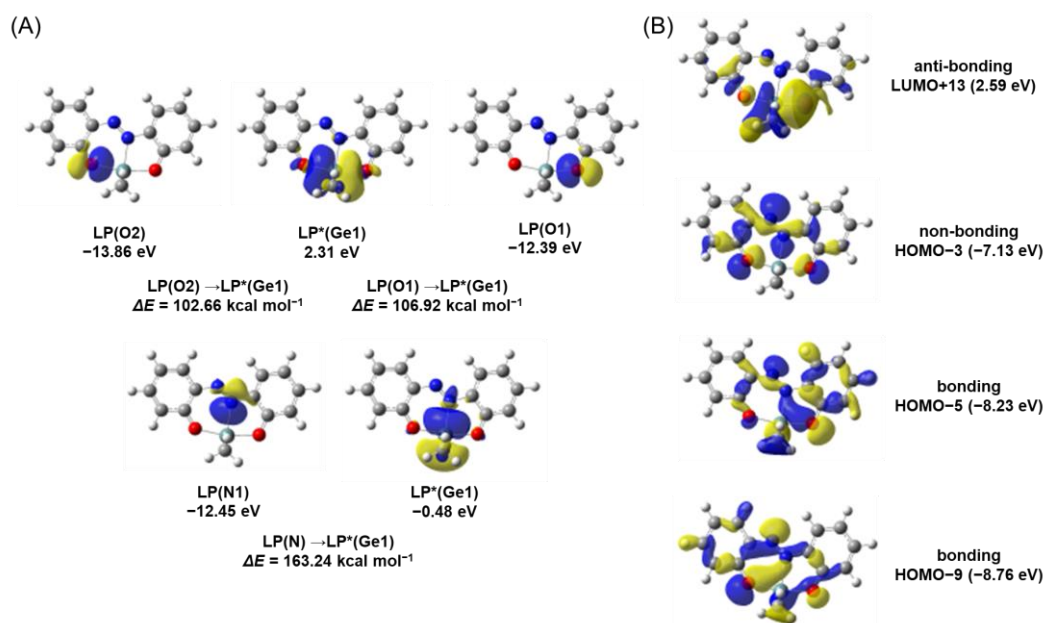
Figure S18. (A) The NBOs and (B) Kohn–Sham orbitals involving 3c-4e bond of **GAzMe-H** and the stabilization energy of donor–acceptor interactions (isovalue = 0.03). ΔE: The second-order perturbation stabilization energy. The split bonding orbitals are found probably by the asymmetric structure.
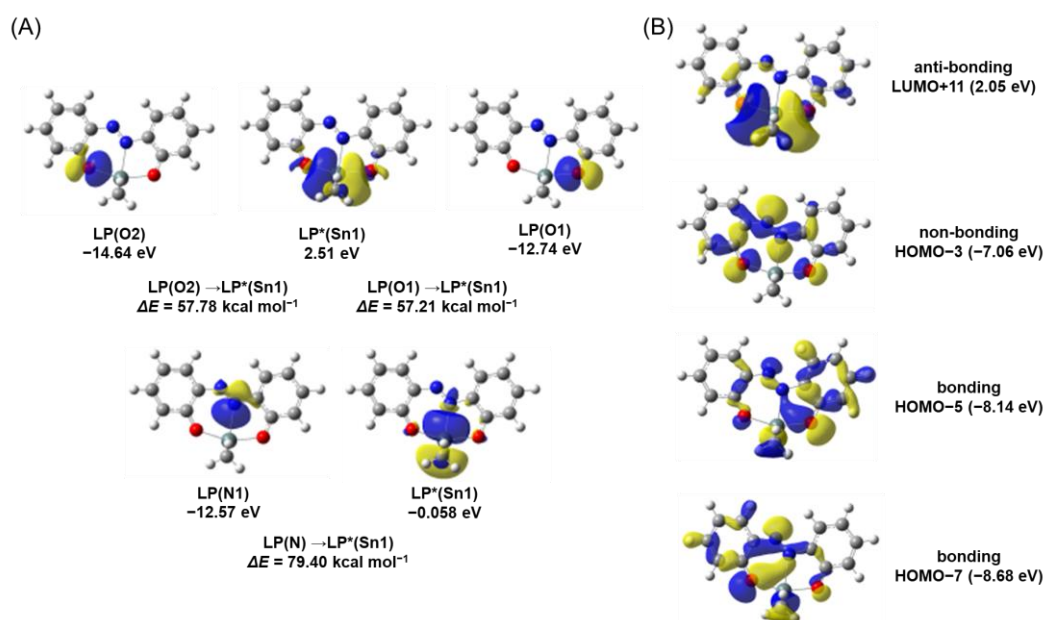
Figure S19. (A) The NBOs and (B) Kohn–Sham orbitals involving 3c-4e bond of **TAzMe-H** and the stabilization energy of donor–acceptor interactions (isovalue = 0.03). ΔE: The second-order perturbation stabilization energy. The split bonding orbitals are found probably by the asymmetric structure.
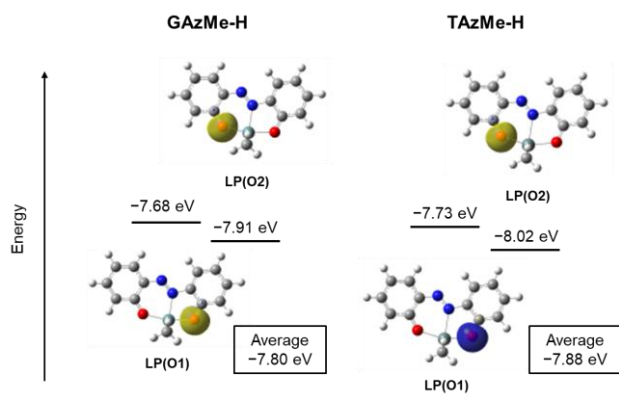
Figure S20. The results of NBO calculations of **GAzMe-H** and **TAzMe-H** focused on energy levels of LP(O1) and LP(O2) (isovalue = 0.03).

References

[1]   T. Higashi, ABSCOR. Program for Absorption Correction.; Rigaku Corporation: Japan, **1995**.

[2]   K. Wakita, Yadokari&XG. Program for Crystal Structure Analysis.; **2000**.

[3]   L. J. Farrugia, *J. Appl. Cryst.* **1997**, *30*, 565.

[4]   A. B. Pangborn, M. A. Giardello, R. H. Grubbs, R. K. Rosen, F. J. Timmers, Safe and Convenient Procedure for Solvent Purification. *Organometallics* **1996**, *15*, 1518–1520.

[5]   H. Tanimoto, T. Nagao, Y. Nishiyama, T. Morimoto, F. Iseda, Y. Nagato, T. Suzuka, K. Tsutsumi, K. Kakiuchi, *Dalton Trans.* **2014**, *43*, 8338–8343.

[6]   M. Gon, K. Tanaka, Y. Chujo, *Chem. Eur. J.* **2021**, *27*, 7561–7571.

[7]   M. Gon, K. Tanaka, Y. Chujo, *Angew. Chem. Int. Ed.* **2018**, *57*, 6546–6551; *Angew. Chem.* **2018**, *130*, 6656–6661.

[8]   D. C. Marelius, E. H. Darrow, C. E. Moore, J. A. Golen, A. L. Rheingold, D. B. Grotjahn, *Chem. Eur. J.* **2015**, *21*, 10988–10992.

[9]   X. Guo, Q. Liao, E. F. Manley, Z. Wu, Y. Wang, W. Wang, T. Yang, Y.-E. Shin, X. Cheng, Y. Liang, L. X. Chen, K.-J. Baeg, T. J. Marks, X. Guo, *Chem. Mater.* **2016**, *28*, 2449–2460.

[10] G. M. Sheldrick, *Acta Cryst.* **2015**, *C71*, 3–8.

[11] a) C. M. Cardona, W. Li, A. E. Kaifer, D. Stockdale, G. C. Bazan, *Adv. Mater.* **2011**, *23*, 2367-2371; b) J. Pommerehne, H. Vestweber, W. Guss, R. F. Mahrt, H. Bässler, M. Porsch, J. Daub, *Adv. Mater.* **1995**, *7*, 551-554.

[12] Gaussian 16, Revision A.03, M. J. Frisch, G. W. Trucks, H. B. Schlegel, G. E. Scuseria, M. A. Robb, J. R. Cheeseman, G. Scalmani, V. Barone, G. A. Petersson, H. Nakatsuji, X. Li, M. Caricato, A. V. Marenich, J. Bloino, B. G. Janesko, R. Gomperts, B. Mennucci, H. P. Hratchian, J. V. Ortiz, A. F. Izmaylov, J. L. Sonnenberg, D. Williams-Young, F. Ding, F. Lipparini, F. Egidi, J. Goings, B. Peng, A. Petrone, T. Henderson, D. Ranasinghe, V. G. Zakrzewski, J. Gao, N. Rega, G. Zheng, W. Liang, M. Hada, M. Ehara, K. Toyota, R. Fukuda, J. Hasegawa, M. Ishida, T. Nakajima, Y. Honda, O. Kitao, H. Nakai, T. Vreven, K. Throssell, J. A. Montgomery, Jr., J. E. Peralta, F. Ogliaro, M. J. Bearpark, J. J. Heyd, E. N. Brothers, K. N. Kudin, V. N. Staroverov, T. A. Keith, R. Kobayashi, J. Normand, K. Raghavachari, A. P. Rendell, J. C. Burant, S. S. Iyengar, J. Tomasi, M. Cossi, J. M. Millam, M. Klene, C. Adamo, R. Cammi, J. W. Ochterski, R. L. Martin, K. Morokuma, O. Farkas, J. B. Foresman, and

D. J. Fox, Gaussian, Inc., Wallingford CT, **2016**.

Coordinates for optimized structures with theoretical calculation

GAz-F (ground state)

Center Number	Atomic Number	Atomic Type	Coordinates (Angstroms)		
			X	Y	Z
1	6	0	-2.66058	-2.69572	-0.09924
2	6	0	-4.03079	-2.63224	-0.14263
3	6	0	-4.62196	-1.35761	-0.14585
4	6	0	-3.90438	-0.1862	-0.1075
5	6	0	-2.49204	-0.23251	-0.06202
6	6	0	-1.86181	-1.5229	-0.05937
7	7	0	-0.52103	-1.75043	-0.02033
8	7	0	0.354509	-0.82021	0.012236
9	6	0	1.701659	-1.21992	0.049601
10	6	0	2.616831	-0.1366	0.068263
11	6	0	3.993691	-0.41905	0.105079
12	6	0	4.394485	-1.73855	0.120998
13	6	0	3.502846	-2.81638	0.102749
14	6	0	2.146667	-2.54641	0.066658
15	8	0	-1.81035	0.867843	-0.02386
16	32	0	0.17075	1.244078	0.013611
17	8	0	2.145438	1.087681	0.051373
18	9	0	5.715874	-2.0108	0.156483
19	9	0	-5.96516	-1.29056	-0.18918
20	6	0	0.09299	2.140401	-1.75511
21	6	0	0.344016	1.142219	-2.89445
22	6	0	1.051023	3.337394	-1.82536
23	6	0	0.074767	2.142349	1.78168
24	6	0	-0.08635	1.119663	2.915462
25	6	0	-1.01406	3.222268	1.828078
26	1	0	-2.14212	-3.64639	-0.09461
27	1	0	-4.65516	-3.51461	-0.17387
28	1	0	-4.40517	0.772641	-0.11265
29	1	0	4.716275	0.385535	0.120752

30	1	0	3.886168	-3.82777	0.117353
31	1	0	1.417584	-3.34483	0.051276
32	1	0	-0.94051	2.492927	-1.81662
33	1	0	-0.36637	0.311162	-2.88144
34	1	0	0.243314	1.643542	-3.8634
35	1	0	1.354502	0.726652	-2.84568
36	1	0	0.836003	4.085111	-1.05639
37	1	0	0.959702	3.833567	-2.79821
38	1	0	2.088398	3.020716	-1.70204
39	1	0	1.058426	2.612008	1.871066
40	1	0	0.715264	0.37638	2.919421
41	1	0	-0.06735	1.627271	3.886181
42	1	0	-1.04131	0.591004	2.843517
43	1	0	-0.86479	3.993302	1.066736
44	1	0	-1.00466	3.720353	2.804251
45	1	0	-2.00588	2.792174	1.677316

GAz-F (excited state)

Center Number	Atomic Number	Atomic Type	Coordinates (Angstroms)		
			X	Y	Z
1	6	0	-2.648143	-2.71459	-0.10656
2	6	0	-4.018073	-2.647905	-0.139045
3	6	0	-4.619331	-1.376941	-0.117762
4	6	0	-3.903978	-0.203418	-0.066327
5	6	0	-2.495471	-0.247472	-0.031929
6	6	0	-1.834426	-1.539238	-0.051587
7	7	0	-0.513268	-1.754662	-0.020891
8	7	0	0.365836	-0.751932	0.025099
9	6	0	1.720339	-1.198615	0.055232
10	6	0	2.664346	-0.130426	0.046111
11	6	0	4.042479	-0.40454	0.072959
12	6	0	4.446216	-1.73761	0.110961
13	6	0	3.548358	-2.782232	0.121003
14	6	0	2.154058	-2.499028	0.093477

15	8	0	-1.824454	0.869252	0.017648
16	32	0	0.115877	1.1953	0.010095
17	8	0	2.17455	1.079726	0.014446
18	9	0	5.775579	-2.0048	0.137284
19	9	0	-5.969308	-1.315329	-0.150577
20	6	0	0.044064	2.148697	-1.745479
21	6	0	0.171605	1.158531	-2.910137
22	6	0	1.067138	3.286567	-1.83988
23	6	0	0.107785	2.166997	1.756504
24	6	0	-0.073552	1.187092	2.922614
25	6	0	-0.940734	3.286564	1.778134
26	1	0	-2.134639	-3.667958	-0.120943
27	1	0	-4.6378	-3.53408	-0.179986
28	1	0	-4.405196	0.755643	-0.052558
29	1	0	4.761649	0.403805	0.064198
30	1	0	3.905475	-3.803527	0.148232
31	1	0	1.433073	-3.304771	0.101177
32	1	0	-0.966058	2.568468	-1.749963
33	1	0	-0.587456	0.372789	-2.872372
34	1	0	0.051032	1.685314	-3.863811
35	1	0	1.1547	0.678868	-2.925299
36	1	0	0.959401	4.011002	-1.027493
37	1	0	0.931799	3.83035	-2.782032
38	1	0	2.090343	2.90697	-1.811211
39	1	0	1.1072	2.606096	1.813783
40	1	0	0.693382	0.408069	2.934859
41	1	0	-0.011627	1.724014	3.87619
42	1	0	-1.051446	0.698354	2.885546
43	1	0	-0.792066	4.011302	0.972462
44	1	0	-0.8791	3.835151	2.725281
45	1	0	-1.952007	2.885466	1.684596

GAz-Cl (ground state)

Center	Atomic	Atomic	Coordinates (Angstroms)

Number	Number	Type	X	Y	Z
1	6	0	-2.575197	-2.652177	-0.071248
2	6	0	-3.946638	-2.628507	-0.10058
3	6	0	-4.586807	-1.372395	-0.099846
4	6	0	-3.892263	-0.184015	-0.070213
5	6	0	-2.476275	-0.189198	-0.038689
6	6	0	-1.809008	-1.458158	-0.040905
7	7	0	-0.461777	-1.646044	-0.015994
8	7	0	0.384075	-0.687868	0.007604
9	6	0	1.742131	-1.04617	0.03014
10	6	0	2.623315	0.062825	0.043123
11	6	0	4.009878	-0.177578	0.065561
12	6	0	4.462014	-1.483599	0.073845
13	6	0	3.592966	-2.585403	0.060788
14	6	0	2.229281	-2.357607	0.038812
15	8	0	-1.831416	0.932991	-0.009133
16	32	0	0.138524	1.373804	0.014659
17	8	0	2.117623	1.273184	0.034851
18	17	0	6.194374	-1.783634	0.102316
19	17	0	-6.33988	-1.333946	-0.138624
20	6	0	0.019625	2.269901	-1.751547
21	6	0	0.300809	1.284458	-2.894898
22	6	0	0.934134	3.500549	-1.821871
23	6	0	0.031431	2.261056	1.787314
24	6	0	-0.076506	1.229249	2.919222
25	6	0	-1.095391	3.300239	1.851746
26	1	0	-2.031791	-3.589108	-0.070924
27	1	0	-4.530497	-3.537708	-0.124047
28	1	0	-4.401446	0.770026	-0.071231
29	1	0	4.691939	0.661234	0.07643
30	1	0	3.990905	-3.590577	0.068219
31	1	0	1.527041	-3.180024	0.028204
32	1	0	-1.026112	2.585445	-1.806915
33	1	0	-0.379434	0.428564	-2.881412

34	1	0	0.177408	1.784875	-3.861599
35	1	0	1.325784	0.905402	-2.852447
36	1	0	0.696317	4.23761	-1.049377
37	1	0	0.820189	3.996208	-2.792494
38	1	0	1.982837	3.220794	-1.705135
39	1	0	0.998385	2.766195	1.865546
40	1	0	0.752147	0.516322	2.91003
41	1	0	-0.063046	1.734384	3.891226
42	1	0	-1.012233	0.665866	2.858757
43	1	0	-0.985219	4.077976	1.090607
44	1	0	-1.090019	3.795921	2.829078
45	1	0	-2.073057	2.834884	1.714104

GAz-Cl (excited state)

Center Number	Atomic Number	Atomic Type	Coordinates (Angstroms)		
			X	Y	Z
1	6	0	-2.566373	-2.668115	-0.081185
2	6	0	-3.93661	-2.63775	-0.102946
3	6	0	-4.589434	-1.384551	-0.08315
4	6	0	-3.889533	-0.195611	-0.042342
5	6	0	-2.479496	-0.201067	-0.018729
6	6	0	-1.782458	-1.472509	-0.038478
7	7	0	-0.456862	-1.650985	-0.019291
8	7	0	0.393999	-0.624008	0.014926
9	6	0	1.757338	-1.026321	0.034106
10	6	0	2.668061	0.069576	0.030839
11	6	0	4.052891	-0.160951	0.049735
12	6	0	4.513724	-1.480347	0.072483
13	6	0	3.633972	-2.549316	0.075755
14	6	0	2.23438	-2.313922	0.057158
15	8	0	-1.84067	0.934465	0.021199
16	32	0	0.090521	1.321069	0.012586
17	8	0	2.139687	1.265725	0.011517
18	17	0	6.246414	-1.778854	0.096276

19	17	0	-6.340889	-1.351552	-0.111858
20	6	0	-0.020725	2.281379	-1.738385
21	6	0	0.129225	1.300849	-2.908277
22	6	0	0.968843	3.448448	-1.831064
23	6	0	0.049039	2.283136	1.765563
24	6	0	-0.107039	1.291848	2.925391
25	6	0	-1.030871	3.372055	1.789177
26	1	0	-2.029878	-3.609032	-0.095525
27	1	0	-4.518049	-3.549387	-0.134919
28	1	0	-4.398048	0.75937	-0.028205
29	1	0	4.732403	0.680718	0.046239
30	1	0	4.008837	-3.564199	0.091839
31	1	0	1.541194	-3.143919	0.060253
32	1	0	-1.042684	2.671198	-1.734345
33	1	0	-0.60739	0.494032	-2.871152
34	1	0	-0.010955	1.829072	-3.858474
35	1	0	1.12551	0.849568	-2.930954
36	1	0	0.845443	4.164424	-1.013459
37	1	0	0.81176	3.993951	-2.768839
38	1	0	2.002576	3.098111	-1.811149
39	1	0	1.03574	2.749451	1.82659
40	1	0	0.681384	0.534556	2.934947
41	1	0	-0.061276	1.825205	3.881883
42	1	0	-1.071139	0.776777	2.884397
43	1	0	-0.9008	4.104507	0.987335
44	1	0	-0.986739	3.917716	2.739004
45	1	0	-2.030179	2.943024	1.691581

GAz-Br (ground state)

Center Number	Atomic Number	Atomic Type	Coordinates (Angstroms)		
			X	Y	Z
1	6	0	-2.519707	-2.480839	-0.046136
2	6	0	-3.891981	-2.483408	-0.063824
3	6	0	-4.555268	-1.238795	-0.059553

4	6	0	-3.883055	-0.037442	-0.037624
5	6	0	-2.465905	-0.016725	-0.018003
6	6	0	-1.775415	-1.272829	-0.023948
7	7	0	-0.424785	-1.435596	-0.010362
8	7	0	0.403141	-0.461469	0.00571
9	6	0	1.767759	-0.794362	0.017018
10	6	0	2.627959	0.330753	0.023553
11	6	0	4.019809	0.116526	0.034803
12	6	0	4.495922	-1.181146	0.03879
13	6	0	3.647558	-2.299541	0.032081
14	6	0	2.279334	-2.096491	0.021124
15	8	0	-1.842093	1.117496	0.003953
16	32	0	0.119168	1.595226	0.01581
17	8	0	2.099837	1.53161	0.019918
18	35	0	6.390768	-1.47302	0.054613
19	35	0	-6.46826	-1.232159	-0.085655
20	6	0	-0.029376	2.49322	-1.747254
21	6	0	0.263872	1.516388	-2.894918
22	6	0	0.860163	3.741872	-1.820133
23	6	0	0.009171	2.477468	1.790846
24	6	0	-0.067198	1.442097	2.922079
25	6	0	-1.138219	3.493042	1.866969
26	1	0	-1.958943	-3.407629	-0.049099
27	1	0	-4.45471	-3.405821	-0.080939
28	1	0	-4.40475	0.909753	-0.035816
29	1	0	4.681823	0.971222	0.04065
30	1	0	4.059532	-3.298927	0.035748
31	1	0	1.592417	-2.931925	0.015714
32	1	0	-1.081496	2.788065	-1.794917
33	1	0	-0.399015	0.647017	-2.879124
34	1	0	0.124132	2.016498	-3.859565
35	1	0	1.296479	1.157835	-2.860058
36	1	0	0.612306	4.472401	-1.044591
37	1	0	0.730731	4.237277	-2.788952

38	1	0	1.914858	3.482664	-1.710156
39	1	0	0.966158	3.002369	1.861302
40	1	0	0.775809	0.746379	2.904268
41	1	0	-0.055273	1.94603	3.894739
42	1	0	-0.99164	0.859601	2.869347
43	1	0	-1.050953	4.273888	1.10604
44	1	0	-1.134341	3.987392	2.844988
45	1	0	-2.107288	3.00783	1.737325

GAz-Br (excited state)

Center Number	Atomic Number	Atomic Type	Coordinates (Angstroms)		
			X	Y	Z
1	6	0	-2.515306	-2.494009	-0.062095
2	6	0	-3.886346	-2.4889	-0.074226
3	6	0	-4.561426	-1.247101	-0.050024
4	6	0	-3.882956	-0.045667	-0.014415
5	6	0	-2.471954	-0.026	-0.000796
6	6	0	-1.752516	-1.284723	-0.025354
7	7	0	-0.423909	-1.439638	-0.015457
8	7	0	0.408693	-0.397537	0.012502
9	6	0	1.778189	-0.774167	0.021885
10	6	0	2.668681	0.338458	0.013176
11	6	0	4.058071	0.133546	0.022337
12	6	0	4.542461	-1.176973	0.040874
13	6	0	3.682324	-2.263001	0.04923
14	6	0	2.279013	-2.053514	0.040485
15	8	0	-1.853642	1.120676	0.034546
16	32	0	0.070936	1.542988	0.01361
17	8	0	2.118181	1.524782	-0.00176
18	35	0	6.437178	-1.470398	0.053576
19	35	0	-6.471988	-1.2453	-0.067814
20	6	0	-0.070813	2.501768	-1.736256
21	6	0	0.091258	1.524703	-2.907406
22	6	0	0.895377	3.687809	-1.834058

23	6	0	0.022108	2.502049	1.768323
24	6	0	-0.107641	1.50657	2.927755
25	6	0	-1.077809	3.570457	1.800141
26	1	0	-1.962281	-3.425369	-0.080014
27	1	0	-4.44723	-3.413229	-0.101828
28	1	0	-4.403524	0.902608	0.003324
29	1	0	4.718034	0.990447	0.014837
30	1	0	4.071739	-3.272271	0.06194
31	1	0	1.601223	-2.896175	0.047597
32	1	0	-1.100157	2.871425	-1.725499
33	1	0	-0.629291	0.703691	-2.86637
34	1	0	-0.064847	2.05048	-3.85647
35	1	0	1.096018	1.092998	-2.936227
36	1	0	0.76318	4.40075	-1.015187
37	1	0	0.721841	4.230733	-2.770424
38	1	0	1.935774	3.3575	-1.820866
39	1	0	1.000341	2.986586	1.823284
40	1	0	0.695113	0.764439	2.931273
41	1	0	-0.065702	2.03966	3.884565
42	1	0	-1.062063	0.973378	2.892513
43	1	0	-0.966905	4.305865	0.998139
44	1	0	-1.037355	4.116092	2.750147
45	1	0	-2.069563	3.122914	1.708991

GAz-I (ground state)

Center Number	Atomic Number	Atomic Type	Coordinates (Angstroms)		
			X	Y	Z
1	6	0	-2.495462	-2.332242	-0.031343
2	6	0	-3.868087	-2.34587	-0.044352
3	6	0	-4.544186	-1.107611	-0.04
4	6	0	-3.879664	0.097791	-0.022258
5	6	0	-2.46148	0.130872	-0.007361
6	6	0	-1.760671	-1.118634	-0.013666
7	7	0	-0.408586	-1.269996	-0.004773

8	7	0	0.410679	-0.288458	0.006995
9	6	0	1.778276	-0.609195	0.013411
10	6	0	2.628284	0.522794	0.016121
11	6	0	4.022869	0.320344	0.02223
12	6	0	4.512814	-0.972054	0.025139
13	6	0	3.672321	-2.096834	0.022204
14	6	0	2.30182	-1.906305	0.01629
15	8	0	-1.848288	1.270986	0.010602
16	32	0	0.109114	1.765519	0.016339
17	8	0	2.090295	1.719469	0.013894
18	53	0	6.628572	-1.277777	0.034865
19	53	0	-6.677782	-1.117111	-0.062188
20	6	0	-0.052819	2.661387	-1.746691
21	6	0	0.246214	1.686772	-2.89474
22	6	0	0.825064	3.918086	-1.822448
23	6	0	-0.002761	2.647894	1.791247
24	6	0	-0.064435	1.612521	2.923392
25	6	0	-1.159735	3.652196	1.871286
26	1	0	-1.927698	-3.254955	-0.034747
27	1	0	-4.416803	-3.276682	-0.058011
28	1	0	-4.401579	1.044881	-0.020205
29	1	0	4.670663	1.185889	0.025111
30	1	0	4.086311	-3.095327	0.024803
31	1	0	1.622961	-2.748494	0.013897
32	1	0	-1.107734	2.946539	-1.79151
33	1	0	-0.408808	0.811507	-2.8768
34	1	0	0.099444	2.185208	-3.85922
35	1	0	1.282074	1.337508	-2.8624
36	1	0	0.572637	4.646611	-1.046483
37	1	0	0.688536	4.411939	-2.791097
38	1	0	1.882354	3.668502	-1.715176
39	1	0	0.949313	3.182201	1.857636
40	1	0	0.78543	0.925293	2.902705
41	1	0	-0.053817	2.117179	3.895703

42	1	0	-0.98318	1.020742	2.874575
43	1	0	-1.08338	4.433108	1.10924
44	1	0	-1.15662	4.147507	2.848831
45	1	0	-2.124509	3.157346	1.746155

GAz-I (excited state)

Center	Atomic	Atomic	Coordinates (Angstroms)		
Number	Number	Type	X	Y	Z
1	6	0	-2.494194	-2.343608	-0.048473
2	6	0	-3.86568	-2.349087	-0.057257
3	6	0	-4.554228	-1.113702	-0.034572
4	6	0	-3.881834	0.091389	-0.003368
5	6	0	-2.470015	0.122884	0.006965
6	6	0	-1.740491	-1.129136	-0.016816
7	7	0	-0.410429	-1.273407	-0.010746
8	7	0	0.413166	-0.223917	0.012185
9	6	0	1.78553	-0.588149	0.01709
10	6	0	2.666417	0.531612	0.007326
11	6	0	4.058095	0.338212	0.01261
12	6	0	4.557521	-0.966722	0.027679
13	6	0	3.703647	-2.05896	0.036662
14	6	0	2.298199	-1.862797	0.032056
15	8	0	-1.862122	1.27524	0.038647
16	32	0	0.059417	1.713997	0.014233
17	8	0	2.106212	1.713492	-0.004907
18	53	0	6.666946	-1.276647	0.035617
19	53	0	-6.678867	-1.128315	-0.049237
20	6	0	-0.094121	2.670541	-1.735554
21	6	0	0.075083	1.694624	-2.90671
22	6	0	0.861203	3.86522	-1.835499
23	6	0	0.00517	2.67252	1.768772
24	6	0	-0.112265	1.67616	2.928813
25	6	0	-1.104781	3.730445	1.803386
26	1	0	-1.934671	-3.271276	-0.065599

27	1	0	-4.412364	-3.281909	-0.081286
28	1	0	-4.401779	1.040025	0.013684
29	1	0	4.703635	1.206026	0.004676
30	1	0	4.094797	-3.067553	0.046862
31	1	0	1.628604	-2.712116	0.039765
32	1	0	-1.12674	3.03095	-1.723608
33	1	0	-0.638017	0.8672	-2.864341
34	1	0	-0.086926	2.218568	-3.855811
35	1	0	1.08361	1.271848	-2.936633
36	1	0	0.723326	4.577666	-1.017115
37	1	0	0.682032	4.405717	-2.772228
38	1	0	1.904531	3.54424	-1.82284
39	1	0	0.978866	3.1664	1.821515
40	1	0	0.697823	0.942035	2.930714
41	1	0	-0.073653	2.209802	3.885469
42	1	0	-1.061403	1.133458	2.895683
43	1	0	-1.002719	4.466931	1.001182
44	1	0	-1.067498	4.27635	2.753387
45	1	0	-2.092413	3.273461	1.714284

GAz-BT (ground state)

Center Number	Atomic Number	Atomic Type	Coordinates (Angstroms)		
			X	Y	Z
1	6	0	12.02262	-2.03207	-0.10901
2	6	0	10.87832	-1.39069	-0.67931
3	6	0	9.849439	-1.26069	0.228726
4	16	0	10.29581	-1.93829	1.786729
5	6	0	11.85728	-2.3869	1.196173
6	6	0	8.534449	-0.65629	0.036185
7	16	0	7.084123	-1.61824	0.228491
8	6	0	6.052052	-0.25415	-0.13966
9	6	0	6.821582	0.856516	-0.39687
10	6	0	8.224168	0.647691	-0.2962
11	6	0	4.595427	-0.37221	-0.14368

12	6	0	3.798545	0.766154	-0.04089
13	6	0	2.391846	0.700931	-0.05969
14	6	0	1.776966	-0.58845	-0.17499
15	6	0	2.603212	-1.73873	-0.27008
16	6	0	3.969171	-1.64469	-0.25888
17	7	0	0.442114	-0.83728	-0.19872
18	8	0	1.69301	1.794414	0.041709
19	7	0	-0.44622	0.084634	-0.12573
20	6	0	-1.78435	-0.32488	-0.15807
21	32	0	-0.27647	2.144881	0.021872
22	6	0	-2.71394	0.742886	-0.09416
23	6	0	-4.08471	0.443915	-0.12641
24	6	0	-4.52906	-0.87656	-0.21029
25	6	0	-3.57534	-1.92579	-0.2628
26	6	0	-2.22413	-1.65273	-0.24035
27	8	0	-2.25501	1.970878	-0.02023
28	6	0	-6.56732	-2.31998	-0.75028
29	6	0	-7.98575	-2.33475	-0.62941
30	6	0	-8.46946	-1.19196	-0.02709
31	16	0	-7.16139	-0.10388	0.396994
32	6	0	-5.95746	-1.1961	-0.24653
33	6	0	-9.85349	-0.83197	0.268136
34	16	0	-10.3771	-0.59965	1.929044
35	6	0	-11.9905	-0.24282	1.420208
36	6	0	-12.1155	-0.30597	0.064807
37	6	0	-10.898	-0.63674	-0.60954
38	6	0	-0.23719	3.139168	-1.7003
39	6	0	-0.30164	2.162664	-2.88476
40	6	0	0.942931	4.109035	-1.83005
41	6	0	-0.28116	2.906324	1.858776
42	6	0	0.82088	3.947922	2.087584
43	6	0	-0.2264	1.783957	2.906143
44	6	0	9.235533	1.741176	-0.50298
45	6	0	10.81491	-0.95308	-2.11663

46	6	0	-8.83754	-3.48594	-1.08855
47	6	0	-10.7854	-0.71961	-2.10683
48	1	0	12.92908	-2.23107	-0.66709
49	1	0	12.55643	-2.88852	1.847596
50	1	0	6.393131	1.813857	-0.66487
51	1	0	4.237776	1.747746	0.082765
52	1	0	2.105791	-2.69684	-0.36093
53	1	0	4.573077	-2.53776	-0.35747
54	1	0	-4.78138	1.272937	-0.10587
55	1	0	-3.91144	-2.95401	-0.29108
56	1	0	-1.48996	-2.44646	-0.27286
57	1	0	-6.01372	-3.12488	-1.21706
58	1	0	-12.7467	-0.00356	2.152084
59	1	0	-13.0451	-0.1084	-0.45456
60	1	0	-1.17288	3.705601	-1.67013
61	1	0	-0.36661	2.717965	-3.82718
62	1	0	-1.17295	1.5055	-2.83089
63	1	0	0.594637	1.536994	-2.93826
64	1	0	0.88615	4.637781	-2.7887
65	1	0	0.947717	4.863592	-1.03928
66	1	0	1.897789	3.581955	-1.79006
67	1	0	-1.25977	3.39092	1.919026
68	1	0	1.812679	3.514222	1.947609
69	1	0	0.760722	4.3353	3.11131
70	1	0	0.729619	4.801154	1.410028
71	1	0	-0.3063	2.205883	3.914243
72	1	0	-1.04181	1.06606	2.786439
73	1	0	0.719734	1.236865	2.856518
74	1	0	10.21334	1.451546	-0.11654
75	1	0	9.35171	1.98299	-1.5648
76	1	0	8.923379	2.656563	0.006798
77	1	0	11.19868	-1.73713	-2.77526
78	1	0	9.791455	-0.72688	-2.41795
79	1	0	11.42242	-0.0582	-2.28936

80	1	0	-9.84636	-3.41757	-0.67986
81	1	0	-8.91813	-3.51336	-2.18055
82	1	0	-8.4037	-4.43813	-0.77089
83	1	0	-11.273	0.138216	-2.57844
84	1	0	-9.74231	-0.7355	-2.42487
85	1	0	-11.2697	-1.62213	-2.49513

GAz-BT (excited state)

Center Number	Atomic Number	Atomic Type	Coordinates (Angstroms)		
			X	Y	Z
1	6	0	-12.044	-1.87299	0.480048
2	6	0	-10.926	-1.01999	0.740048
3	6	0	-9.84904	-1.31099	-0.07395
4	16	0	-10.223	-2.65299	-1.15195
5	6	0	-11.815	-2.79699	-0.49695
6	6	0	-8.54204	-0.67599	-0.12695
7	16	0	-7.08904	-1.63999	0.053048
8	6	0	-6.04904	-0.237	-0.13795
9	6	0	-6.83004	0.892006	-0.31695
10	6	0	-8.22704	0.661007	-0.32095
11	6	0	-4.60804	-0.346	-0.09795
12	6	0	-3.80004	0.796003	-0.03695
13	6	0	-2.40204	0.729002	-0.00695
14	6	0	-1.76004	-0.578	-0.03695
15	6	0	-2.60704	-1.733	-0.09495
16	6	0	-3.96704	-1.628	-0.12395
17	7	0	-0.45204	-0.824	-0.01895
18	8	0	-1.70403	1.829001	0.053048
19	7	0	0.452964	0.157	0.032048
20	6	0	1.778964	-0.293	0.043048
21	32	0	0.253966	2.13	0.107048
22	6	0	2.744965	0.761998	0.101048
23	6	0	4.105965	0.453996	0.120048
24	6	0	4.538964	-0.881	0.079048

25	6	0	3.562963	-1.905	0.018048
26	6	0	2.199963	-1.618	0.001048
27	8	0	2.269966	1.982998	0.143048
28	6	0	6.541962	-2.45901	0.318048
29	6	0	7.958962	-2.46801	0.250048
30	6	0	8.479963	-1.21501	-0.02495
31	16	0	7.194964	-0.03301	-0.21295
32	6	0	5.953963	-1.23001	0.089048
33	6	0	9.869964	-0.81201	-0.17495
34	16	0	10.39996	0.000991	-1.64295
35	6	0	12.01996	0.11499	-1.05295
36	6	0	12.14396	-0.43901	0.188048
37	6	0	10.92096	-0.96801	0.708048
38	6	0	0.230967	2.976	1.919048
39	6	0	0.268966	1.894	3.008048
40	6	0	-0.93003	3.953001	2.133048
41	6	0	0.289967	3.115	-1.63195
42	6	0	-0.78703	4.201001	-1.73995
43	6	0	0.215966	2.125	-2.80295
44	6	0	-9.23503	1.749008	-0.57395
45	6	0	-10.932	0.023009	1.823048
46	6	0	8.774961	-3.72101	0.413048
47	6	0	10.80996	-1.56101	2.085048
48	1	0	-12.978	-1.80599	1.024048
49	1	0	-12.486	-3.55799	-0.86795
50	1	0	-6.40603	1.873006	-0.48595
51	1	0	-4.23603	1.786004	0.006048
52	1	0	-2.11804	-2.699	-0.12095
53	1	0	-4.56804	-2.527	-0.18095
54	1	0	4.808965	1.275996	0.184048
55	1	0	3.874962	-2.94	-0.03895
56	1	0	1.462962	-2.408	-0.05095
57	1	0	5.968961	-3.35101	0.534048
58	1	0	12.78297	0.585989	-1.65295

59	1	0	13.07696	-0.45901	0.737048
60	1	0	1.176967	3.524999	1.941048
61	1	0	0.343966	2.362	3.997048
62	1	0	1.123965	1.222999	2.897048
63	1	0	-0.64204	1.288001	3.004048
64	1	0	-0.85403	4.407001	3.128048
65	1	0	-0.92903	4.767001	1.402048
66	1	0	-1.89603	3.448002	2.064048
67	1	0	1.277967	3.581999	-1.63095
68	1	0	-1.79003	3.776002	-1.67395
69	1	0	-0.69903	4.715001	-2.70495
70	1	0	-0.69103	4.958001	-0.95795
71	1	0	0.318967	2.661	-3.75395
72	1	0	1.009965	1.373999	-2.76395
73	1	0	-0.74503	1.602001	-2.82595
74	1	0	-10.195	1.336009	-0.88395
75	1	0	-9.40503	2.355008	0.322048
76	1	0	-8.88203	2.422008	-1.35895
77	1	0	-11.399	-0.36999	2.730048
78	1	0	-9.91904	0.342009	2.074048
79	1	0	-11.5	0.91101	1.525048
80	1	0	9.782961	-3.59301	0.015048
81	1	0	8.864961	-4.00901	1.466048
82	1	0	8.30496	-4.55601	-0.11295
83	1	0	11.36296	-0.95501	2.808048
84	1	0	9.770963	-1.61501	2.412048
85	1	0	11.22796	-2.57201	2.123048

GAzMe-H (ground state)

Center	Atomic	Atomic	Coordinates (Angstroms)		
Number	Number	Type	X	Y	Z
1	6	0	2.775234	2.287075	0.007958
2	6	0	4.140362	2.142797	0.007019
3	6	0	4.691393	0.842862	-0.002021

4	6	0	3.888304	-0.27753	-0.009635
5	6	0	2.476396	-0.162966	-0.008047
6	6	0	1.915979	1.155818	0.000877
7	7	0	0.586418	1.452868	0.001351
8	7	0	-0.3321	0.564315	-0.001003
9	6	0	-1.662471	1.018143	-0.001628
10	6	0	-2.616448	-0.028874	0.004988
11	6	0	-3.982041	0.312588	0.004873
12	6	0	-4.358815	1.644664	-0.001276
13	6	0	-3.401381	2.674795	-0.007758
14	6	0	-2.053862	2.362794	-0.007959
15	8	0	1.740434	-1.232333	-0.016426
16	32	0	-0.239028	-1.498223	0.001252
17	8	0	-2.190085	-1.272775	0.011373
18	1	0	-5.413503	1.897604	-0.001207
19	1	0	5.769422	0.721479	-0.003097
20	6	0	-0.204546	-2.395844	-1.731473
21	1	0	-0.268392	-1.647885	-2.524287
22	1	0	-1.063303	-3.06219	-1.811318
23	6	0	-0.181652	-2.382357	1.740344
24	1	0	-0.225895	-1.627886	2.528324
25	1	0	0.748738	-2.941115	1.837204
26	1	0	2.30359	3.262435	0.014234
27	1	0	4.787955	3.010413	0.0128
28	1	0	4.30612	-1.276924	-0.016869
29	1	0	-4.712262	-0.487191	0.009949
30	1	0	-3.71834	3.710494	-0.012804
31	1	0	-1.291552	3.130288	-0.012928
32	1	0	0.728416	-2.948065	-1.839819
33	1	0	-1.043829	-3.041541	1.840174

TAzMe-H (ground state)

Center Number	Atomic Number	Atomic Type	Coordinates (Angstroms)		
			X	Y	Z

1	6	0	2.827965	2.467316	0.002547
2	6	0	4.194382	2.325958	0.002011
3	6	0	4.745411	1.028699	-0.001658
4	6	0	3.938412	-0.090114	-0.004589
5	6	0	2.52831	0.020904	-0.003775
6	6	0	1.96453	1.339797	-0.000187
7	7	0	0.63467	1.662763	0.000156
8	7	0	-0.296942	0.789067	-0.000715
9	6	0	-1.619528	1.268642	-0.000932
10	6	0	-2.614754	0.254782	-0.000301
11	6	0	-3.965924	0.651876	-0.000718
12	6	0	-4.297857	1.994851	-0.001615
13	6	0	-3.303926	2.989463	-0.002224
14	6	0	-1.970493	2.626467	-0.001921
15	8	0	1.803248	-1.062542	-0.006917
16	50	0	-0.237587	-1.46317	0.001005
17	8	0	-2.26449	-1.015203	0.000639
18	1	0	-5.343272	2.283871	-0.001883
19	1	0	5.823156	0.905153	-0.002232
20	6	0	-0.22041	-2.436724	-1.883119
21	1	0	-0.245923	-1.685178	-2.674212
22	1	0	-1.099122	-3.074071	-1.982391
23	6	0	-0.21437	-2.421574	1.892917
24	1	0	-0.236876	-1.663754	2.6781
25	1	0	0.695184	-3.012189	2.002437
26	1	0	2.35623	3.442565	0.005073
27	1	0	4.839593	3.195441	0.004234
28	1	0	4.354991	-1.090077	-0.007519
29	1	0	-4.722907	-0.122677	-0.000254
30	1	0	-3.581892	4.036398	-0.002993
31	1	0	-1.180629	3.365467	-0.002444
32	1	0	0.689166	-3.027598	-1.990888
33	1	0	-1.092996	-3.057747	2.000256